TU Delft

Delft University of Technology

Document Version
Final published version

Citation (APA)
Jain, V. (2025). *Towards Sickness-free Automated Driving: Control Algorithms for Motion Sickness Mitigation in Automated Vehicles and Enhanced Immersion in Driving Simulators*. [Dissertation (TU Delft), Delft University of Technology]. https://doi.org/10.4233/uuid:d3d1e107-a9f3-4aaf-918a-7a4b9d1274c2

Important note
To cite this publication, please use the final published version (if applicable).
Please check the document version above.

Copyright
In case the licence states “Dutch Copyright Act (Article 25fa)”, this publication was made available Green Open Access via the TU Delft Institutional Repository pursuant to Dutch Copyright Act (Article 25fa, the Taverne amendment). This provision does not affect copyright ownership.
Unless copyright is transferred by contract or statute, it remains with the copyright holder.

Sharing and reuse
Other than for strictly personal use, it is not permitted to download, forward or distribute the text or part of it, without the consent of the author(s) and/or copyright holder(s), unless the work is under an open content license such as Creative Commons.

Takedown policy
Please contact us and provide details if you believe this document breaches copyrights.
We will remove access to the work immediately and investigate your claim.

This work is downloaded from Delft University of Technology.

TOWARDS SICKNESS-FREE AUTOMATED DRIVING

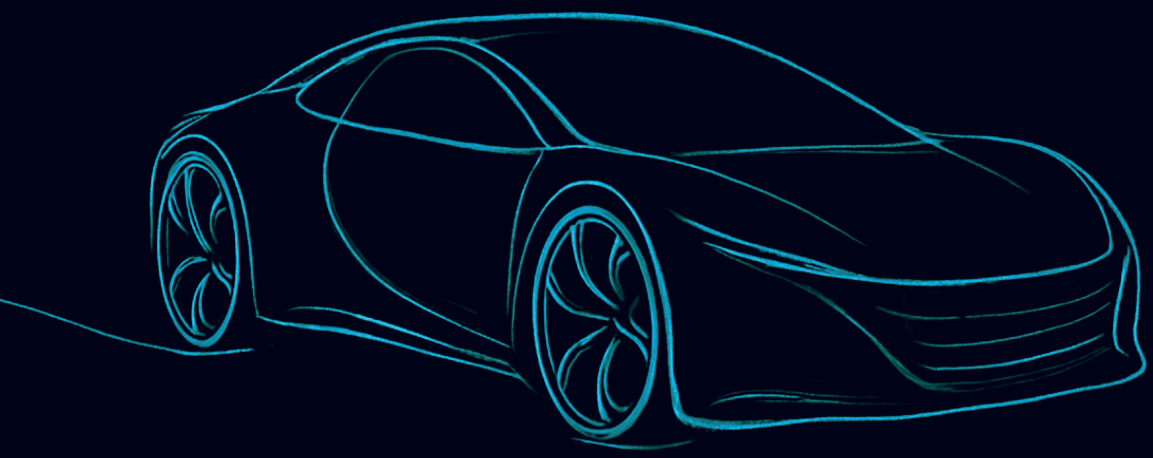

CONTROL ALGORITHMS FOR MOTION SICKNESS MITIGATION IN AUTOMATED VEHICLES AND ENHANCED IMMERSION IN DRIVING SIMULATORS

VISHRUT JAIN

TOWARDS SICKNESS-FREE AUTOMATED DRIVING

CONTROL ALGORITHMS FOR MOTION SICKNESS MITIGATION IN AUTOMATED VEHICLES AND ENHANCED IMMERSION IN DRIVING SIMULATORS

TOWARDS SICKNESS-FREE AUTOMATED DRIVING

CONTROL ALGORITHMS FOR MOTION SICKNESS MITIGATION IN AUTOMATED VEHICLES AND ENHANCED IMMERSION IN DRIVING SIMULATORS

Dissertation

for the purpose of obtaining the degree of doctor
at Delft university of Technology,
by the authority of the Rector Magnificus, prof. dr. ir. T.H.J.J. van der Hagen,
chair of the Board for Doctorates
to be defended publicly on
Thursday 18^{th}, December 2025 at 10:00 a.m.

by

Vishrut JAIN

Master of Science in
Mechanical Engineering,
TU Delft, Delft, The Netherlands.
Born in Jabalpur, Madhya Pradesh, India.

This dissertation has been approved by the promotors.

promotor: Prof. dr. ir. R. Happee
promotor: Dr. B. Shyrokau

Composition of the doctoral committee:

Rector Magnificus	Chairperson
Prof. dr. ir. R. Happee	Delft University of Technology, promotor
Dr. B. Shyrokau	Delft University of Technology, copromotor
Independent members:	
Prof. dr. H. Vallery	Delft University of Technology, The Netherlands
Prof. dr. A. Beghi	University of Padua, Italy
Dr. R. Romano	University of Leeds, UK
Dr. L. Ferranti	Delft University of Technology, The Netherlands
Dr. H. Asadi	Deakin University, Australia
Reserve member:	
Prof. dr. ir. M. Wisse	Delft University of Technology, The Netherlands

This doctoral research was carried out in collaboration with and funded by Toyota Motor Europe.

Keywords: Automated driving, Driving simulators, Motion planning, Model Predictive Control, Motion cueing, Human-in-the-loop, Model predictive control, Perceived fidelity, Pre-positioning

Printed by: ProefschriftMaken

Cover Front & Back: Alysia-Lara Kitir

ISBN 978-94-6518-194-3

An electronic version of this dissertation is available at
http://repository.tudelft.nl/.

CONTENTS

SUMMARY

As mobility advances toward full automation, the role of the human within the vehicle is undergoing a profound transformation. Automated vehicles promise enhanced safety, increased convenience, and optimised traffic flow. Yet, these benefits introduce new challenges in user experience, chief among them is motion comfort. When passengers relinquish control and assume a passive role, conflicts between what is seen and what is expected become more prominent. This mismatch can lead to motion sickness and disengagement, and in more severe cases, undermine user acceptance and trust in automated systems.

This thesis confronts the motion sickness problem from both sides of the human-machine interaction. On one hand, it introduces a method for planning vehicle motion that inherently considers motion sickness-inducing stimuli. On the other, it proposes algorithms that ensure that driving simulators can deliver more immersive and perceptually accurate feedback, enabling both effective evaluation and real-world deployment of comfort-aware automated driving strategies.

In Chapter 2, the Motion Sickness Mitigating (MSM) Trajectory Planner is developed using a model-based optimal control framework, where motion sickness, quantified via the motion sickness dose value (MSDV) metric, is embedded directly in the cost function. Rather than optimising solely for traditional performance metrics such as travel time or energy efficiency, the approach integrates a human-centric discomfort metric into the planning process. This is achieved through a model-based optimal control framework that generates trajectories which are both dynamically feasible and better suited to reducing motion sickness.

Subjective evaluations demonstrated a reduction in motion sickness of over 65% among participants. However, this improvement came at the cost of a 50% increase in travel time. These results underscore an inherent trade-off in automated mobility: more comfortable trajectories may require longer durations, while faster trajectories can increase passenger discomfort. The findings highlight the potential for future trajectory planners to be adaptive, not only to traffic and environmental conditions, but also to individual user preferences or physiological states.

However, evaluating and tuning such comfort-aware planners requires tools capable of faithfully reproducing the specific forces experienced during real driving. This leads to the second core contribution of the thesis: the design of motion cueing algorithms (MCAs) for high-fidelity driving simulators. These systems must accurately replicate vehicle motion within the constraints of limited motion platforms, ensuring that the experience inside the simulator closely mimics that of the road. This fidelity is crucial when assessing human-centered metrics like motion sickness. Additionally, since the primary focus of this thesis is on automated driving, motion cueing strategies were specifically designed and implemented for passive driving cases where the driver becomes the passenger.

A central development in this domain is presented in Chapter 3, where the frequency-splitting MPC-based MCA is introduced. The proposed MCA decomposes the motion signal into frequency components, delivering low-frequency cues via tilt coordination, high-frequency cues through translational motion, and incorporating full vehicle accelerations to reconstruct the total specific force. By leveraging the predictive capabilities of the MPC framework, the frequency-splitting MCA improves cueing accuracy and constraint handling.

Compared to the widely used filter-based Adaptive Washout algorithm, the frequency-splitting MCA demonstrates significantly higher physical accuracy in reproducing specific forces. Subjective evaluations further confirm participants' preference for frequency-splitting MCA over Adaptive Washout.

However, a key perceptual limitation remains: pre-positioning, where anticipatory tilt movements occur before large accelerations. Although mathematically justified, often yielding a net-zero specific force, these motions can appear perceptually unnatural to human occupants, disrupting immersion and causing false cues.

To overcome this issue, a more refined control strategy, Autoscaling MCA, was developed in Chapter 4. This algorithm reduces the manual scenario-specific tuning effort by introducing a dynamic scaling mechanism that automatically adapts to the reference input. Crucially, it scales only the tilt-coordination component, prioritising motion reproduction via translational movement, which produces a more perceptually congruent experience (as accelerations in real vehicles are majorly translational). This innovation solves two problems in MPC-based motion cueing: it minimises pre-positioning artifacts and removes the burden of tuning scaling factors for different driving scenarios. The result is a more realistic, adaptable, and immersive simulation experience, crucial not only for user testing but also for driver training and vehicle development. Moreover, the computational efficiancy is further improved compared to the frequency-splitting MCA,

Returning to the primary goal of reducing motion sickness, Chapter 5 proposes a fundamental shift in motion cueing via the Subjective Vertical Conflict MCA (SVC-MCA), the first MCA to embed a predictive motion sickness model within an MPC framework. By simulating how the brain resolves discrepancies between visual and vestibular inputs, the algorithm proactively adjusts the simulator's motion to reduce predicted sickness. It introduces a tunable control balance between physical accuracy (specific force tracking) and motion sickness mitigation, enabling flexible operation across a wide range of simulator scenarios. This marks a fundamental shift in cueing philosophy—from merely replicating physical dynamics to intelligently accounting for human perception and comfort.

Objectively, the SVC-MCA algorithm demonstrated an effective trade-off between specific force fidelity and sickness reduction. Subjectively, user studies revealed significant reductions in reported motion sickness levels with marginal loss in realism or immersion. These results confirm that embedding perceptual models within the control loop can enhance comfort without compromising simulator effectiveness.

Yet, MPC-based MCAs are inherently computationally demanding, due to the complexity of optimising system dynamics in real time. To support real-time execution, Chapter 6 develops a Hybrid MPC framework that combines an offline-trained explicit

MPC component—using regression-based lookup tables—with an online implicit MPC solver. The explicit component provides a warm-start estimate, enabling the implicit MPC to converge more quickly. This hybrid approach balances model complexity with computational efficiency, improving the feasibility of deploying MCAs in operational simulators.

Across all of these efforts, from planning AV trajectories that respect human comfort to building simulator control systems that adapt to both physical and perceptual constraints, this thesis delivers a unified, perception-aware framework for reduced sickness in automated mobility. It makes the case that motion sickness is not merely a side effect to be tolerated, but a design constraint to be actively managed. By integrating knowledge from vehicle dynamics, control systems, and human perception, this research redefines how we think about comfort and control in the age of autonomy.

Ultimately, this thesis advocates for a new direction in automated vehicle design, one that moves beyond raw performance and embraces the complexity of human experience, encompassing the subjective dimensions of ride comfort, motion sickness, and perceptual coherence. It shows that with thoughtful modelling, clever control, and an emphasis on perception, we can design automated systems that are not only capable and efficient but also deeply comfortable and genuinely human-centred.

1

Introduction

Aim for the moon.
If you miss, you may hit a star.

William Clement Stone

Dream the impossible. Dream big.
You have to believe in yourself and work hard for your dreams.

Sir Lewis Hamilton

1

1.1. OVERVIEW

The advent of automated vehicles (AVs) is driving a major shift in the transportation landscape, with significant implications for safety, traffic efficiency, and cost reduction. Predictions indicate that by 2050, AVs could account for as much as 50% of all vehicle sales, signaling a fundamental change in how society perceives and utilizes transportation [1], [2]. This shift brings new opportunities but also presents challenges related to passenger comfort, particularly as more people transition to passive roles during travel. Among these, motion sickness (MS) emerges as a major impediment to the widespread acceptance and daily use of AVs.

Traditionally, MS has been an issue primarily associated with maritime and aerial transport. However, as AVs free occupants from the task of driving and offer opportunities to engage in non-driving activities while unable to view the external environment, the probability of MS increases significantly [3]. This is primarily due to the sensory mismatch between vestibular, visual, and proprioceptive cues, often exacerbated when passengers look at screens or read while in motion. As such, MS must be addressed not as a secondary concern but as a core design objective in AV systems.

In parallel, the advancement of AV technology requires extensive testing and validation, particularly regarding the interaction between automated systems and human passengers. Driving simulators are playing an increasingly important role in providing a safe, controlled environment for testing these systems, enabling engineers to evaluate performance and refine algorithms without the risks and costs of real-world trials. Yet, they too can induce discomfort through simulator sickness, stemming from visual-vestibular conflicts due to imperfect motion cueing. As simulation fidelity improves, the demand for more perceptually accurate and physiologically compatible motion cueing algorithms increases.

This thesis addresses the overarching challenge of motion sickness in the context of automated driving and simulation. It contributes to the body of knowledge by proposing control strategies that explicitly consider human discomfort, integrating physiological models into motion planning and cueing processes. The work bridges the domains of control systems, vehicle dynamics, human factors, and perceptual psychology, presenting a unified framework for sickness-free mobility.

1.1.1. AUTOMATED VEHICLES

Automated vehicles (AVs) are typically classified into six levels of automation as defined by the Society of Automotive Engineers (SAE) in the SAE J3016 standard. These levels describe the extent to which the vehicle's automated systems can control driving tasks, ranging from fully manual control by the driver to full autonomy. The levels are as follows:

- **Level 0** (No Driving Automation): The driver is entirely responsible for controlling the vehicle, with no automation support.
- **Level 1** (Driver Assistance): The vehicle may assist the driver with either steering or acceleration/braking, but not both at the same time. The driver remains fully engaged in the driving task. Examples include adaptive cruise control or lane-keeping assist.

- **Level 2** (Partial Driving Automation): The vehicle can take over acceleration, braking, and steering in specific conditions, but the driver must remain engaged and monitor the environment. Tesla's Autopilot [4] is an example of this level.
- **Level 3** (Conditional Driving Automation): The vehicle can handle all aspects of driving under certain conditions, including environmental monitoring, but the driver must be available to take over if necessary. Audi's Traffic Jam Pilot [5] is an example of Level 3.
- **Level 4** (High Driving Automation): These vehicles can fully control all driving tasks within specific conditions (e.g., designated geographical areas or weather conditions) without human intervention. Waymo's robotaxi is an example of Level 4 automation [6].
- **Level 5** (Full Driving Automation): The vehicle is fully autonomous, capable of handling all driving tasks in any environment, under any conditions, without human intervention. No such vehicle/system exists to date.

As automation levels increase, AVs offer passengers the opportunity to engage in non-driving tasks such as work or leisure, which could redefine societal expectations of comfort and productivity during travel [7]. However, this shift towards passive occupancy introduces challenges, particularly with regard to motion sickness. Passengers who focus on non-driving activities without a view of the external environment are at greater risk of experiencing MS, a problem that worsens as automation increases. To ensure widespread adoption of AVs, addressing these comfort-related challenges is essential.

1.1.2. MOTION SICKNESS

Motion sickness is a condition that can arise when an individual is exposed to motion, leading to a mismatch between the signals detected by the inner ear (vestibular system) and the expected sensory input based on prior experience. This discrepancy between perceived movement and expectation can trigger symptoms such as nausea, dizziness, headaches, and general discomfort. Motion sickness is commonly experienced in various modes of transportation, including cars, planes, boats, and trains, particularly when passengers are exposed to unfamiliar or irregular motion patterns.

The most widely accepted explanation for motion sickness is the sensory conflict theory, which posits that symptoms arise from a mismatch between the motion sensed by the body (via vestibular, visual, and proprioceptive systems) and the motion expected by the brain's internal models. This conflict can occur even in the absence of visual input, indicating that motion sickness is not solely due to visual-vestibular mismatch. It is especially prevalent during conditions involving unexpected accelerations or limited motion predictability.

Motion sickness manifests as discomfort and nausea when an individual is subjected to specific motion stimuli. The primary symptoms include nausea and vomiting, accompanied by objective signs such as retching, pallor, sweating, belching, yawning, and salivation. The aversive nature of motion sickness has been exploited historically, both as a form of punishment [8] and as a peculiar form of therapy [9].

There are several theories on how motion sickness is induced in humans. The most widely accepted explanation is the Sensory Conflict Theory [8], which indicates that motion sickness arises due to conflicts between different sensory systems: visual, vestibular, and non-vestibular proprioceptors. This conflict occurs when the perceived motion does not match the actual motion, triggering motion sickness. Hence, the condition arises when sensory information contradicts one's expectations based on past experiences. Another widely accepted theory is the Postural Instability Theory [10], which suggests that motion sickness symptoms occur when an individual has not yet adapted to postural instability, particularly in response to motion stimuli.

A third theory, the Eye Movement Theory, proposed by Ebenholtz [11], [12], attributes motion sickness to the stimulation of the vagus nerve due to specific eye movements (such as optokinetic nystagmus and vestibular ocular response). These eye movements cause tension in the eye muscles, which in turn stimulates the vagus nerve, resulting in motion sickness symptoms. However, studies, such as those by Irmak et al. [13], show that even blindfolded individuals exposed to motion stimuli experience motion sickness symptoms. This suggests that eye movements may exacerbate symptoms but are not the sole cause of motion sickness.

In the case of driving simulators, due to two different stimuli arrising from the visual cues and the motion of the platform, the case of motion sickness can be exacerbated and hence a higher chance of motion sickness development occurs. This is generally termed as simulator sickness.

1.1.3. DRIVING SIMULATORS

The development of automation technology in AVs requires extensive testing to ensure the systems are safe, reliable, and comfortable for passengers. Driving simulators play a pivotal role in this process by providing a controlled, crash-free environment where different driving scenarios can be replicated without the risks and costs associated with real-world trials. These simulators allow developers to evaluate the performance of automated systems, such as perception algorithms, control strategies, and user interfaces, while interacting with human users, under a wide variety of dynamic conditions.

One of the key advantages of simulators is their ability to replicate extreme or rare events that are difficult to test on real roads, thereby reducing risk while accelerating the development cycle. Additionally, simulators are invaluable for testing human factors, including how passengers interact with autonomous systems at varying levels of automation. This is crucial for understanding user behaviour and acceptance as AVs transition from semi-autonomous to fully autonomous systems.

Simulators also provide a potential tool for evaluating passenger comfort, particularly in terms of motion sickness. As AVs transition to higher levels of automation, passengers no longer need to focus on driving, which can lead to discomfort and MS. By using simulators, developers can test how different motion cues and control strategies influence MS symptoms in a safe and controlled environment. This allows for the identification and resolution of comfort-related issues before AVs are deployed on the road.

Moreover, simulators enable the validation of emerging automated driving technologies. These technologies need to be tested in a controlled virtual environment to ensure they are safe and reliable before being implemented in real-world vehicles. Beyond test-

ing the algorithms themselves, simulators also offer a means of evaluating human acceptance of these new technologies, which is critical for their successful deployment.

In summary, driving simulators are essential tools for advancing automated driving technology, allowing for safe testing, validation, and refinement of both the systems and human interactions with these systems. This thesis will explore how driving simulators can be used to address the challenges of motion sickness and improve the human acceptance of automated driving technologies, contributing to the broader goal of developing safe and comfortable AVs.

Driving simulators are increasingly integral to the development and validation of automated driving systems, especially in domains involving human perception, comfort, and motion sickness. Central to these simulators are Motion Cueing Algorithms (MCAs), which aim to replicate the forces experienced in real vehicles using limited physical motion. These algorithms blend platform translations and tilt-coordination to recreate high- and low-frequency vehicle accelerations respectively, ensuring that the induced specific force mimics real driving experiences without exceeding human perceptual thresholds for motion [14]–[16].

Filter-Based Approaches: Early MCAs relied on classical washout filters, which use high-pass and low-pass filtering to distribute specific force tracking between translation and tilt. These were later extended into adaptive washout filters, which dynamically scale reference signals based on workspace limits and motion perception mismatches [17], [18]. Collectively, these are known as filter-based MCAs.

Model Predictive Control (MPC)-Based Approaches: Recent advancements in simulator fidelity have been driven by MPC-based MCAs, which leverage predictive models and platform constraints to optimize motion cues [19]–[21]. These algorithms offer enhanced realism, especially for complex dynamic maneuvers. However, their computational complexity remains a key barrier for real-time applications. Strategies to mitigate this include:

- Linearised actuator models for reduced solver complexity [22].
- Explicit MPC approaches that pre-compute control policies and use them as look-up tables [23].
- Hybrid MPC frameworks combining explicit and implicit control for faster convergence [24].

Integration of Perception Models and Learning-Based Techniques MPCs have also been enhanced by integrating human perception models, allowing the algorithm to track perceived, rather than raw, vehicle accelerations [19], [20], [25]. This perceptual filtering further aligns motion cues with what humans actually experience.

Recent studies have explored parameter tuning via genetic algorithms [26], [27], as well as reinforcement learning (RL) techniques—including deep RL for direct control and RL-based horizon selection for faster convergence [28], [29]. Dynamic algorithm switching has also been proposed using sequential MCAs to adaptively choose the best algorithm for each situation [30].

Limitations and Gaps: While several studies have compared classical and MPC-based MCAs both objectively and subjectively [20], [25], [31], the focus has largely been on improving specific force fidelity. However, no existing work explicitly addresses simulator sickness mitigation as a design goal within the motion cueing algorithm.

Furthermore, a recent meta-analysis of simulator sickness studies indicates modest but significant sickness levels across simulator configurations. Notably, active driving in simulators tends to result in higher simulator sickness than passive driving, though this contrast is not observed in real vehicles, where passive occupants are more susceptible [32]. Studies comparing different motion cueing strategies found improved perceived fidelity with motion-enabled platforms but did not show corresponding reductions in sickness [33].

This thesis addresses this critical research gap by proposing and validating motion cueing strategies that explicitly target the reduction of simulator sickness, in addition to enhancing motion fidelity and computational efficiency. Additionally, since the primary focus of this thesis is on automated driving, motion cueing strategies were specifically designed and implemented for passive driving cases where the driver becomes the passenger—an aspect that has been largely overlooked in prior simulator fidelity research.

1.2. RESEARCH OBJECTIVES

The core objective of this thesis is to reduce motion sickness in both AVs and driving simulators through optimal control strategies. The specific research objectives include:

- **R1:** Developing trajectory planning algorithms for AVs that minimise motion sickness by optimising velocity and curvature profiles.
- **R2:** Designing motion cueing algorithms for simulators that balance motion fidelity, workspace limitations, and computational efficiency.
- **R3:** Integrating 6-DoF sensory conflict models into control frameworks to predict and reduce human discomfort in real-time.
- **R4:** Validating the effectiveness of these control strategies using both simulation tools and human-in-the-loop experiments.

1.3. STRUCTURE OF THE THESIS

This dissertation is organized into seven chapters, each building upon the previous to develop a comprehensive strategy for sickness-free automated mobility.

- In Chapter 1, the motivation, research challenges, and overall structure of the thesis are introduced.
- A trajectory planning framework based on nonlinear model predictive control is presented in Chapter 2, where motion sickness is reduced by minimising the motion sickness dose value (MSDV) during automated vehicle navigation. This chapter addresses research objective **R1**.

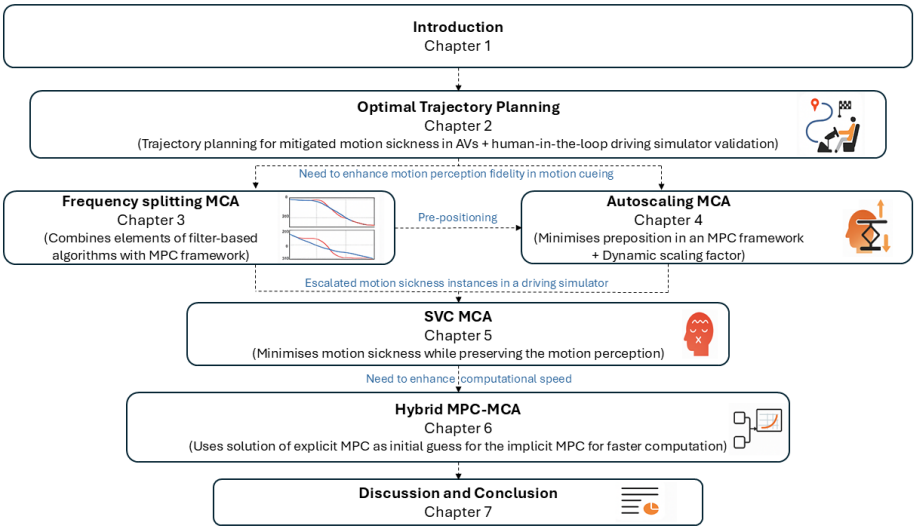

Figure 1.1: Structure of the Thesis

- In Chapter 3, motion perception in simulators is enhanced through a frequency-splitting MPC-based motion cueing algorithm that integrates filter-based techniques, enabling realistic cueing under platform constraints. This chapter addresses research objective **R2** and is further validated with human-in-the-loop experiments in a driving simulator, thereby also addressing research objective **R4**.

- Autoscaling MCA is proposed in Chapter 4, where perceptual accuracy is improved by minimising unnatural pre-positioning effects associated with tilt coordination. This chapter addresses research objective **R2** and, through validation with human driving simulator experiments, also addresses research objective **R4**.

- A perceptually motivated motion cueing strategy is developed in Chapter 5, incorporating a 6 DoF Subjective Vertical Conflict motion sickness model, within an MPC framework to actively minimise predicted simulator sickness. This chapter addresses research objective **R3** and, following algorithm development, is validated with human experiments in a driving simulator, thereby also addressing research objective **R4**.

- In Chapter 6, a hybrid motion cueing approach is introduced to improve the computational efficiency of MPC-based algorithms. While the methods in Chapter 2–5 rely on implicit MPC—effective for handling nonlinear systems but computationally demanding—the hybrid formulation combines explicit and implicit MPC, where the explicit solution is used as a warm-start for the implicit solver to enhance real-time applicability. This chapter addresses research objective **R2** by tackling the problem of computational expense within an MCA.

- In Chapter 7, the findings are synthesized, broader implications are discussed, and potential directions for future research and application are outlined.

Each chapter is validated through a combination of simulation and human subject studies, ensuring both technical soundness and practical relevance. An exception is Chapter 6, where simulation alone was sufficient to evaluate the computational performance of the proposed methods. The work concludes by emphasising the need for continued interdisciplinary collaboration to develop mobility systems that are not only intelligent but also comfortable, acceptable, and aligned with human physiology.

By centering motion sickness within the control design space, this thesis contributes a paradigm shift in automated transport—moving from performance-centric to human-centric design. The methodologies proposed have direct implications for AV deployment, simulator fidelity, and the broader field of human-centered mobility engineering.

1.4. SCIENTIFIC CONTRIBUTIONS

This thesis makes several novel contributions to the domains of trajectory planning and motion cueing for automated driving and driving simulators. The work spans algorithmic development, simulation-based validation, and human-in-the-loop experiments, resulting in both theoretical and practical insights. The scientific contributions per component of the thesis are as follows:

OPTIMAL TRAJECTORY PLANNING FOR MOTION COMFORT

- We use a standardised motion sickness dose value metric instead of solely minimising jerk, acceleration or both. At the same time, we not only consider this metric for the current prediction horizon, but also take into account travel time and the accumulation of sickness across the entire journey.
- To improve the accuracy, in addition, we use a non-linear bicycle model as the internal model for the optimal control problem, instead of the commonly used point mass model, which oversimplifies the dynamics of a real vehicle.
- We perform a first-ever human-in-the-loop experimental validation to subjectively validate an MS mitigation algorithm, using a moving-base driving simulator. Motion cueing parameters were selected to optimally transmit the sickening stimuli, resulting in close to full vibration transmission above 0.2 Hz. Results confirm the effectiveness of the proposed trajectory planning in reducing motion sickness.

FREQUENCY-SPLITTING MOTION CUEING ALGORITHM

- We developed a novel frequency-splitting algorithm that integrated elements of classical washout and model predictive control-based motion cueing, combining the strengths of both approaches within a single framework.
- We demonstrated through objective analysis that the proposed algorithm significantly outperformed conventional adaptive washout in specific force tracking, while also achieving higher computational efficiency than traditional MPC-based cueing algorithms.

- We conducted human-in-the-loop evaluations in an automated driving scenario, where participants clearly preferred the proposed algorithm compared to adaptive washout. In specific manoeuvres, the algorithm also effectively reduced the perception of false cues.

AUTOSCALING MOTION CUEING ALGORITHM

- Proposed a novel autoscaling strategy for model predictive control-based motion cueing, developed in response to the prepositioning issues observed in the frequency-splitting algorithm. This strategy dynamically scales the tilt contribution based on simulator constraints and human perceptual thresholds, improving motion fidelity by better aligning the onset of motion with visual cues.

- Eliminated the need for manual tuning of scaling factors for vehicle acceleration across driving scenarios by dynamically adjusting the acceleration magnitude, while maintaining motion realism and minimising undesirable pre-positioning.

- Improved immersion and adaptability of driving simulations by modifying the reference signal to comply with human perceptual thresholds, ensuring realistic motion without disrupting immersion.

SENSORY CONFLICT MODEL-BASED MOTION CUEING (SVC-MCA)

- Incorporated a six-degree-of-freedom Subjective Vertical Conflict motion sickness model, for the first time, directly into a motion cueing algorithm as part of its cost function.

- Formulated a multi-objective optimisation framework that jointly considers motion sickness reduction and reproduction of motion perception compared to real-world driving.

- We demonstrated that the inclusion of the motion sickness model allows for an adjustable trade-off between motion fidelity and predicted motion sickness, enabling the algorithm to prioritise either physical realism or passenger comfort based on application-specific requirements. The highest motion sickness reduction was predicted with negligible motion, and a compromise was found balancing fidelity and sickness.

- Conducted human-in-the-loop experiments confirming that the proposed algorithm effectively mitigates motion sickness symptoms, while having minimal impact on motion perception.

HYBRID MOTION CUEING ALGORITHM

- We proposed a hybrid motion cueing algorithm that integrates an explicit model predictive control formulation into an existing implicit MPC-based structure. While the other model predictive control-based cueing algorithms presented in this thesis are purely implicit, this hybrid approach significantly enhances computational efficiency without degrading specific force tracking performance.

- Demonstrated superior computational efficiency over state-of-the-art implicit model predictive control-based cueing algorithms in simulation scenarios representative of urban and highway driving.
- Established a foundation for future work which can extend the hybrid model predictive control approach to non-linear systems, offering a pathway to real-time deployment of human-centred optimised cueing algorithms.

2

OPTIMAL TRAJECTORY PLANNING FOR MITIGATED MOTION SICKNESS: SIMULATOR STUDY ASSESSMENT

You have to sacrifice something
in order to achieve something greater.

David Brooks

Trade-offs have always been a part of life.
The trick is in knowing which ones to make.

C. S. Lewis

This chapter is based on ***V. Jain***, *S. Kumar, G. Papaioannou, R. Happee and B. Shyrokau, "Optimal trajectory planning for mitigated motion sickness: Simulator study assessment." in IEEE Transactions on Intelligent Transportation Systems 24, no. 10 (2023): 10653-10664.[34].*

2

ABSTRACT

In the transition from partial to high automation, occupants will no longer be actively involved in driving. This will allow the use of travel time for work or leisure, where high comfort levels preventing motion sickness are required. In this paper, an optimal trajectory planning algorithm is presented in order to minimise motion sickness in automated vehicles. A predefined path is provided as an input to the algorithm, to generate an optimal path with limited lateral deviation and the corresponding optimal velocity profile, for the minimisation of motion sickness. An optimal control problem is formulated with a cost function combining both motion sickness and travel time. For a sickening curvy road, the algorithm reduced the motion sickness dose value (MSDV) up to 52% depending on the allowed lateral deviation and the weighting on travel time. The efficacy of the proposed algorithm has been evaluated via human-in-the-loop experiments using a moving-base driving simulator. Motion cueing parameters were selected to optimally transmit the sickening stimuli resulting in close to full vibration transmission above 0.2 Hz. During the experiment, the participants were asked to rate their experience based on the standard MIsery SCore ratings. According to these, sickness levels were reduced on average by 65% with reduced motion sickness in all 16 participants.

2.1. INTRODUCTION

AUTOMATED vehicles (AVs) are projected to be safer than manual driving, efficient in terms of traffic flow and cheaper in the cost of transportation [1]. In fact, by 2050, AVs are predicted to have a market share of about 50% of all on-road vehicle sales [2]. The wide adoption of this disruptive innovation could create a massive impact on public mobility. With higher automation levels, the occupants are not required to be actively involved in driving. This will enable the productive use of travel time for work or leisure [7], an appeal that is a major driving force behind the adoption of AVs by the public [35]. However, when using the time inside the vehicle for non-driving tasks, where there is limited awareness about the surrounding of the AV, the ride experience and comfort for the passengers will deteriorate, making them more prone to motion sickness (MS) [3]. Hence, high levels of comfort should be achieved within AVs, preventing MS and excessive body motion, both of which can lead to discomfort. In this direction, the "AV driving style" should not only be carefully designed, but also experimentally tested to check the comfort perceived by occupants, when exposed to this driving style.

This work aims to reduce sickening stimuli by planning the vehicle motion around a predefined path, using optimal control, and thus mitigating its sickening effects on passengers in automated vehicles. While generating an optimal path that is more suitable for mitigating MS, the algorithm also searches the optimal velocities for different sections of the path as well as deceleration and acceleration profiles negotiating curves. The effectiveness of the proposed algorithm in reducing MS has been assessed via human-in-the-loop experiments. The occupants of an AV are expected to be involved in non-driving tasks, without the visual awareness of the surrounding environment. Therefore, in the conducted experiment, the participants performed a non-driving task in absence of visual cues related to the road. This ensures participants' exposure to an environment similar to that of an AV and eliminates any additional sickening effects of the sensory conflicts arising through visual cues.

The contributions of the paper are as follows:

- We use a non-linear bicycle model as the internal model for the optimal control problem (OCP), instead of the commonly used point mass model which oversimplifies the dynamics of a real vehicle.
- We use a standardized motion sickness metric (MSDV) instead of solely minimising jerk, acceleration or both. At the same time, we not only consider this metric for the current prediction horizon, but also take into account travel time and the accumulation of sickness across the entire journey.
- We perform a first ever human-in-the-loop experimental validation to subjectively validate an MS mitigation algorithm, using a moving-base driving simulator. Motion cueing parameters were selected to optimally transmit the sickening stimuli resulting in close to full vibration transmission above 0.2 Hz. Results confirm the effectiveness of the proposed trajectory planning in reducing motion sickness.

The chapter is organized as follows: Section 2.2 discusses the existing works in the domain of driving comfort and MS reduction; Section 2.3 provides the details of the pro-

posed algorithm and formulates the optimal control problem (OCP); section 2.4 presents the experiment design for the validation of the proposed algorithm; Section 2.5 illustrates the results of the experiments; then, Section 2.6 follows, where the results are analysed and their significance is discussed; finally, conclusions are extracted in Section 2.7.

2.2. EXISTING STUDIES

Various geometric, constraint and optimisation-based motion control methods have been investigated to enhance occupants' comfort in automated driving [36]. Geometric-based and heuristic-based methods mainly address path generation, while optimal control-oriented methods focus on generation of a feasible trajectory, by assigning a velocity profile over a pre-defined path.

Geometrical methods employ clothoids, bezier curves, and others to generate a smooth path or to smooth an existing one [37]–[39]. In addition to the design of the path, quintic bezier curves have been used to assure smooth and continuous velocity and acceleration profiles [40]. Constraint-based methods set upper comfort limits to acceleration and jerk [41], while iterative numerical methods that restrict vehicle acceleration and jerk within a comfortable range have also been explored [42]. The restrictions are set according to comfort limits. Then, the solution is searched for the vehicle to have the maximum allowable jerk according to the comfort range. This search runs in a loop, where if the solution fails or is unachievable, the jerk values are reduced and a new search starts until a feasible solution is achieved. Numerical iterative methods for minimum time velocity planning utilize the upper limits of the defined jerk range to obtain minimum travel time [43]. However, constraint-based methods predominantly work in the defined upper limits to plan the motion, which may lead to accumulated discomfort over long periods.

Although the restriction of jerk and acceleration, using numerical methods, demonstrates positive effects on motion comfort, a more common approach is the use of optimisation for motion planning. By applying cost functions for the translation of vehicle motion to perceived comfort, higher levels of comfort can be obtained in comparison to methods only constraining acceleration, velocity, and jerk. Motion planning has been conducted minimising the lateral and longitudinal accelerations using optimisation [44]. The addition of journey time in the cost function, to make the algorithm time efficient and comfortable has also been explored [45]. Trajectory planning has also been conducted using a combination of jerk, acceleration, and travel time as the cost function to be minimised [46]. Additionally, velocity and yaw rate inclusion in the cost function has been analysed [47]. Moreover, several studies explore combinations of the above-mentioned strategies, to achieve a more comfortable ride. Optimisation over a smooth path for the planning of vehicle motion has been investigated using geometric curves [48], [49]. Where a path is first smoothed using quintic bezier curves, an optimal velocity planning is then run over this path. These studies focus on motion comfort through minimisation of acceleration and jerk over a wide frequency range. To address motion sickness, low-frequency motion requires particular attention and different approaches have been considered.

Emphasising MS mitigation, use of vibrational cueing in the seat, to generate anticipation of the future motion of the vehicle, has been explored [50]. Vibrational cues resulted in lower MS levels for the participants of the study. However, no MS model

was involved in this work. Only a few studies use MS models to plan vehicle motion. A vehicle-following algorithm has been designed, which minimises the sensory conflict obtained through the 6-DoF Subjective Vertical Conflict model [51]. The use of optimisation to obtain velocity profiles to reduce MS is explored [52]. The effectiveness of MS mitigation was gauged numerically, comparing the respective motion sickness incidence (MSI) obtained using different cost functions. The results showed that adaptive MS cost was the most effective in MS mitigation; however, acceleration cost showed very similar results, with a significantly lower computational expense. This indicates that the acceleration cost is a promising candidate for MS mitigation. However, in this study, the lateral dynamics were simplified using a point mass vehicle model. The model only considered longitudinal jerk as the input, the lateral accelerations were calculated using longitudinal velocity and road curvature. Similarly, an optimal velocity profiling architecture using optimal control-oriented methods is proposed using Motion Sickness Dose Value (MSDV) as a cost function for minimisation [53]. Such an approach allowed deviation of the vehicle from the predefined path and showed substantial MSDV reduction when more lateral deviation is allowed. However, the adopted point mass model does not accurately represent the dynamics of a real vehicle, and thus the algorithm may provide sub-optimal results. A frequency-shaping approach to motion planning has also been proposed, which uses frequency-weighted MSDV as a cost function in the OCP framework [54]. This approach reduced acceleration in the frequency range which provokes motion sickness to the occupants. However, the effectiveness of the algorithm wasn't confirmed using any human-in-the-loop experiment. Moreover, the vehicle model was highly simplified. At the same time, the journey time was not included in the cost function, and the motion planner could conclude in long rides that can decrease the occupant's satisfaction. Our proposed algorithm considers a more sophisticated vehicle model, which allows the algorithm to look for a more suitable path for mitigating MS. The algorithm also considers journey time minimisation along with MSDV to reach the destination within a desirable time, illustrating the trade-off between comfort and travel time. Additionally, our study involved human-in-the-loop driving simulator experiments, which demonstrated the effectiveness of the algorithm in mitigating MS. Motion sickness modelling is known to require objective measures capturing low-frequency motion and representing sickness accumulation over longer time periods [13]. This work accounts for the accumulation of motion sickness over longer periods. This is achieved by optimizing motion over the shifting-control horizon window N_c, using the current MSDV as an initial state representing MS accumulation due to past motion. Finally, results are presented recalculating MSDV over the entire trip. Furthermore, to the best of authors' knowledge, the proposed algorithms to date have been analysed only via simulation. However, human beings are differently susceptible to motion sickness, and no single metric represents this individuality accurately and hence can't effectively evaluate the efficacy of such algorithms in mitigating motion sickness. Therefore, experimental validation with human participants was performed, using a driving simulator.

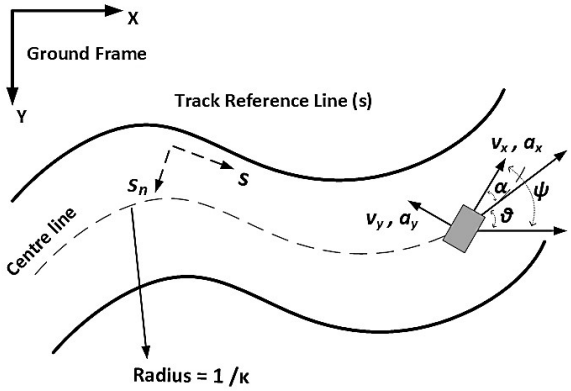

Figure 2.1: Depiction of the vehicle on the road

2.3. OPTIMAL CONTROL STRATEGY

This section describes our novel AV trajectory planning algorithm for MS mitigation. The problem is defined as an OCP applied to driving on a predefined path without other road users. The cost functions are considered to represent MS accumulation and journey time. Constraints secure the feasibility of the optimal solutions.

2.3.1. VEHICLE MODEL

A 3-DOF nonlinear bicycle model with linear tyre model is used to represent the vehicle dynamics. The modeling equations are given in vehicle's frame of reference. Figure 2.1 depicts the variable nomenclature used in the modeling. The vehicular accelerations (a_x and a_y), and yaw rate (r) are defined as:

$$\dot{v}_x = a_x + v_y r \tag{2.1}$$

$$\dot{v}_y = -\left(\frac{C_{\alpha f} + C_{\alpha r}}{m v_x}\right) v_y + \left(\frac{l_r C_{\alpha r} - l_f C_{\alpha f}}{m v_x} - v_x\right) r + \frac{C_{\alpha f}}{m}\delta \tag{2.2}$$

$$\dot{r} = \left(\frac{l_r C_{\alpha r} - l_f C_{\alpha f}}{I_z v_x}\right) v_y \tag{2.3}$$

where v_x and v_y are the longitudinal and lateral velocities respectively; δ is the road wheel angle; $C_{\alpha f}$ and $C_{\alpha r}$ are the front and rear cornering stiffness respectively; m is the mass of the vehicle; I_z is the inertia moment of vehicle about vertical axis; l_f and l_r are the distances of the vehicle centre of gravity from the front and the rear axles, respectively.

The road is defined using curvilinear coordinates. The road co-ordinates and the road heading angle θ are described by:

$$\frac{dx}{ds} = cos\theta; \quad \frac{dy}{ds} = sin\theta; \quad \frac{d\theta}{ds} = \kappa(s); \tag{2.4}$$

where κ is the road curvature. Additionally, the distance covered by the vehicle (s), the lateral deviation of the vehicle from the lane center (s_n) and the deviation of the vehicle heading angle from the road heading angle ($\alpha = \psi - \theta$) are given as:

$$\dot{s} = \frac{v_x cos\alpha - v_y sin\alpha}{1 - s_n \kappa(s)} \tag{2.5}$$

$$\dot{s_n} = v_x sin\alpha + v_y cos\alpha \tag{2.6}$$

$$\dot{\alpha} = r - \dot{s}\kappa(s) \tag{2.7}$$

2.3.2. OPTIMAL CONTROL PROBLEM

The problem is to find a reference trajectory for the vehicle to follow. It is assumed that the vehicle shall approximately follow a predefined path from an initial position (s_0) to a final position (s_f). As objective a weighted combination of MS metric and travel time is considered, to reduce the sickening effect of the ride and incorporate time efficiency as well.

MOTION SICKNESS METRIC

MSDV is a metric quantifying motion sickening accumulation in time as defined in ISO 2631 standard [55]. This metric accounts for the frequency related sickening stimuli by weighting the acceleration for different frequency ranges, as MS depends on the frequency of motion an individual is subjected to [56]. The metric is defined as:

$$MSDV = \sqrt{\int_0^T [a_{x,w}(t)]^2 dt} + \sqrt{\int_0^T [a_{y,w}(t)]^2 dt} \tag{2.8}$$

where $a_{x,w}(t)$ and $a_{y,w}(t)$ are frequency weighted accelerations in longitudinal and lateral directions in time domain; t, dt is the time increment, and T is the exposure time. The weighting curve constitutes of a 0.02-0.63 Hz bandpass filter based on [57]. The weightings for the longitudinal and lateral acceleration are assumed to be the same in this study, as there is no clear guideline in the literature for the longitudinal filters.

COST FUNCTION

The cost function for the prediction horizon is given by:

$$J_c = \sum_{i=0}^{N_c} w_m MSDV_i + w_t T_i \tag{2.9}$$

where w_m and w_t are the weighting coefficients for MSDV and travel time respectively, and N_c is the length of the prediction horizon.

As travel time is one of the criteria to be minimised, the problem is solved in space domain instead of time domain. The whole state space is converted from time domain to space domain using the relation given in Equation 2.10.

$$\frac{dp}{ds} = p' = \frac{dp}{dt}\frac{dt}{ds} = \dot{p}\dot{s}^{-1} \tag{2.10}$$

where p is the time dependent variable represented in space domain instead of time. Thus the OCP horizon is expressed in distance instead of time.

The travel time can be represented as:

$$T = \int_0^T dt = \int_{s_0}^{s_f} \frac{dt}{ds} ds = \int_{s_0}^{s_f} \dot{s}^{-1} ds \tag{2.11}$$

For the dynamics of the problem as defined in Subsection 2.3.1, the feasibility and continuity of the acceleration and road wheel angle should be considered. Thus, their time derivatives i.e. jerk, J_x and rate of road wheel angle, d_δ, are chosen as the control inputs. Hence, the vehicle model is described as:

$$x'_v = f_v(x_v, u) \tag{2.12}$$

where $x_v = [v_x \ v_y \ r \ s_n \ \alpha \ a_x \ \delta]^T$ are the vehicle states, and $u = [J_x \ d_\delta]$ are the control inputs.

The constraints on the state s_n are kept non zero allowing some deviation from the predefined path (lane centre line) to obtain a further reduction in MS levels. Along with the constraints on the states of the vehicle model, an additional constraint representing the friction circle is added to the problem, to ensure that the vehicle remains in its functional limits. The friction circle defines the maximum acceleration that the vehicle can attain due to limited friction between road and the tyre. This constraint is defined as :

$$\sqrt{a_x^2 + a_y^2} \leq \mu m g \tag{2.13}$$

where μ is the road friction coefficient and g is the acceleration due to gravity.

The OCP is formulated as:

$$\min_{u \in U} \quad J_c \tag{2.14}$$

$$s.t. \quad x'_v = f_v(x_v, u) \tag{2.15}$$

$$\phi(x_v, u) \leq 0 \tag{2.16}$$

$$b\left(x(s_0), x\left(s_f\right)\right) = 0 \tag{2.17}$$

The dynamics of the system are represented in Equation 2.15 using equality constraints, defined by the function f_v. The parameter ϕ in Equation 2.16 defines/represents the constraints on the vehicle limits (acceleration, velocities, etc.) including the friction circle constraint represented in Equation 2.13. Lastly, function $b(x(s_0), x(s_f)))$ in Equation 2.17 defines/represents the boundary conditions for the vehicle i.e. the initial states and the final states of the vehicle.

The optimal driving style obtained by the algorithm will hereon be referred to as '*Motion sickness mitigation drive*' (MSM drive).

The optimisation is conducted with the ForcesPro solver [58], using sequential quadratic programming. The optimisation was run for the whole road but due to the long length of the road, a sliding window (where the optimisation is solved as smaller OCPs, sliding the prediction horizon forward by a defined number of steps over the complete horizon) has been applied to reduce the computational load on the solver. The

detailed settings can be referred to in Appendix A.4. The shifting-control horizon window N_c was chosen to be 100 steps (100 m) to reduce the computation time. It should be emphasised that as a sliding window approach has been used, MSDV is added as a state during the optimisation. This allows us to initialise MSDV with its current value, which ensures that accumulation of the sickness dose over the entire journey is considered. The number of solver iterations is chosen to be 2000, to ensure convergence and avoid sub-optimal solutions. The optimisation has been performed on Intel(R) Xeon(R) W-2223 CPU @3.60GHz with 32GB RAM.

With the above-mentioned settings, the computation time for the algorithm is reported. The time taken for the algorithm to arrive at a solution varies based on the complexity of the road and the initial guess provided to the algorithm. To analyse the effect of the length of the shifting-control horizon, simulations were conducted considering 100, 150, 200 and 250 steps as prediction horizon respectively (for even larger horizons ForcesPro failed to converge). The simulations were conducted for a reduced drive with a length of 500 steps, keeping all the conditions apart from the prediction horizon the same. The obtained results are presented in Figure 2.2.

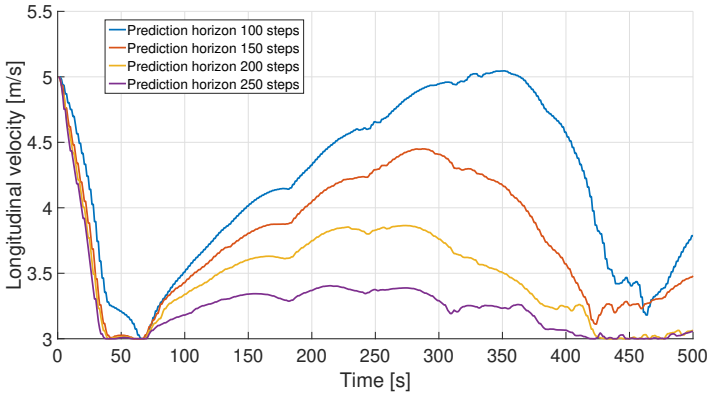

Figure 2.2: Velocity profiles for horizon lengths of 100, 150, 200 and 250 steps respectively

Comparing the different horizons, a similar trend in acceleration and deceleration is observed, however, there is a difference in the resultant velocity profile. This behaviour aligns with the expectation. For a smaller prediction horizon, the algorithm takes more aggressive actions due to the lack of information about the future. The obtained travel time and MSDV at the end of the 500 m (500 step) journey, along with the time taken for the OCP solution is reported in Table 2.1

Table 2.1: Obtained travel time, MSDV and the computation time for different prediction horizon lengths

Prediction horizon	Travel time [s]	MSDV [m/s$^{1.5}$]	Computation time [s]
100 steps	122	6.97	39
150 steps	133	6.00	54
200 steps	144	5.58	69
250 steps	154	5.47	79

This indicates that reducing the size of the prediction horizon makes the solution much faster. Thus a smart choice of prediction horizon should be made for obtaining desired MS reduction and at the same time keeping the algorithm computationally inexpensive.

As can be observed from Table I, using the above-mentioned PC configuration, for a 122 second simulation the algorithm takes a simulation time of 39 seconds. This corresponds to a real-time factor of 0.32. Thus, the algorithm is real-time implementable, as it takes less computation time than the real-time factor permits.

The pseudo-code for the OCP is presented in Algorithm 1:

Algorithm 1 NL-OCP for MSM drive

choose $s_0 = 0, s_f = end\ distance$
Input: $\mathbf{x}_0, \mathbf{x}^{\text{guess}}, \mathbf{u}^{\text{guess}}, w_m, w_t, s_0, s_f, \kappa(s) \forall s_0 \rightarrow s_f$
  while $k + N_c \leq s_f$ **do**
    $\forall\ k \rightarrow k + N_c$
    Calculate: cost function using Equation 2.8
    Solve: OCP using Equations 2.14-2.17
    Find: $u_{opt}\ \underset{u}{minimise}\ J$
    Calculate: $\mathbf{x}(k \rightarrow k + N_c)$ with u_{opt} with Equation 2.12
    Update: $\mathbf{x}_0$=$\mathbf{x}$, $\mathbf{x}^{\text{guess}}$, $\mathbf{u}^{\text{guess}}$
    Shifting window: $k = k + 1$
  end while
Return NL-OCP solution : states and control inputs ($\mathbf{x}$,$\mathbf{u}$) **Display** v_x, a_x, a_y, s_n, MSDV, travel time for MSM drive

2.4. EXPERIMENT DESIGN

To assess the efficacy of the trajectory planning algorithm in reducing MS, experiments need to be performed to subjectively assess the occupants' MS levels. In this direction, a driving simulator is employed and human participants are tested regarding the accumulated MS levels using different driving styles. This section entails the design of the experiment and presents the justification for using the selected settings.

2.4.1. APPARATUS

DRIVING SIMULATOR

Delft Advanced Vehicle Simulator (DAVSi, Figure 2.3) is used for assessing the effectiveness of optimal trajectories obtained from the proposed algorithm, in the mitigation of motion sickness via human-in-the-loop experiments. DAVSi is a 6-DoF motion platform driving simulator [20], capable of generating acceleration up to 1 g in all directions and can simulate motions in the wide frequency range up to 10 Hz. The half-car Toyota Yaris mock-up with a controllable interface via CAN (levers, buttons, air-con, etc.) is used and extended by the control loading system to provide haptic feedback. The simulator is operated in hard real-time using a dSPACE Scalexio system.

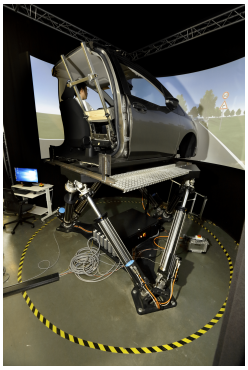

Figure 2.3: Delft Advanced Vehicle Simulator

A high-fidelity vehicle model in IPG CarMaker is used to simulate the optimal solutions obtained from the algorithm. The high-fidelity vehicle model, which is the digital twin of the Toyota Yaris, was parameterized using mass-inertia parameters obtained from a vehicle inertia measuring facility. The suspension kinematics and compliance were measured on a Kinematics and Compliance test rig for wheel suspension characterization, and finally, validated using field tests by Toyota.

2.4.2. DRIVING SCENARIO

To investigate the sickness of the participants within a limited time of 45 min, an accelerated sickening road path is designed providing high magnitude sickening stimuli. The design of this road path can be found in Appendix A.1. The path consists of abundant curves and corners eliciting sickening lateral accelerations within the curvy sections. Along with the lateral acceleration, the vehicle also decelerates before the curve and accelerates after exiting the curve. This reduces lateral acceleration, but increases longitudinal sickening stimuli. The sickening path is designed with a limited lateral displacement to better (but not completely) fit the motion range of the driving simulator.

In the OCP described in Section 2.3, the desired path is defined using its curvilinear co-ordinates, distance and curvature. Additionally, the operational driving limits were restricted to comply with highway driving. Along with these driving limits, several constraints related to comfort and actuators were introduced (Table 2.2). Limits on lateral

deviation were defined to offer the vehicle lateral maneuverability and help the algorithm to find a better path for MS mitigation, while staying within the road boundaries.

Table 2.2: Motion & actuators constraints

Quantity	**Lower limit**	**Upper limit**
Longitudinal velocity (v_x)	3 m/s	40 m/s
Longitudinal acceleration (a_x)	$-1.5\,\mathrm{m/s^2}$	$1.5\,\mathrm{m/s^2}$
Lateral acceleration (a_y)	$-4\,\mathrm{m/s^2}$	$4\,\mathrm{m/s^2}$
Longitudinal jerk (J_x)	$-1\,\mathrm{m/s^3}$	$1\,\mathrm{m/s^3}$
Deviation from road centre line (s_n)	−2 m	2 m
Rate of road wheel angle (d_δ)	−0.22 rad/s	0.22 rad/s
Road wheel angle (δ)	−0.52 rad	0.52 rad
Yaw rate (r)	−0.1 rad/s	0.1 rad/s

The travel time and the MSDV vary with the change in weights on their cost terms, w_m and w_t. Considering the restriction on experiment duration of 45 min, the trade-off between the accumulated MSDV over the journey, and the distance travelled was analysed for different configurations of the ratio w_m/w_t (see Figure 2.4). As the solution remains invariant when both weights w_m and w_t are scaled with the same factor, only the ratio w_m/w_t affects the results. Based on Figure 2.4, an increase in the distance travelled results in high MSDV. Since every individual is differently susceptible towards MS [59], there are no unique settings suitable for all passengers. Different settings can be used in accordance with the occupant's preference. In this study, we further selected settings represented by the larger black dot in Figure 2.4 which results in around 60% reduction of MSDV, when compared to the least MS mitigating setting (red dot in Figure 2.4) from the simulated cases. The selected settings resulted in an MSDV of $34\,\mathrm{m/s^{1.5}}$ and travel distance of 16.7 km. This setting was chosen for the MSM drive in the following analysis.

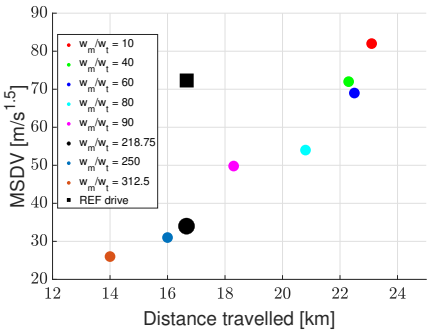

Figure 2.4: Effect of OCP cost function weight factor on MSDV and travel distance. Dots represent OCP results where the large black dot represents the selected MSM drive. The square represents the more aggressive reference drive.

2.4.3. REFERENCE DRIVING STYLE

To compare the effectiveness of the proposed algorithm in reduction of MS, a benchmark case has been defined based on the driver model used in IPG CarMaker [60]. For the longitudinal control, the artificial driver model (aggressive driving with a speed limit of 40 m/s) is used, coupled with path-following lateral control. From here on, the benchmark algorithm will be referred to as '*reference automation drive*' (REF drive). The acceleration limits are kept the same as in the MSM drive, to create a dynamic yet not overly aggressive driving style.

The resultant MSDV for the REF case is 72.7 m/s^2, which is higher than the selected settings for MSM drive, but 12% lower when compared to the least MS mitigating setting (red dot in Figure 2.4) from the simulated cases. The REF drive is also 1.5 times faster in completing the journey.

2.4.4. MOTION CUEING TUNING

The moving-base simulator has a limited workspace envelope. Therefore, a motion cueing algorithm (MCA) is adopted and the MCA parameters were tuned to utilise the workspace of the simulator as much as possible, but at the same time ensuring that the workspace limits are not violated. Maximum utilisation of simulator workspace results in a higher motion range and corresponding motion sickening stimuli. To that end, an adaptive washout filter was used for motion cueing; as this filter is known to be more effective in terms of reducing false cueing [61]. Various gains and cut-off frequencies for fore-aft and sway motion have been explored to maximise workspace utilisation and to obtain the maximum sickening stimuli (Table 2.3). According to Table 2.3, with setting 3, the simulator realises the highest MSDV of 17.1 which is around 50% of the MSDV resulting from the actual vehicle acceleration. However, setting 3 obtains a much higher MSDV as compared to setting 6 which applies a quite common 50% motion scaling allowing a larger motion bandwidth. In both REF drive and MSM drive, the same motion cueing parameters are adopted for a uniform comparison.

Table 2.3: Motion cueing parameters

Setting	**Cut-off frequency** (rad/s)	**Gain**	**MSDV**
1	2	0.9	12.1
2	1	0.9	15.54
3	1	1	17.1
4	0.5	0.8	15.4
5	0.4	0.5	16.2
6	0.5	0.5	10.4

To verify the simulator capability for recreation of the desired accelerations, power spectral analysis of the accelerations was performed (Figure 2.6 and Figure 2.7). According to Figure 2.6, the longitudinal acceleration power spectra for the virtual vehicle and the driving simulator overlap after 0.25 Hz. Similarly, based on Figure 2.7, the lateral

acceleration power spectrum for the simulator and the virtual vehicle are fairly close beyond 0.2 Hz. Based on these figures, motions beyond 0.2 Hz are sufficiently replicated with the selected motion cueing algorithm parameters.

2.4.5. EXPERIMENTAL PROCEDURE

Figure 2.5: Participant performing the non-driving task in the simulator

All participants gave informed consent before participation. The Human Research Ethics Committee of TU Delft, Netherlands approved the experiment protocol under application number 1675.

In total, 16 participants from the pool of students and employees of TU Delft participated in the study (mean age: 24.9, std: 1.61 years, 1 female, 15 males). All participants were subjected to both MSM and REF drive. To avoid habituation [62] to the simulator motions, there was at least a week's gap between the two sessions for any participant. Additionally, for the same reason, half the participants were subjected to the MSM drive first and the rest to the REF drive first. Before the initiation of the experiment, the participants were given a safety briefing, which was then followed by the motion sickness susceptibility questionnaire (MSSQ). This questionnaire gives information on the susceptibility of an individual towards getting motion sick. Two-way communication between the researchers and the participants was established via bluetooth headphones and microphones. Although the participants were not intended to reach retching, sick bags were positioned within easy reach. The participants were also instructed to not consume food at least two hours before the experiment.

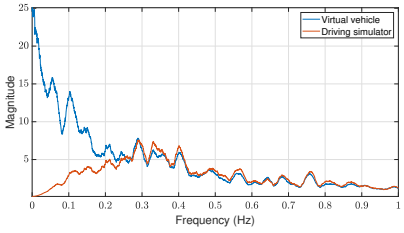

Figure 2.6: Longitudinal acceleration in the virtual vehicle and the driving simulator for MSM drive

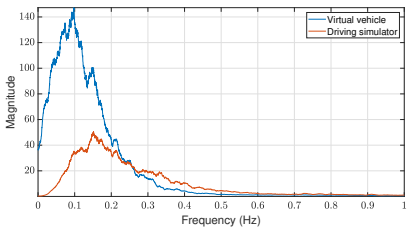

Figure 2.7: Lateral acceleration in the virtual vehicle and the driving simulator for MSM drive

As soon as the participants were ready to start the experiment, they were driven in

fully automated mode for 45 min in case of MSM drive and 30 min in case of REF drive. The distance travelled in both drive cases was kept constant (16.7 km), resulting in a longer duration for the MSM drive, enabling a fair comparison between the accumulated sickness over the trip for the two driving styles. During the driving session, the participants performed a non-driving task, answering a simple yes/no question quiz on a tablet. During the non-driving activity, the participants were instructed to place the tablet in front of them, around chest level, while operating it (see Figure 2.5). They were also asked to not look out of the simulator, resulting in 'internal vision' (eyes-off-the-road), which is a representative scenario for automated driving.

During the experiment, sickness ratings were queried based on the 11-point subjective MIsery SCale (MISC) [63] in 30 s intervals and their verbal responses were recorded. If the participant reached a MISC level of 6, the experiment was terminated, because this level corresponds to the inception of slight nausea and is deemed an appropriate threshold as observed in pilot runs. Upon the completion of an experimental session, the participants filled out the Motion Sickness Assessment Questionnaire (MSAQ). In this questionnaire, the participant rated the severity of experienced symptoms of MS in detail, at the end of the experimental session.

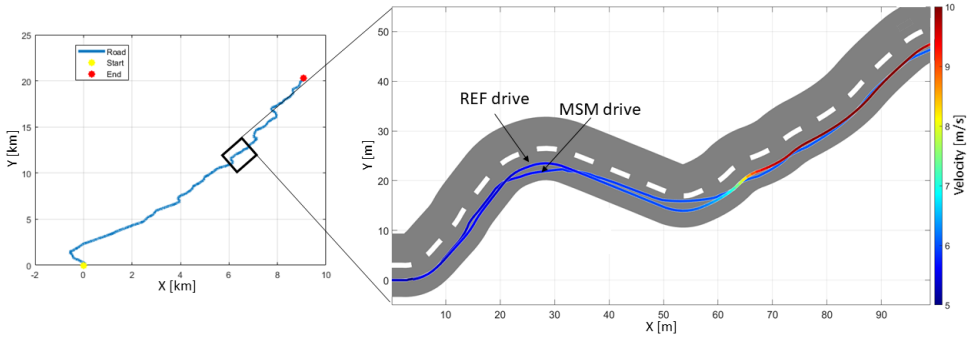

Figure 2.8: Trajectories of MSM drive and REF drive for a small section of the path

2.5. RESULTS

2.5.1. OPTIMAL TRAJECTORY PLANNING

VELOCITY AND PATH PROFILE

The optimal velocity and path for a small section of the path is presented in Figure 2.8. According to the figure, the velocity for the displayed part of the path ranges from 5 m/s to 10 m/s, and between 5 m/s and 6 m/s for the REF drive and the MSM drive, respectively. Similarly, for the entire journey (road path), the velocity ranges from 5 m/s to 22 m/s, and between 3 m/s and 10 m/s for the REF drive and the MSM drive, respectively. The REF drive executes a limited reduction in its velocity while approaching the corners. Whereas, in case of MSM drive, the vehicle slows down to velocities near 3 m/s (lowest allowed velocity). Moreover, the MSM drive does not follow the center-line of the path and cuts the corners within the selected limits, to reduce the lateral acceleration.

This driving behavior provides a more suitable path for reducing the motion sickening stimuli.

ACCELERATION

The G-G diagram obtained from the simulation is presented in Figure 2.9. The blue and the red dots depict the acceleration achieved through the REF and the MSM drive, respectively. Based on the figure, higher longitudinal accelerations are achieved in the REF drive, whereas the lateral acceleration ranges are similar in both drives. Furthermore, Figure 2.9 shows that higher accelerations have a lower occurrence in the MSM drive rather than in the REF drive. Occasionally the defined acceleration constraints are violated in the MSM drive. The latter occurs as the optimal solution is obtained using a 3-DOF vehicle model, but the G-G diagram is extracted after simulating the optimal solution with a high-fidelity vehicle model. Due to the low occurrence of high amplitude accelerations, the MSDV obtained for the MSM drive is 34 $m/s^{1.5}$, whereas the MSDV obtained for the REF drive is 72.7 $m/s^{1.5}$. This indicates a significant decrease in motion sickening stimuli.

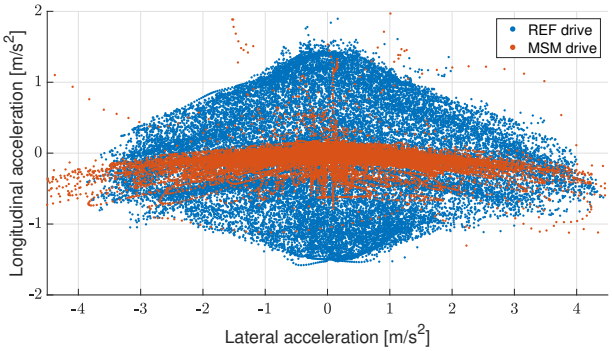

Figure 2.9: G-G diagram of the virtual vehicle acceleration achieved for REF and MSM drive

LATERAL DEVIATION

The proposed algorithm was analyzed for the effect of allowed lateral deviation from the road lane centre. The cases considered were from 0.5 to 2 m with steps of 0.5 m. No values lower than 0.5 m were considered, as constraining the lateral deviation to a lower value resulted in infeasible optimisation at some stages (horizons of the sliding window). A possible reason for this occurrence is the complexity of the path, for which the solver could not converge to a feasible solution that follows the path without violating the constraints.

According to Table 2.4, when the allowed lateral deviation was increased, the MSDV through the whole path reduced. Moreover, the travel time reduced with increased lateral deviation; as corner cutting allows the vehicle to continue at slightly higher velocities (as the lateral accelerations reduce with corner cutting) and also reduces the actual overall distance travelled marginally. Specifically, when the lateral deviation was increased

from 0.5 m to 1 m the MSDV reduced by 19.25%. Increasing it further from 1 m to 1.5 m, the MSDV reduced by 6.78%, and finally from 1.5 m to 2 m, the reduction in MSDV was 3.38%. This illustrates that the initial increment in the lateral deviation has the highest impact on MS reduction, and as the lateral deviations are increased further the impact on MS mitigation reduces.

Regarding the travel time, it also showed decrements with the increase of lateral deviation. Particularly, when the lateral deviation was increased from 0.5 m to 2 m the travel time reduced by 15.6%. Increasing it from 0.5 m to 1 m reduced the travel time by just 3.96%. Increasing it further from 1 m to 1.5 m reduced the travel time by 8.45% and lastly, increasing it from 0.5 m to 2 m reduced the travel time by 4.08%.

Table 2.4: Effects of allowed lateral deviation from the road center line on MSDV and travel time

Allowed deviation	MSDV	Travel time
0.5 m	46.74 m/s$^{1.5}$	53.0 min
1.0 m	37.75 m/s$^{1.5}$	50.9 min
1.5 m	35.19 m/s$^{1.5}$	46.6 min
2.0 m	34.0 m/s$^{1.5}$	44.7 min

2.5.2. DRIVING SIMULATOR VALIDATION

REALISED ACCELERATIONS

Figure 2.10 shows the G-G diagram for the accelerations realised in the driving simulator. According to Figure 2.9 and Figure 2.10, the accelerations attained by the two drives are lower in magnitude inside the simulator, which is expected due to limited simulator workspace. However, based on Figure 2.6 and Figure 2.7, the power is reduced below 0.2 Hz, but is replicated fairly beyond that point. Thus, the selected MCA parameters retain motion characteristics above 0.2 Hz in the applied driving simulator motion.

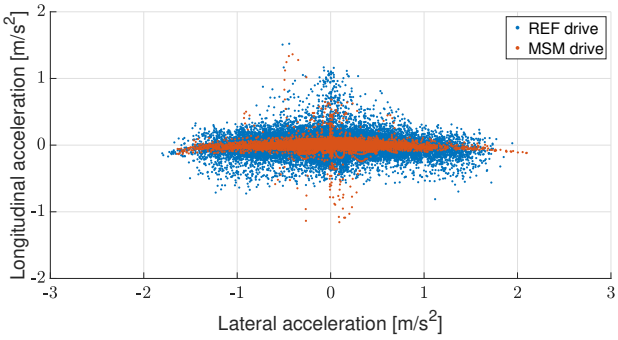

Figure 2.10: G-G diagram of the simulator platform acceleration realised in the driving simulator for REF and MSM drive

PARTICIPANTS' SICKNESS LEVELS

General motion sickness susceptibility assessed prior to the experiment yielded a mean MSSQ of 17.14 with a standard deviation of 10.03 over the selected participants. This mean translates to a percentile of 69%, which indicates that our participants have a slightly above-average motion sickness susceptibility. The standard deviation translates to 52.94% to 81.49% percentiles, indicating that our participants cover a reasonable range of susceptibility.

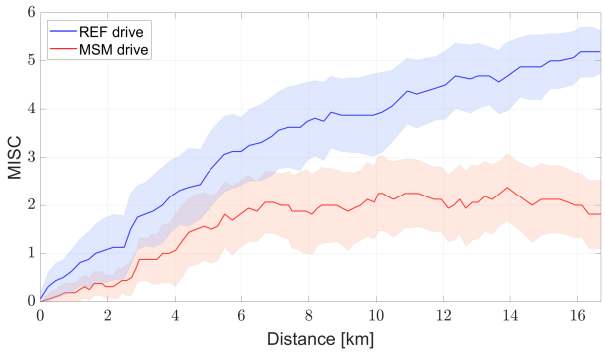

Figure 2.11: Mean MISC scores for MSM and REF drive

For the MSM drive only one participant dropped out reaching MISC level of 6, whereas in case of REF drive 7 out of 16 participants dropped out of the experiment. Hence, the algorithm was effective in motion planning to reduce the amount of participants stopping the experiment approaching retching levels. The mean MISC scores representing the sickness levels of the participants are shown in Figure 2.11. The blue line depicts the mean MISC for the REF drive, whereas the red line shows the mean MISC for the MSM drive. The shaded areas around the plotted lines depict the standard deviation of MISC ratings for the participants. It should be noted that, in cases of a participant stopping the experiment, their MISC score was considered to be 6 till the end of the experiment for the calculation of mean MISC (in practice it should rise further).

According to Figure 2.11, the MSM drive is less sickening during the entire journey. In fact, the mean MISC value at the end of the experiment for MSM drive is 65% lower compared to REF drive. Overall, the participants showed a very high variability in the MISC scores during the experiment due to their motion sickness susceptibility. Even with this variability in the MISC scores, all the participants had reduced sickness levels when they were subjected to MSM drive, compared to REF drive (Figure A.1 in Appendix A.2).

The onsets of increasing motion sickness levels were analysed through boxplots in Figure 2.12. The onsets up to MISC level of 3 are provided, as, with the MSM drive, not many participants reached a MISC level beyond 3. This is another indication of the algorithm's ability to successfully mitigate motion sickness. Furthermore, the mean distance travelled before a participant reaches a specific MISC level and its standard deviation are given in Table 2.5. This shows that the distance travelled by the participants before

reaching each and every MISC level is more in case of MSM drive compared to REF drive.

Table 2.5: Distance travelled by participants before reaching specific MISC levels

MISC level	AV driving style	Mean distance (std), km
1	MSM drive	2.8 (1.83)
	REF drive	1.52 (1.29)
2	MSM drive	6.3 (4.21)
	REF drive	3.14 (2.01)
3	MSM drive	6.91 (2.82)
	REF drive	4.47 (2.04)

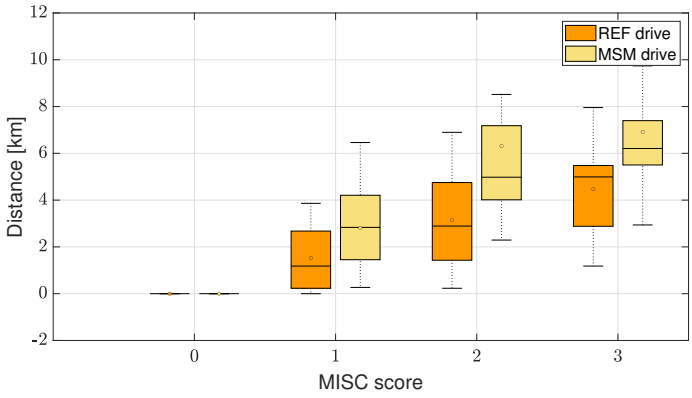

Figure 2.12: Boxplot of onset of the levels of motion sickness with respect to distance travelled

Along with the continuous MISC measurements during the experiment, post experiment MSAQ ratings were collected. For REF drive the mean MSAQ for all the participants was 65.56 with a standard deviation of 18.91, whereas, for MSM drive, the mean MSAQ for all the participants was 37.69 with a standard deviation of 17.71. All the participants reported a reduced MSAQ score with MSM drive. The results of the single-tailed t-test ($p = 4.9e-4$) on this dataset confirm the assertion that the algorithm effectively mitigates MS.

Finally, the general sickness susceptibility using MSSQ prior to the experiment was evaluated in relation to the actual sickness. Based on Table 2.6, the correlation of MSSQ with any of the sickness indicators is not significant. This implies that MSSQ is not a reliable metric to predict the susceptibility of an individual to motion sickness in the conditions tested. This is coherent with [64] reporting a moderate correlation with MSSQ ($\rho = 0.5, p = 0.05$) in 0.3 Hz fore-aft motion.

Table 2.6: Correlation coefficients between MSSQ scores and different sickness indicators and their respective p-values

Data-set	Correlation coefficient	p-value
Max MISC: MSM drive case	0.3493	0.1849
Max MISC: REF case	0.1877	0.4864
MSAQ: MSM drive case	0.3623	0.1679
MSAQ: REF case	0.4349	0.0922

2.6. DISCUSSION

The effectiveness of the optimal trajectory planning for mitigating MS has been evaluated. This was conducted by comparing the optimal MSM drive with REF drive (baseline) in human-in-the-loop experiments using a moving-base driving simulator.

In MSM drive, the vehicle reduces its velocity during the corners, leading to decreased lateral accelerations that a passenger is subjected to. This is a desired behaviour to reduce the sickening stimuli. The algorithm also modifies the pre-defined path allowing the vehicle to perform corner cutting. Such adjustments to the path led to a further reduction in lateral acceleration, since corner cutting increases the turning radius. This renders the ride more comfortable and less sickening.

The G-G diagram in Figure 2.9 indicates a large reduction in longitudinal and lateral accelerations in MSM drive. The objective of the algorithm is to minimise MSDV; hence, the algorithm limits the velocity reduction in cornering, attaining a higher lateral acceleration, but limiting the longitudinal deceleration. This results in a lower overall MSDV.

For the selected weight settings, the MSDV for the journey reduced by 53% with the proposed MSM algorithm. This aligns with the projections made in the literature [52], [53], as expected due to the presence of MSDV in the cost function. According to Figure 2.4 as the weight ratio w_m/w_t is increased, the MSDV through the journey reduces. Moreover, as MSDV minimization reduces the vehicle velocities/accelerations, a very high ratio of the weight, w_m/w_t, would result in an optimal solution with very low velocities, which are preferable for MS mitigation. However, the excessive reduction of velocity leads to the occupants' dissatisfaction [65], [66]; as the journey time will be too long, violating their expectation for travelling long distances in a short period of time. An alternative would be to prompt users to watch the road during sickening road sections, and avoid engagement in non-driving tasks.

The experimental study in the driving simulator was conducted to gauge the effectiveness of the proposed method in reducing MS using human beings. The recent state-of-the-art studies for MS mitigation assess their proposed algorithms only via simulations and lack experimental validation with humans. The experiments in this study demonstrate that the proposed algorithm is effective in reducing experienced motion sickness with human participants across a substantial range of individual susceptibility. In general, our results are in line with the simulation studies mentioned earlier. Regarding the efficiency of the driving simulator, the accelerations (Figure 2.6 and Figure 2.7) beyond 0.2 Hz were replicated closely in the driving simulator, whereas the accelerations

below that frequency could not be captured due to the limited workspace of the simulator. Although the range of frequency for human susceptibility to motion sickness is from 0.1 Hz to 0.8 Hz, the tuned settings of the simulator allowed us to replicate the frequency range beyond 0.2 covering a large part of the focus range.

Regarding the experiment, an accelerated sickening path was used to seek the optimal solution and subjectively test the occupants' motion sickness levels. During the experiment, only one participant dropped out when the proposed algorithm was used, i.e. in MSM drive. Meanwhile, even this participant travelled a longer distance until dropping out compared to the REF drive. This indicated that the algorithm had a positive effect on MS mitigation for each and every individual, when compared to the REF drive which tries to follow the lane center and is not close to human-like negotiating curves. Our proposed algorithm is expected to outperform any human-like driving algorithm since it optimises both velocity and path for the mitigation of MS. However, such comparison is considered as scope for future study. The proposed algorithm suffers from certain limitations as well. All the participants showed differing MS susceptibility during the experiment. Thus, there is no single weight setting for the cost function that would suit the entire population. Weight sets need to be defined for different individuals or different susceptibility groups. We recommend performing user groups studies to assess if different comfort pre-sets would provide a benefit to more people.

The algorithm also makes a trade-off between the travel time and sickness reduction, which adheres to the findings from [53]. In the conducted experiment, the travel time of the journey increased by 50% with mitigation of MS. The road profile used for the experiment was high on sickening stimuli. For paths with lower sickening stimuli as occurring in many highways, the vehicle velocity will often be constrained by speed limits, and hence the travel time increase will be limited.

2.7. CONCLUSION

Trajectory planning for mitigation of motion sickness in automated vehicles through optimal control has been proposed. The algorithm outputs a comfortable reference velocity profile. Moreover, it generates a preferred path through corner cutting within the allowable road area. This allows the vehicle to corner with lower lateral acceleration reducing the sickening motion stimuli.

The effectiveness of the proposed algorithm in reduction of motion sickness was studied using a driving simulator experiment. The proposed algorithm successfully reduced the levels of motion sickness for the 16 participants, where, the mean MIsery SCale scores reported by the participants reduced by 65% compared to the benchmark controller. Each and every participant reported reduced levels of sickness, when subjected to the proposed driving style, and the number of dropouts reduced from 6 to 1. The overall journey was also rated as more comfortable by the participants, indicated by a 57.48% reduction in the mean score of Motion Sickness Assessment Questionnaire, which confirms the algorithm's capability in reduction of motion sickness in each and every individual.

Although all participants reported reduced motion sickness with the proposed algorithm, the individual sickness levels displayed a substantial variance. This calls for subject-specific comfort settings in automated vehicles.

3

Frequency-Splitting: Bridging Filter-Based and Optimization-Based Motion Cueing with Human-in-the-Loop Driving Simulator Validation

Great things are not done by impulse,
but by a series of small things brought together.

Vincent van Gogh

Parts of this chapter have been published in **V. Jain**, A. Lazcano, R. Happee, B. Shyrokau “Motion Cueing Algorithm for Effective Motion Perception: A frequency-splitting MPC Approach”. In: Proceedings of the Driving Simulation Conference 2023 Europe, Antibes, France. 2023 [67], and will serve as a basis for future publication V. Jain, A. Lazcano, R. Happee, B. Shyrokau "Frequency-Splitting: Bridging Filter-Based and Optimization-Based Motion Cueing with Human-in-the-Loop Driving Simulator Validation".

3

ABSTRACT

Motion cueing algorithms in driving simulators ensure coherence with the scenario's visualisation. Model predictive control is a promising motion cueing technique, but its widespread real-time application is hindered by its high computational demands.

This paper introduces a novel algorithm that combines filter-based and optimisation-based methods to enhance specific force tracking while improving computational efficiency. The proposed frequency-splitting algorithm decomposes reference vehicular acceleration into low- and high-frequency components. The high-frequency component guides translational motion, avoiding workspace limits, while the low-frequency component guides tilt coordination to replicate sustained accelerations. This guidance enhances computational efficiency and tracking performance. The total acceleration acts as a reference for specific force, with the highest priority, ensuring optimal specific force tracking.

The performance of the proposed approach was evaluated in comparison to state-of-the-art model predictive control-based motion cueing and conventional adaptive washout. The proposed approach at least matches, if not outperforms, the state-of-the-art model predictive control-based cueing algorithm in specific force tracking. It also demonstrates potential for real-time implementation in driving simulators.

To complement the objective findings, we conducted a comprehensive human-in-the-loop assessment. We gathered user feedback to validate the effectiveness in providing a realistic driving experience in passive driving representative of being driven by an automated vehicle. The algorithm was rated equally or more realistic compared to adaptive washout by 76.3% of the participants, with a reduction of false cues in specific manoeuvres. It was also rated to be more aggressive by 68.4% of participants, demonstrating that it captures the aggressiveness of the original drive better.

3.1. INTRODUCTION

In the realm of moving-based driving simulators, achieving realism in motion cueing algorithms (MCAs) has been a long-standing challenge. Despite the advancements in cueing algorithms based on model predictive control (MPC) over the years, adaptive washout filter-based approaches continue to prevail in industry applications. The dominance of washout filter-based algorithms is primarily attributed to their computational efficiency, a critical factor for real-time application in driving simulators.

While MPC-based algorithms offer superior fidelity in motion cueing, their computational demands often outweigh their benefits, making them less practical for widespread adoption in real-time applications.

To address this gap, this paper introduces a novel frequency-splitting motion cueing algorithm that integrates the computational efficiency of washout filters with the optimal control capability of MPC-based MCAs. The key idea is to decompose the reference specific force signal into low- and high-frequency components, as illustrated in Figure 3.1. The MPC now jointly uses three references. The high-frequency component guides the translational motion of the platform, while the low-frequency component guides the tilt coordination, similar to classical washout schemes. The total acceleration acts as a reference for specific force, with the highest priority, ensuring optimal specific force tracking.

Within this framework, the MPC formulation ensures optimal workspace utilization by adapting to varying driving scenarios and respecting platform constraints. This approach is motivated by the need for computationally efficient yet perceptually accurate motion cueing in next-generation simulators used for human-in-the-loop testing and automated driving research. By maintaining real-time performance without sacrificing motion realism, the proposed method offers a practical solution for automotive and research simulators alike.

The contributions of the work are outlined below:

- Development of a novel frequency-splitting algorithm including elements of classical washout and MPC-based motion cueing algorithms, combining advantages of both approaches within a single algorithm.
- Objective analysis demonstrating that the proposed algorithm strongly outperforms conventional adaptive washout in terms of specific force tracking, while also achieving higher computational efficiency than traditional MPC-based MCAs.
- Human-in-the-loop evaluation replicating an automated driving scenario, showing a clear preference among participants for the proposed algorithm. Additionally, for specific manoeuvres, the algorithm effectively reduces perceived false cues.

The paper is structured as follows: Section 3.2 discusses the existing works in the domain of motion cueing and driving simulator experiments; Section 3.3 provides the details of the proposed algorithm and formulates the optimal control problem; Section 3.4 establishes the configuration of the frequency-splitting MCA; Section 3.5 compares the proposed MCA to two benchmark MCAs through objective metrics, followed by human experiment design and subjective validation in Section 3.6; Section 3.7 discusses the results presented in previous sections. The conclusion is laid out in Section 3.8.

3.2. RELEVANT STUDIES

Motion cueing algorithms implemented in driving simulators aim to emulate the motion of a vehicle through various control strategies. The typical approach is to recreate low-frequency translational accelerations with tilt-coordination, and high-frequency accelerations by linear accelerations of the platform [14]–[16]; such MCAs are referred to as "washout" filters.

As a next step, optimisation-based washout-filter algorithms have been established. These algorithms adaptively scale the reference accelerations based on the current states of the platform and the mismatch in motion perception [17], [18]. These MCAs are generally referred to as "adaptive washout".

Classical and adaptive washout algorithms, are collectively referred to as filter-based approaches, and remain widely used due to their simplicity, low computational cost, and suitability for real-time implementation. Their intuitive structure and fast execution make them particularly attractive for industrial applications, despite their limited ability to explicitly handle motion constraints.

A more enhanced approach is based on using model predictive control [19]–[21]. By anticipating future states, MPC-based MCAs optimise motion control inputs, providing more optimal solutions compared to (adaptive) washout MCAs.

Nonlinear Model Predictive Control (NMPC)-based MCAs enable the prediction and optimization of future system behavior while explicitly considering nonlinearities and constraints. This approach allows more accurate control actions and improved workspace utilization, as the controller is aware of the motion system's physical limitations including actuator capabilities.

Previous studies [68], [69], have explored the inclusion of actuator dynamics and constraints within NMPC-based MCAs. By modeling the nonlinear actuator behavior, these works demonstrated enhanced performance and more efficient use of the platform workspace, leading to smoother and more realistic motion rendering.

Restriction of motion through additional constraints is also explored. Dynamic constraints utilise a non-linear combination of acceleration, velocity, and displacement to reduce abrupt motion of the platform, aiding in better workspace utilisation [23]. A decoupled MPC-based motion cueing strategy has also been proposed, in which vehicular translational and rotational motions are controlled independently [70]. In this architecture, translational accelerations—sensed by the otolith organs—are handled by one MPC, while rotational cues—sensed by the semicircular canals—are handled by a separate MPC. The rotational motion arising from the vehicle dynamics is combined with the tilt coordination component, and the resulting signal is applied to the tilt channel to reproduce both the vehicle rotations and part of the specific force. This decoupling relaxes the constraint of imposing tilt perception thresholds on vehicular rotations, as the vehicle rotations themselves do not need to remain below the human perception threshold.

However, MPC-based MCAs face a drawback in terms of their high computation time, which poses a limitation for real-time applications.

To reduce computational costs, explicit (offline) MPC has been used to pre-compute solutions and use these as look-up table. This significantly reduces online computation time [23]. While explicit MPC reduces online computation time, it encounters challenges

related to memory storage and limitations on utilising large prediction horizons with fast sampling rates. Thus, a more practical alternative is needed to address these challenges. As an alternative, a four DoF MCA is proposed using a combination of explicit (offline) and implicit (online) MPCs [24]. The four DoF explicit MPC provides an initial educated guess to the implicit MPC, resulting in faster convergence.

It is interesting to note that, for real-time implementation, short prediction horizons are often explored in MPC-based MCAs. While this reduces computational effort, it typically compromises stability. To mitigate this, terminal weights have been introduced to retain stability even with short horizons [71]. Exponential weighting of the future predicted trajectory has been shown to accelerate convergence [72], although this comes at the cost of reduced tracking performance.

Both washout and MPC-based MCAs include several parameters which can be selected by users to enhance performance for specific driving scenarios. These parameters include scaling factors for vehicular accelerations, filter frequencies, penalisation weights for washout (to bring back the platform to its neutral position), jerk penalisation, etc. The performance of an MCA can depend heavily on these parameters. The use of genetic algorithms has been explored [26] to tune the algorithm parameters, eliminating the need for weight tuning based on user feedback. A genetic algorithm has also been employed to scale the reference signal online to achieve better specific force tracking. The scaling is based on the workspace available for the upcoming motion and the motion perception error [27].

While MPC-based MCAs generally use the specific force as a reference to be tracked, human perception models have been added to MPCs to enhance perceptible motion while ignoring the motion that humans do not perceive [19]–[21], [25], [70], [73]. In these studies, human perception models are included to convert the actual vehicle accelerations into perceived accelerations, and then the MPC aims to recreate these perceived accelerations through the platform motion. However, we found no comparison quantifying benefits, including and excluding human perception model, using simulations nor via subjective experimental evaluation.

Sequential motion cueing algorithms, where the most suitable algorithm is selected for each situation, have also been explored [30]. In this approach, different motion cueing algorithms were switched dynamically to utilize the best-suited MCA or MCA setting at the appropriate instances.

Reinforcement learning (RL) has also been investigated in the field of motion cueing to enhance fidelity. Prior studies have explored RL for selecting the prediction horizon length [29] and deep reinforcement learning (DRL) for directly controlling platform actuation based on reference signals [28]. The use of RL to adaptively determine the horizon length demonstrated reduced computation times for MPC-based MCAs. Meanwhile, the DRL-based MCAs demonstrated the ability to learn the underlying control strategy directly and improve motion cue realism and immersion quality based on a human perception model, outperforming optimised filter-based classical washout algorithms in objective evaluations. However, such machine learning approaches face the drawback of limited generalizability when encountering unforeseen scenarios. The use of deep neural networks to derive explicit MPC formulation for an MCA has also been explored [74]. A Gaussian radial basis function–based neural network (RBF-NN) was

developed in [75]; however, the resulting explicit MPC formulation exhibited degraded performance compared to conventional approaches.

Several studies report objective comparisons of washout algorithms and MPC-based MCAs (e.g. [20], [25]) and demonstrate that MPC-based algorithms outperform washout algorithms in terms of specific force tracking. However, only few studies compare subjective evaluation of multiple MCAs with human in the loop experiments.

Experimental subjective validation [31] compared a classical filter-based algorithm and MPC-based MCA. Participants rated the perceived mismatch between the motion profile and the visual stimuli continuously during the simulation via a knob mechanism. The mismatch rating using the classical filter-based algorithm was scored approximately 2.5 times higher (based on the conducted MANOVA test). Experimental validation in [21] also indicated that 70% of the participants rated the motion rendered through a non-linear MPC-based MCA as more realistic compared to a filter-based algorithm.

This work proposes a novel algorithm combining elements of classical washout filter-based and MPC-based approaches. It utilises an MPC framework to incorporate workspace and dynamic constraints. The three references for the algorithm are the total specific force and filtered accelerations, with high frequency for translational acceleration and low frequency for tilt coordination. The proposed frequency-splitting algorithm is evaluated through a comparative analysis with a benchmark MPC based MCA and with a widely employed adaptive washout algorithm with optimisation-based workspace management [76].

Ample studies evaluate driving simulator fidelity as perceived by active drivers. Considering that driving simulators have started to be intensively used in research and development regarding comfort in automated vehicles, we validate the proposed algorithm from the perspective of passive driving. We evaluate simulator fidelity by examining visual and motion realism, as well as assessing aggressiveness and motion sickness. To guide our evaluation, we utilise a questionnaire inspired by a validation study on cyclist behavior in a bike simulator [77]. This approach ensures a comprehensive assessment of the simulation experience, focusing on key factors that contribute to overall realism and user comfort.

3.3. METHODOLOGY

This section describes the proposed frequency-splitting MCA, which combines elements from both filter-based and MPC-based MCAs. The algorithm utilises high-pass and low-pass (first-order) filters to split the reference acceleration signal into high and low-frequency components (cut-off frequency, ν_{FS} =0.5 Hz). The high-frequency component serves as a reference for translational platform accelerations, while the low-frequency component guides tilt coordination, resembling the washout-filter approach. Furthermore, the algorithm incorporates an MPC framework to address workspace constraints.

While several studies include vestibular perception models in MPC-based MCA (see Section 3.2), this increases computational complexity. Our preliminary exploration indicated that incorporating these models (second-order transfer functions for otoliths and semicircular canals) adversely affected computation load with no significant change in specific forces. Given that our MCA already tracks specific forces effectively without a vestibular model, we decided against including it.

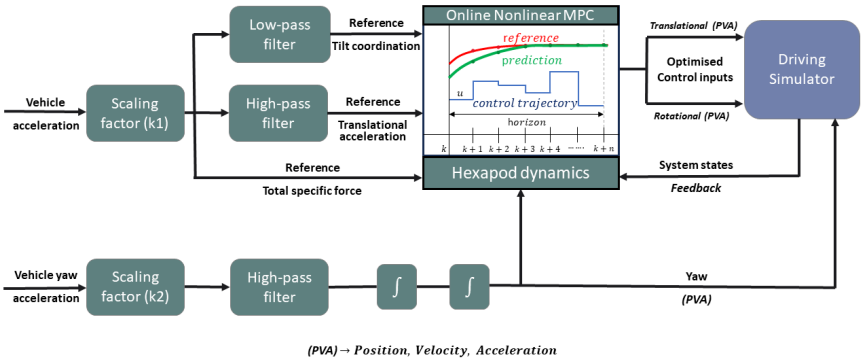

Figure 3.1: Structure of the five DoF frequency-splitting algorithm

Within the MPC framework, control is exercised over four DoFs responsible for pitch, roll, and translation in both longitudinal and lateral directions. The vertical motion is ignored in this study assuming a perfectly flat road. Due to no contribution of yaw for specific force generation, it can be decoupled from the MPC framework. It is directly incorporated into the simulator's rotational channel input after passing through a washout filter. The schematic representation of the algorithm's structure is depicted in Figure 3.1. In this study, pitch and roll corresponding to vehicle motion are neglected, as they remain below 2 degrees through the entire maneuver for the used experimental real driving data. However, these can be directly added to the rotational inputs (which are the rotational optimised control inputs to the driving simulator in Figure 3.1).

3.3.1. HEXAPOD/DRIVING SIMULATOR DYNAMICS

The motion of the hexapod platform is defined in a state space form to facilitate implementation in the MPC. The base states include hexapod position (s_{hex}) and angular orientation (θ_{hex}). These base states are added to the state-space model with the relation

$$\dot{x}_{hex} = A_{hex} x_{hex} + B_{hex} u_{hex} \tag{3.1}$$

where the state vector, x_{hex}, comprises of the position, s_{hex}, translational velocity, v_{hex}, angular orientation, θ_{hex}, and angular velocity, ω_{hex}, of the hexapod and the input vector, u_{hex}, comprises of translational acceleration, a_{hex} and angular acceleration, α_{hex}. The matrices A_{hex} and B_{hex} represent the double integrator systems of the states and inputs, adapted from [78].

As the algorithm is designed for both longitudinal and lateral degrees of freedom, each state comprises of components in x and y directions (roll and pitch for orientation). In this study, positive values correspond to forward, left, and upward orientations along the x, y, and z axes, with counterclockwise rotations indicated as positive.

3.3.2. MPC FORMULATION

To achieve realistic motion perception, vehicular accelerations are tracked using specific forces generated by the driving simulator. These specific forces encapsulate the

combined effects of accelerations and gravity as perceived by the human via the otoliths (part of the vestibular system). Therefore, the specific force is calculated at the estimated head location.

The translational component is the acceleration of the platform. The gravitational force vector G_{loc}, at the estimated head location, is defined by the relation

$$G_{loc} = R^T [0\ 0\ g]' \tag{3.2}$$

where R is the transformation matrix that resolves gravitational force corresponding to longitudinal, lateral and vertical directions and g is the acceleration due to gravity, acting on the occupant's body vertically.

The total specific force is then defined as

$$f_{spec} = a_{hex} + G_{loc} \tag{3.3}$$

where a_{hex} is the translational acceleration of the platform. The tilt component, G_{loc}, provides an additional pseudo acceleration to the occupant of the simulator.

The specific force is the quantity to be tracked to achieve realistic motion perception. Additionally, it is essential to restrict the platform rotation rates to levels below the human perception threshold to prevent the rotations from being perceived. This threshold is generally kept between 2-4 deg/s [20], [21], [79]. For this work, we selected 3 deg/s as the perception threshold. To ensure a more robust specific force tracking, this limit is incorporated as a soft constraint rather than a hard constraint. This means that the constraint is allowed to be violated when necessary to enhance specific force tracking.

OBJECTIVE / COST FUNCTION

The cost function minimises the squared error between the reference values and the actual values of the outputs y_k, inputs u_k, and states x_k, over a prediction horizon of N future samples. The structure of the cost function used for this work is adapted from [80] and is given by

$$\begin{aligned} J_c = [&\underbrace{(Y(x_k,u_k) - \hat{Y}_k)^T W_Y (Y(x_k,u_k) - \hat{Y}_k)}_{output\ terms} \\ &+ \underbrace{(X_k - \hat{X}_k)^T W_X (X_k - \hat{X}_k)}_{state\ terms} + \underbrace{J_k^T W_J J_k}_{jerk\ terms} \\ &+ \underbrace{(U_k)^T W_U (U_k)}_{input\ terms} + \underbrace{\delta^T w_\delta \delta}_{slack\ term} \ ] \end{aligned} \tag{3.4}$$

$$Y(x_k,u_k) = [f_{spec}\ a_{hex}\ G_{loc}] \tag{3.5}$$

$$W_Y = [w_{f,spec}\ w_{f,trans}\ w_{G,loc}] \tag{3.6}$$

$$J_k = [j_{trans}\ j_{ang}] \quad W_J = [w_{j,trans}\ w_{j,ang}] \tag{3.7}$$

In MPC-based MCAs, it is common practice to penalise the difference between the simulator and vehicle motion output, i.e. specific force, as the reference output term.

In this work, we include two additional references (see Equation 3.4 and 3.5) for the tilt-coordination G_{loc} and the translational acceleration a_{hex}, which are the high-frequency and low-frequency components of the reference specific force respectively.

Additionally, penalising jerk in the cost function of an MPC-based MCA is a well established practice to reduce oscillations in the specific force. We approximate jerk using the acceleration change over time-steps divided by the time-step $j(k) = \frac{a(k)-a(k-1)}{Ts}$. This approach avoids the need to add jerk as a system state, thereby decreasing the computational complexity of the optimal control problem. The state term $(x_k - \hat{x}_k)$ introduces 'washout' to the platform by consistently attempting to return it to its neutral position $\hat{x}_k$. The input term $(U_k - \hat{U}_k)$ penalises high input values.

In Equation 3.4, the main user defined (tunable) parameters are represented by the weighting matrices W_Y, W_U, W_X and w_δ. It is worth mentioning that W_X is a diagonal matrix with weights corresponding to the states being its diagonal elements. The weights for washout namely w_s and w_θ are defined in Subsection 3.3.2 (Workspace Management).

The slack variable, denoted as δ, in the cost function represents the deviation of the tilt-rate from the soft constraint limit (the perception threshold).

The optimal control problem is then formulated as

$$\min_{u \in U} \quad J_c \tag{3.8}$$

$$s.t. \quad x'_k = f(x_k, u_k) \tag{3.9}$$

$$\phi(x_k, u_k) \leq 0 \tag{3.10}$$

$$b(x(s_0)) = 0 \tag{3.11}$$

The dynamics of the system, as defined in Subsection 3.3.1, are used as equality constraints in Equation 3.9. The function ϕ in Equation 3.10 represents the inequality constraints on the system as defined in Subsection 3.3.2. Lastly, function $b(x(s_0))$ in Equation 3.11 defines the boundary conditions for the platform, i.e. the initial states of the platform.

CONSTRAINTS

Unlike a real vehicle, in a driving simulator, movements are restricted to a maximum displacement and maximum tilt angle. These quantities are specific to the simulator being used. In this work, the workspace limitations of Delft Advanced Vehicle Simulator (DAVSi) are used. DAVSi is a 6-DoF moving-based driving simulator [20], capable of generating acceleration up to 1 g in all directions and can simulate motions in the wide frequency range up to 10 Hz. The considered limits of the platform motion are given in Table 3.1. It is worth mentioning that, as the algorithm includes yaw washout as a separate controller, conservative limits are chosen for translational and rotational displacement.

Additionally, the soft constraint used to define the tilt-rate perception limit is formulated as

$$\begin{aligned} -\omega_{thd} &\leq \omega_{hex} + \delta \\ \omega_{hex} - \delta &\leq \omega_{thd} \\ 0 &\leq \delta \end{aligned} \tag{3.12}$$

Table 3.1: Limits for the simulator and the used MPC limits

Quantity	Platform physical limit	Defined MPC limit
θ_{hex}	$\pm 30 deg$	$\pm 20 deg$
v_{hex}	$\pm 7.2 m/s$	$\pm 7.2 m/s$
a_{hex}	$\pm 9.81 m/s^2$	$\pm 9.81 m/s^2$
s_{hex}	$\pm 0.5 m$	$\pm 0.3 m$

where ω_{thd} is the perception threshold limit (3 deg/s). δ is a positive slack variable which is penalised in the cost function to keep its value low. Hence, the tilt-rate soft constraint limit is allowed to be violated, however, any violation of the constraint is penalised, to minimise it.

WORKSPACE MANAGEMENT

The MPC takes these constraints into account over the MPC prediction horizon, thereby optimally using the workspace to generate realistic motion. For proper workspace management, two additional strategies are employed, namely washout and dynamic constraints.

Washout: The simulator platform has the maximum potential of recreating the specific forces at its neutral position. Hence, it is a common practice to consistently push the platform back to its neutral position. This is done by penalising the states of the platform in the cost function as described in Subsection 3.3.2 (Objective/Cost function). In this work, we use non-linear weights (based on the platform orientation and position) for the washout instead of constant weights. This allows a single non-linear setting for all scenarios rather than tuning the washout weights for each scenario.
The non-linear weights are defined as

$$w_s = \frac{g_1}{g_2 * (|s_{hex}| - s_{lim})^2 + \Delta} \tag{3.13}$$

$$w_\theta = \frac{g_1}{g_2 * (|\theta_{hex}| - \theta_{lim})^2 + \Delta} \tag{3.14}$$

where the parameters g_1, g_2 and g_3 define the shape of the weight function, s_{lim} and θ_{lim} are the defined limits for the platform for displacement and tilt angle. Δ (here 0.01) is a small value added to the denominator to avoid singularity. The values selected for the algorithm are $g_1 = 1$, $g_2 = 50$ and $g_3 = 0.1$, these values ensure that the penalisation is low near the neutral position while being high close to the platform limits. The values were manually tuned to obtain a desirable response. The resulting weight variation with the platform displacement can be seen in Figure 3.2.

Dynamic constraints: In this study, we incorporate a dynamic bound on the position and orientation of the platform rather than fixed bounds. The constraints proposed in [23], as 'braking constraints', are incorporated in this work. These dynamic constraints restrict the platform from taking actions which may drive the platform out

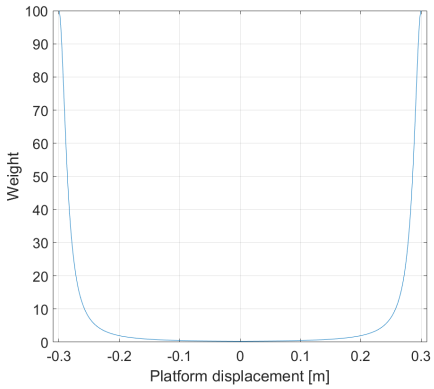

Figure 3.2: Non-linear position weight for the platform displacement (Equation 3.13)

of the workspace limits. The formulation of the constraints is

$$s_{hex,min} \leq s_{dyn} \leq s_{hex,max} \tag{3.15}$$

$$\theta_{hex,min} \leq \theta_{dyn} \leq \theta_{hex,max} \tag{3.16}$$

with

$$s_{dyn} = s_{hex} + c_v v_{hex} T_{dyn,s} + 0.5 c_u a_{hex,tran} T_{dyn,s}^2 \tag{3.17}$$

$$\theta_{dyn} = \theta_{hex} + c_w \omega_{hex} T_{dyn,\theta} + 0.5 c_u a_{hex,rot} T_{dyn,\theta}^2 \tag{3.18}$$

where, $c_v = 1, c_w = 1, c_u = 0.45, T_{dyn,\theta} = 0.5,\ T_{dyn,s} = 2.5$ and s_p, θ_p limits are 0.3 m and 20 deg respectively. The selected values were adopted from [73]. When the platform approaches its limits, the platform's acceleration and velocity reduce, aiding in maintaining the platform within the workspace envelope.

3.3.3. YAW CHANNEL

The fifth DoF, yaw, is controlled separately using a parallel washout channel, ensuring reduced computational complexity. The first-order high-pass filter used for this purpose is given as

$$HP = \frac{s}{s + 2\pi\nu_{yaw}} \tag{3.19}$$

where ν_{yaw} is the cutoff frequency for the high pass filter. In this work, we use the value of 0.0159 Hz for the cutoff frequency. The choice of the selected value is motivated in Subsection 3.4.2 (Yaw Channel).

3.4. ALGORITHM CONFIGURATION

This section outlines the simulation settings employed for the results presented in this study. A cut-off frequency ν_{FS} = of 0.5 Hz was chosen for the filters utilised to split the

reference accelerations. This selection was informed by human-in-the-loop pilot tests conducted to establish the experimental parameters.

For the simulations presented in this work, the optimisation is performed using `ForcesPro` [58], using the Primal dual interior point (PDIP) algorithm. The maximum iterations are chosen to be 100, to ensure convergence and avoid sub-optimal solutions. The optimisation has been performed on Intel(R) Xeon(R) W-2223 CPU @3.60GHz with 32GB RAM.

3.4.1. PENALISATION WEIGHTS FOR THE OUTPUT TERMS

The frequency splitting algorithm requires three weighting factors for tracking specific force, acceleration and tilt. We selected W_y = [5 1 1], as defined in Equation 3.6. This weighting prioritizes the tracking of the specific force, with a modest weighting of acceleration and tilt. Varying this weighting had modest effects on the solution (see Figure B.4 in Appendix B.7); therefore, the authors proceeded with this weight selection.

3.4.2. SENSITIVITY ANALYSIS

This section describes the procedure for configuring the FS-MCA parameters using real driving data (described in Subsection 3.5.2).

TIME STEP

The DAVSi can well attain frequencies up to 10 Hz, corresponding to a Nyquist frequency with a time step of 0.05 s. While smaller time steps can yield smoother responses, they impede real-time implementation of the MPC algorithm. Consequently, a time step of 0.05 s is selected to discretise the control inputs in the MPC.

PREDICTION HORIZON LENGTH

The length of the MPC prediction horizon was varied between 20 and 120 steps with an increment of 20 steps to examine the performance of the algorithm with different look-ahead times.

As depicted in Figure 3.3, the algorithm exhibits nearly identical responses for prediction horizon lengths of 60 steps and above. Increasing the prediction horizon length affects the algorithm's computation complexity adversely (this can be seen in Table B.3a in Appendix B.4). It can also be observed that the prediction horizon of 60 steps has real-time capability. Thus, a prediction horizon length of 60 steps is chosen for most simulations in this work.

ANGULAR JERK PENALISATION

Undesirable abrupt changes in tilt rate, which are not achievable by the simulator platform, are mitigated by introducing a penalty on angular jerk.

The angular jerk weight was varied between 1e-2 and 1e2. Weights below unity led to significant oscillations, and increasing the weight above unity negatively affected the specific force tracking. Consequently, a weight of 1 was chosen.

TRANSLATIONAL JERK PENALISATION

The weight for the translational jerk was varied between 1e-2 and 1e2, similar to the analysis of the angular jerk sensitivity. While different weights yielded similar results,

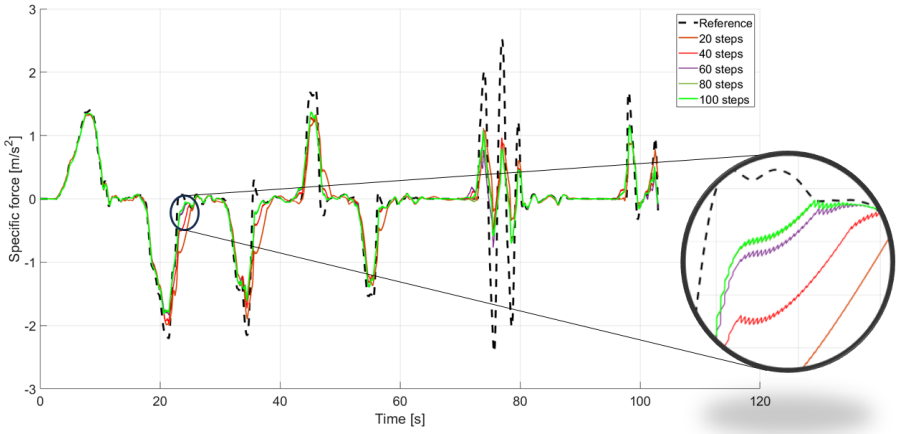

Figure 3.3: Real-drive data tracking performance in lateral direction of the proposed algorithm for various prediction horizon lengths (results for 80 and 100 steps practically coincide)

a weight of 1 was chosen for translational jerk penalisation as it resulted in the closest specific force tracking. The authors believe that selecting another value within this range is unlikely to affect the results significantly.

SLACK VARIABLE

A high penalty on the slack variable indicates a stricter adherence to the tilt rate constraint. In this study, we restrict the maximum tilt rate to $3deg/s$. However, some flexibility is given to this limit to avoid instability (described in [67]). This was done using soft constraints as described in Equation 3.12. A penalisation weight, w_δ, of 1e5 resulted in the tilt-rate staying desirably close to the limit of $3deg/s$. Increasing this weight further caused undesirable oscillation in the tilt-rate when it reached or exceeded the tilt-rate limit.

YAW WASHOUT

The tuning parameter for the yaw washout was the cut-off frequency ν_{yaw} of the washout filter. This cut-off frequency was varied between 0.0159 Hz (0.1 rad/s) and 0.1592 Hz (1 rad/s). The yaw response is shown in Figure 3.4.

Since human perception is primarily sensitive to rotational velocities, the cut-off frequency is chosen based on yaw velocity tracking rather than yaw angle or acceleration. Additionally, it is essential to ensure that the yaw angle remains within acceptable limits (20 deg for this work, considering the simulator's maximum of 30 deg and potential coupled motion effects coming from the MPC framework). Based on these considerations, a cut-off frequency of 0.0159 Hz is chosen for this study.

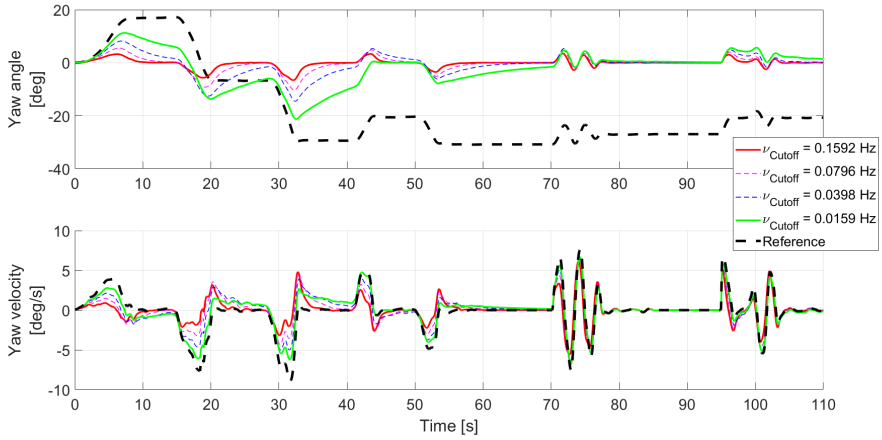

Figure 3.4: Yaw response for different cut-off frequencies ν_{yaw} for the real driving described in Subsection 3.5.2

3.5. SIMULATION ASSESSMENT

This section presents two benchmarking algorithms and the scenarios considered for this work. An objective comparison is then carried out with both benchmark algorithms.

3.5.1. BENCHMARK MCAS

For comparison, we employ two algorithms: a state-of-the-art MPC-based MCA and an Adaptive Washout (AW) MCA.

MPC-BASED MCA

The benchmark MPC-based MCA retains the structure of the proposed FS MCA with the absence of tilt-coordination and translational acceleration tracking terms in the cost function (W_y = [5 0 0] as defined in Equation 3.6). To ensure a fair comparison, all other settings are kept the same as the proposed algorithm.

ADAPTIVE WASHOUT

The adaptive washout algorithm dynamically adjusts the scaling of the reference signal according to the platform's current state, including the available workspace and motion perception error. It should be noted that the adaptive washout MCA does not incorporate any knowledge of upcoming maneuvers, whereas the proposed MCA has access to perfect preview of the future trajectory. This provides the proposed approach with a fundamental advantage in terms of anticipatory control. Nevertheless, the AW MCA is included as a benchmark since it represents the state-of-the-art in industrial motion simulation. For benchmarking, we employ an industrial state-of-the-art AW algorithm with MPC-based direct workspace management [76].

This adaptive washout consists of the following components

- Translation channels: 1st order high-pass filter

- Rotation channels: 3rd order high-pass filter
- Tilt coordination: 2nd order low-pass filter

The used configuration of the adaptive washout is kept consistent with the proposed algorithm for a fair comparison. The used values are summarised in Table 3.2

Table 3.2: Configuration of the adaptive washout algorithm

Parameter	Value
Cut-off frequency (long. and lat.)	0.5 Hz
Max tilt angle (roll and pitch)	30 deg
Maximum tilt rate (roll and pitch)	3 deg/s
Scaling Factor (Lateral)	0.4
Scaling Factor (Longitudinal)	0.3

3.5.2. SCENARIOS

This study employs two scenarios for benchmarking: one for objective and one for both objective and subjective evaluation.

An artificially generated step signal is used for the objective benchmark, focusing on evaluating the algorithm's capability to reproduce specific forces. The artificially generated step signal, although not intended for subjective comparison due to its non-realistic nature, plays a crucial role in objectively evaluating the algorithm's proficiency in replicating specific forces. In contrast, real driving data is selected for subjective evaluation, aiming to assess the realism and immersion of the algorithm in the driving simulator.

STEP SIGNAL

The step signal introduces a sudden increment in the reference specific force, simulating an extreme dynamic maneuver. This signal includes a rest period, followed by a consistent magnitude of +0.8 m/s^2 for 8 seconds and another rest period. It serves as a reference in both longitudinal and lateral directions and has also been employed in other works to evaluate MCA tracking performance [24], [73].

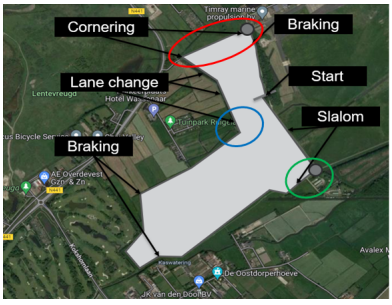

Figure 3.5: Valkenburg track

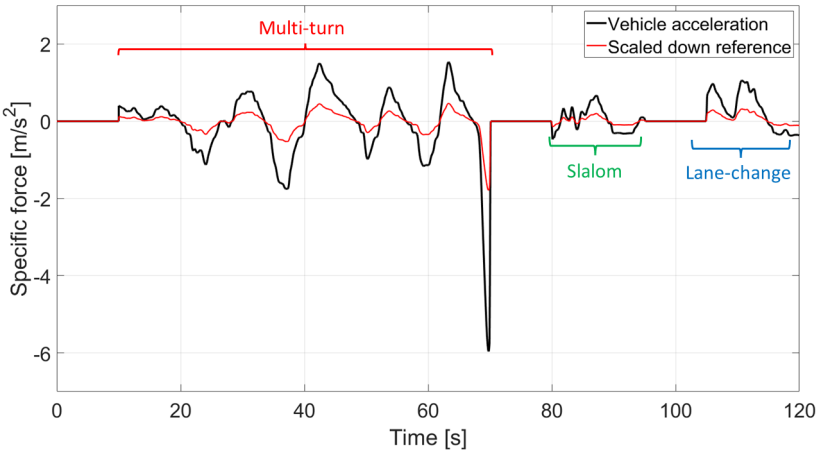

Figure 3.6: Longitudinal acceleration for the real driving data

REAL DRIVING DATA

To compare the realism and immersion of the algorithm in the driving simulator, real-experiment driving data from the Valkenburg experiment conducted by our group was utilised [81] (the track can be seen in Figure 3.5). The experiment focused on motion sickness development during dynamic driving in our automated Prius vehicle. Given the experiment's duration, specific sections were chosen for this study. These sections included multi-turns with acceleration and braking, a slalom maneuver, and a lane change maneuver, capturing various naturalistic driving scenarios.

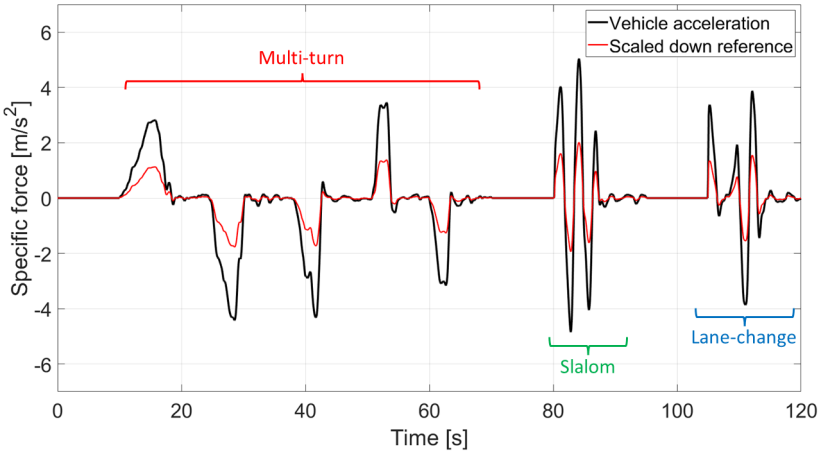

Figure 3.7: Lateral acceleration for the real driving data

The overall scenario duration was intentionally kept brief at 110 seconds to minimise

the risk of inducing simulator sickness and introducing bias to the study (see Subsection 3.6.1 for details on the algorithm sequencing process implemented to mitigate potential biases). Scaling factors of 0.3 and 0.4 were applied to the longitudinal and lateral directions, respectively, based on participant feedback obtained during pilot studies to enhance realism. This choice aligns with the general trend of using scaling factors between 0.2 and 0.6 [21], [82]. Moreover a recent paper found no effect on perceived fidelity when reducing scaling factors from 0.8-0.4 [83].

Figure 3.6 and Figure 3.7 show the acceleration profile extracted from the different sections of the drive utilised for the simulations.

3.5.3. STEP RESPONSE

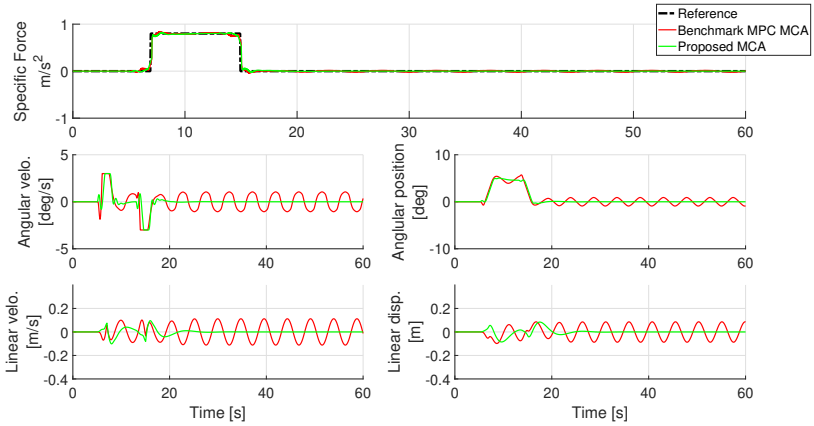

Figure 3.8: Step signal tracking for benchmark MPC-based MCA and the proposed MCA

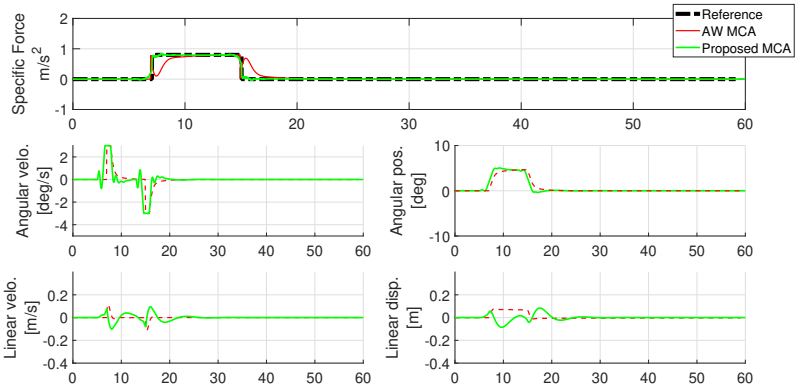

Figure 3.9: Step signal tracking for adaptive washout and the proposed algorithm

BENCHMARK WITH MPC-BASED MCA

The step response plot depicted in Figure 3.8 illustrates this comparison. In the case of the benchmark MPC-based MCA, major oscillations in platform acceleration and tilt are observed, resulting in a combined motion that yields zero specific force. These oscillations are obtained with a prediction horizon of 20 steps. This abnormality can be resolved by using longer and more effective prediction horizons. However, this example illustrates that the additional references of the frequency splitting MCA enhance convergence towards realistic motion cues.

BENCHMARK WITH ADAPTIVE WASHOUT

The responses for the same step signal, through the adaptive washout algorithm, are depicted in Figure 3.9. Notably, the adaptive washout algorithm exhibits limitations in generating desirable outcomes, manifesting as high-magnitude false cues at the beginning and end of the step signal. In contrast, the proposed algorithm consistently produces favourable results.

3.5.4. SIMULATIONS WITH REAL DRIVING DATA

The performance of the algorithms in terms of specific force tracking, computation time, and workspace utilisation is presented for the benchmark MPC-based MCA, the proposed algorithm, and the adaptive washout approach in Table B.3a and Table B.3b in Appendix B.4. Both tables also illustrate the effect of varying the MPC prediction horizon on tracking accuracy, real-time feasibility, and workspace usage. With a horizon of 60 steps (3 seconds) or higher both MPC-based solutions provide a better specific force tracking compared to adaptive washout. The proposed algorithm either outperforms the benchmark MPC algorithm or matches its performance while achieving faster convergence. Even with short horizons the proposed algorithm provides stable responses with low error values due to the presence of the filtered references for the translation and tilt-coordination. With longer horizons the proposed algorithm remains more efficient computationally, whereas results remain close to the benchmark MPC.

The similar RMSE values observed between the two algorithms indicate that their expected performance in terms of motion fidelity would also be similar. Additionally, in pilot studies, participants reported no discernible differences. Thus it was not expected that the subjective evaluation for the two algorithms would differ significantly and thus the MPC-based MCA was dropped from the experimental validation.

Additionally, prolonged exposure to driving simulations increases the likelihood of motion sickness in participants, which could bias the results and compromise the validity of the evaluation. Hence the experimental comparison was kept between only FS MCA and AW MCA.

We further adopt a horizon of 60 steps for the proposed MCA and illustrate the specific force tracking in time for longitudinal motion in Figure 3.10 and for lateral motion in Figure 3.11. The response of the proposed MCA is quite similar to that of the adaptive washout in the longitudinal direction, but the proposed algorithm provides an overall better specific force tracking, with a root mean squared error (RMSE) for the adaptive washout being 0.0846 m/s^2, and that for the proposed algorithm being 0.0608 m/s^2. The distinction in performance of the algorithms is more evident in the lateral direction,

where the adaptive washout loses tracking in various sections, resulting in false cues, whereas this occurrence is minimal for the proposed algorithm. The RMSE for adaptive washout was found to be 0.3283 and that for the proposed algorithm was 0.2536.

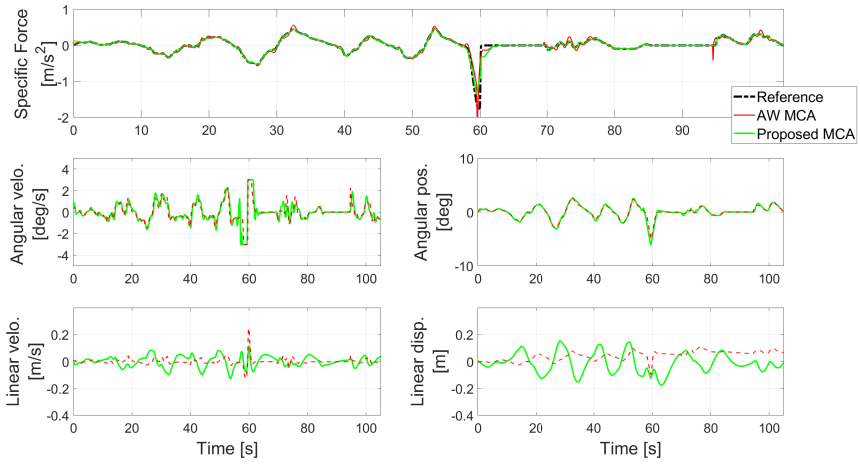

Figure 3.10: Real-drive data tracking in longitudinal direction for the adaptive washout and the proposed algorithm

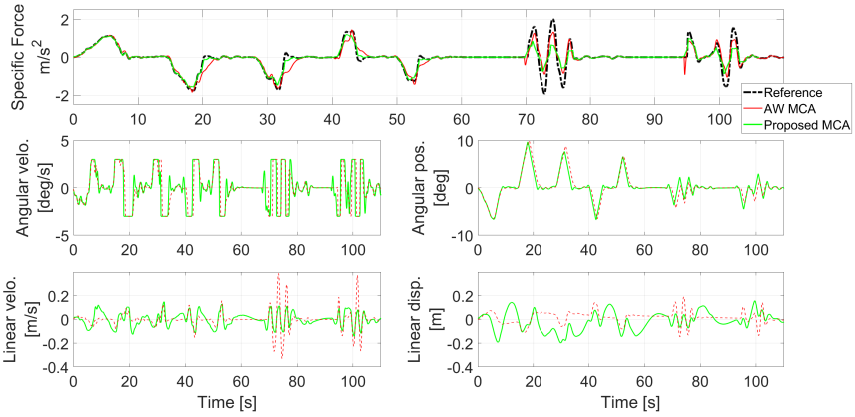

Figure 3.11: Real-drive data tracking in lateral direction of the adaptive washout and the proposed algorithm

Hence, substantial differences between adaptive washout and the proposed algorithm were observed in the specific force, and the applied platform translation and rotation also show marked differences, particularly at the onset of dynamic manoeuvres.

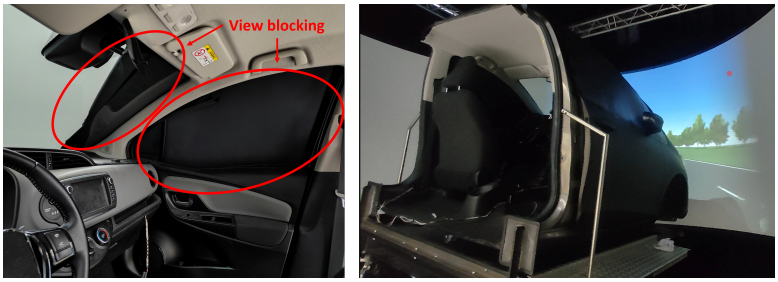

Figure 3.12: Driving simulator with side window and part of the windshield covered for frontal visual focus on the left; right side featuring visualisation projection

Therefore, we expect the two algorithms to differ substantially in terms of subjective evaluation and selected these MCAs for human-in-the-loop evaluation.

3.6. HUMAN-IN-THE-LOOP EVALUATION

This section describes the human-in-the-loop driving simulator experiment and its subjective evaluation results. Perceived driving simulator fidelity was evaluated from the perspective of passive users, representative of users of automated vehicles. In pilot studies, we even aimed to evaluate perceived fidelity with the eyes off the road using a tablet for a non-driving task. However, with vision limited to the vehicle interior, the MCAs were not perceived as representative of driving. This was resolved by adding exterior vision and instructing participants to observe the road.

3.6.1. EXPERIMENTAL PROCEDURE

All participants gave their informed consent prior to participating. The Human Research Ethics Committee of TU Delft, The Netherlands, approved the experiment protocol under application number 3965.

In total, 38 participants from the pool of students and employees of TU Delft participated in the study (mean age: 28.45, std: 4.81 years, 10 females, 28 males). All participants were subjected to both the proposed algorithm and adaptive washout drives. The two algorithms were played sequentially in a randomised order within one session to compare the subjective evaluation of the realism and feel of the MCAs.

Before the experiment, the participants underwent a concise briefing session to familiarise themselves with the questionnaire and to understand the objective of the experiment. During the experiment, two-way communication was established between the experimenter and the participant via bluetooth headphones and microphones.

Measures were taken to ensure that the video remained their sole visual focus, including blocking side window views and part of the windshield to eliminate external cues indicating platform tilt (see Figure 3.12).

Following the briefing, participants underwent a series of two-minute rides in fully automated mode, following the scenario outlined in Subsection 3.5.2. After each drive, participants completed an absolute grading questionnaire (refer to Appendix B.1) to as-

Table 3.3: Subjective evaluation and statistical analysis (on a scale from 0–5). P-values below 0.05 are considered statistically significant.

Criterion	Algorithm	All data				Inconsistent responses	Data excluding inconsistent responses			
		mean	std.	median	p-value		mean	std.	median	p-value
Coherence with the video	AW	3.61	0.69	4	0.0266	3	3.64	0.68	4	0.0672
	FS	3.88	0.69	4			3.87	0.68	4	
Cornering realism	AW	3.21	0.84	3	0.0546	3	3.27	0.79	3	0.0730
	FS	3.58	0.85	4			3.57	0.85	4	
Braking realism	AW	2.84	1.01	2.5	2.9e-5	4	2.82	1.04	2.5	1.2e-5
	FS	3.55	0.86	3.5			3.63	0.86	3.75	
Aggressiveness: Multi-turn	AW	2.95	0.93	3	2.3e-3	3	2.94	0.94	3	0.0013
	FS	3.41	0.97	3.5			3.44	1.01	3.5	
Aggressiveness: Slalom	AW	2.49	0.91	2.25	6.5e-5	5	2.50	0.95	2	0.0053
	FS	2.92	0.75	3			2.85	0.77	3	
Aggressiveness: Lane change	AW	2.28	0.78	2	5.7e-5	6	2.33	0.79	2.25	0.0072
	FS	2.67	0.79	2.5			2.65	0.82	2.5	
Sickening	AW	2.04	0.96	2	0.6588	-	2.04	0.96	2	0.6588
	FS	1.99	0.90	2			1.99	0.90	2	
Unnatural motions	AW	2.49	0.80	2.25	0.5935	0	2.49	0.80	2.25	0.5935
	FS	2.45	0.96	2			2.45	0.96	2	

sess various aspects of the driving experience. Subsequently, participants engaged in a second drive, with minimal time between drives to facilitate a clear comparison.

To ensure a consistent evaluation, each scenario was played a total of six times: three times using the proposed algorithm and three times using the adaptive washout MCA. The first round of each algorithm ride aimed to immerse participants in the simulation environment and was not graded. Participants provided ratings in a 5-point scale for the second and third rounds based on the provided questionnaire. At the end of the experiment, the participants were asked to fill in a comparative questionnaire (refer to Appendix B.1). To ensure fair comparison, the sequence of algorithms was randomised for different participants, maintaining either the pattern (A B A B A B) or (B A B A B A), where A represents AW and B represents FS algorithm.

Additionally, to analyze the instances of false cues, which can be perceived as unnatural motion, the participants were asked to report any instances of unnatural motions by saying 'Now'. The participants were briefed to consider any motion that does not resemble a real vehicle motion to be unnatural. The time stamps of such instances were recorded to study the reason for their occurrence.

Additionally, at any point, participants could indicate their desire to terminate the experiment.

3.6.2. SUBJECTIVE EVALUATION

This subsection draws the comparison of the algorithms based on the conducted experiment. The obtained responses are presented in Figure 3.13 and detailed including statistical significance in Table 3.3.

Inconsistencies in a participant's response to the questionnaire pose a challenge to the reliability of evaluations. To address this issue, a method was established. Each algorithm was rated twice by each participant. If the discrepancy in ratings for a criterion within the same algorithm exceeded 2 points (40%), the question was excluded for that specific participant's analysis. This method was not followed for the sickness criterion, as sickness may develop over time with exposure to multiple simulations. A total of 24 (8%) inconsistencies were eliminated from the pool of 304 responses. Table 3.3 lists the results without removal (left), the number of inconsistent responses per question (mid) and results when removing these inconsistent responses (right).

The realism, in this work, was evaluated based on three factors.

- *Coherence of the motion with the video*: For an immersed experience within the simulator environment, the motion of the simulator should always be coherent with the video.

- *Cornering realism*: In recreating the accelerations of the vehicle, an algorithm should generate motions that follow the dynamics of the vehicle and should feel like motion in a real vehicle.

- *Braking realism*: Just like cornering, the vehicle's deceleration should also resemble a real-vehicle motion.

Additionally, the aggressiveness of the three sections (Figure 3.5.2) of the experiment scenario was evaluated separately.

The proposed algorithm was rated higher for all questions related to realism and aggressiveness in matching the actual scenario. Initially, five measures showed a significant difference, but after omitting inconsistent responses, this dropped to four.

COHERENCE OF THE MOTION WITH THE VIDEO

In general, both the algorithms are rated high by the participants in terms of realism of the simulation. For coherence with the video, the proposed algorithm, on average, was rated 3.88 out of 5 which translates to approximately 78% realism, compared to 73% (avg. 3.61) for the adaptive washout, with the median for both the algorithms being 4. This indicates that both the algorithms rendered motion coherent with the video, not significantly different with the removed inconsistent responses (see Table 3.3 right side). It is worth mentioning that the quality of the video was the limiting factor restricting the realism of the simulation and not the coherence of the motion, as indicated by the participants' verbal feedback after the experiment.

CORNERING REALISM

The proposed algorithm was rated 3.57, and the adaptive washout MCA was rated 3.27 on average, with their medians being 4 and 3 respectively, with no statistically significant difference.

Seven participants (18%) observed pre-positioning of the platform before approaching a corner with the proposed algorithm. This is discussed further in Subsection 3.6.2 where these instances of false cues are reported (see Figure 3.14). Pre-positioning is described further in Appendix B.6. The response describing prepositioning is also presented in Figure B.3. This figure also illustrates the components of the specific force, the translational and tilt components, cancelling each other to create a zero net specific force in the periods before the corners. Pre-positioning is inherent in MPCs, which prepares the platform for optimal tracking of the specific force looking at the upcoming manoeuvre. On the other hand, for adaptive washout, after the corner, the platform returns to its neutral position slowly without any compensation through translational acceleration (see Figure 3.11). This causes a drifting sensation because the platform keeps moving even after the turn has ended. This drifting phenomenon was perceived by 12 participants (32%) in adaptive washout MCA. Seven participants (18%) observed a similar drifting phenomenon in the proposed algorithm as well, however, it was reported to be milder than in adaptive washout MCA.

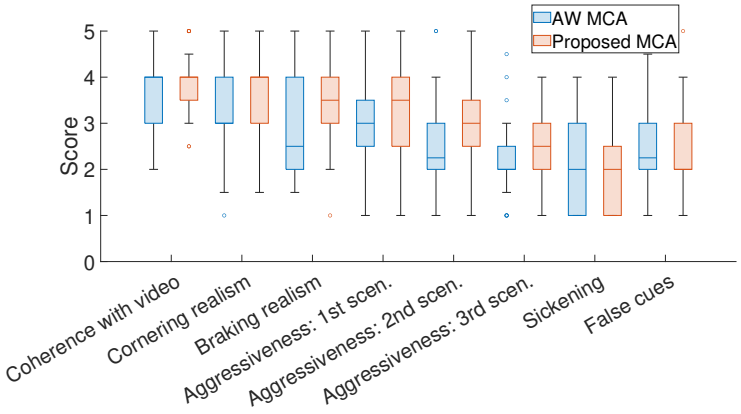

Figure 3.13: Subjective responses obtained during the experiment. Boxes represent the interquartile range (IQR) with the lower quartile (Q1) at the bottom and the upper quartile (Q3) at the top. The line inside the box indicates the median. Whiskers extend to the minimum and maximum values within 1.5 times the IQR from the quartiles. Points outside this range are considered outliers and are plotted individually.

REALISM OF BRAKING

The proposed algorithm was rated 3.63, and the adaptive washout MCA was rated 2.82 on average, with a statistically significant difference ($p = 2.9e-5$).

This more realistic perception can be attributed to the fact that the proposed algorithm uses more translational motion to recreate the specific forces, whereas, the adaptive washout MCA predominantly relies on the tilt-coordination of the platform.

Overall realism

In the comparative questionnaire, the proposed algorithm was rated as the algorithm

that provided a more realistic experience by 23 participants, 9 participants indicated adaptive washout algorithm to be more realistic and 6 participants rated the algorithms to be equally realistic. This indicates that 75% of the participants either preferred or found the motion to be equally realistic for the proposed algorithm compared to adaptive washout MCA.

AGGRESSIVENESS

The aggressiveness of the different sections was also enquired from the participants of the experiment via the absolute grading questionnaire. The recorded scenario corresponds to an aggressive drive (evident from the vehicle accelerations in Figure 3.6 and Figure 3.7). Thus, preserving this aggressiveness in the simulation within the driving simulator is important.

The scenario was divided into 3 different sections: multi-turn, slalom and lane change. All three sections were graded separately in the questionnaire.

Aggressiveness of section 1: Multi-turn
The proposed algorithm was rated 3.44, and the adaptive washout MCA was rated 2.94 on average, with their medians being at 3.5 and 3 respectively, with a statistically significant difference.

Aggressiveness of section 2: Slalom
The proposed algorithm was rated 2.84, and the adaptive washout MCA was rated 2.5 on average, with their medians being at 3 and 2 respectively, with a statistically significant difference.

Aggressiveness of Section 3: Lane change
The proposed algorithm was rated 2.65, and the adaptive washout was rated 2.33 on average, with their medians being at 2.5 and 2.25 respectively, with a statistically significant difference.

These results demonstrate that the proposed algorithm provided a more aggressive drive in every section of the experiment. Likewise, according to the comparative questionnaire, 26 participants (68.4%) found the proposed algorithm to be more aggressive compared to the adaptive washout, 11 participants (28.9%) found adaptive washout to be more aggressive and one participant marked both the algorithms to be equal in terms of aggressiveness.

After the completion of the experiment many participants verbally indicated that both algorithms fall short in recreating the aggressiveness corresponding to the described/briefed scenario. However, as outlined above, the proposed algorithm was rated as more aggressive and thereby more realistic.

SICKNESS

The experiment consists of six two minute drives, which limits the probability of motion sickness development. After exposure to each ride, the participants rated the sickness intensity induced by the algorithms. The average rating for the proposed algorithm is

1.99 and that for adaptive washout MCA is 2.04, with both their medians lying at 2. This demonstrates that there is no significant difference between the sickening effect of the motion profiles generated by the two algorithms. A reason for this occurrence may be that both algorithms do not take into account motion sickness within their framework.

UNNATURAL MOTION/ FALSE CUES

The participants rated the proposed algorithm 2.45 on average and the adaptive washout MCA was graded 2.49 on average, with their median values lying at 2 and 2.25 respectively, with no significant difference.

Based on the comparative questionnaire, 16 participants indicated that the adaptive washout MCA caused higher instances of false cues, 13 participants suggested that the proposed algorithm has higher unnatural motions (false cues), whereas 9 participants rated them to be equal in terms of unnatural motion.

Based on the recorded instances of unnatural motion, a total of 76 false cues were reported for the adaptive washout algorithm, compared to 40 for the proposed algorithm. These instances were classified into 5 main events:

- *Acceleration/deceleration*: corresponding to pitch and longitudinal translations.
- *Coupled motion*: When both longitudinal and lateral motion have varying acceleration.
- *Pre-positioning of the platform*: the platform positions itself in anticipation of the manoeuvre so that when the manoeuvre is performed, it recreates the desired specific forces better (described above and in Appendix B.6).
- *Corner/turning*: When the vehicle and the video are turning.
- *Exiting a corner*: After a corner is over and the vehicle is expected to go straight.

Figure 3.14 presents the false cues observed during the above defined events. It can be seen that the proposed algorithm in general produces fewer instances of false cues compared to the adaptive washout. However, pre-positioning of the platform before the corner is observed only for the proposed algorithm.

3.7. DISCUSSION

In conventional washout-filter-based algorithms, both tilt-coordination and translational acceleration rely on their defined references. If translational acceleration fails to replicate its reference, no compensatory mechanism is present through tilt-coordination and vice-versa.

On the other hand, in the benchmark MPC-based algorithm, the objective is to track the overall specific force. Hence the two components, translation and tilt coordination, work together to systematically follow the reference specific force. However, as various

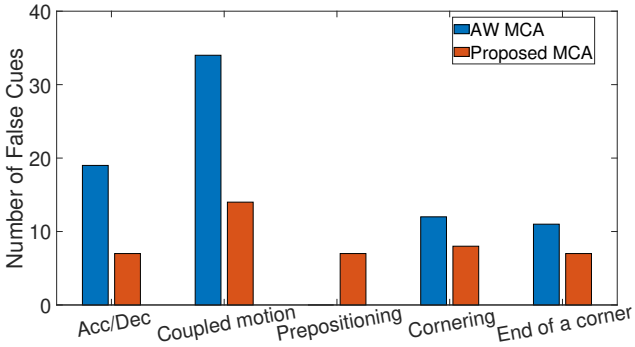

Figure 3.14: False cues observed during different events

platform motions can result in the same specific force, the algorithm may output sub-optimal results. This sub-optimal solution may even lead to oscillating platform motions, as observed in the step response with short MPC horizon (Figure 3.8).

The proposed frequency splitting algorithm is guided by additional references for tilt-coordination and translational motion. These references push the algorithm to converge to a consistent combination of translational and tilt motion, similar to classical washout cueing algorithms. The total specific force is used as the primary reference, with the highest level of penalisation for deviations. This approach enables the compensatory mechanism in the proposed algorithm, allowing it to adjust for any missing component in translation or tilt coordination. Unlike washout algorithms, if one component fails to meet its reference, the other component can compensate, as long as the platform remains within its defined workspace limits. As these references guide the platform motion, the computational efficiency of the algorithm also improves. This can be clearly observed from Table B.3a, where the computation time needed to generate the solution for the proposed algorithm is lower than that for the benchmark MPC-based MCA. Table B.3a also indicates that the proposed algorithm outperforms the benchmark MPC in terms of tracking performance with short prediction horizons. This is due to the sub-optimality of the obtained solutions for the benchmark MPC with short prediction horizons. It can also be seen that for very long prediction horizons (100 steps and above [5s + look-ahead]), the benchmark MPC produces slightly better tracking performance. This is due to the fact that it only has total specific force as the reference, which for long prediction horizons generates a solution that is closer to optimal than the components obtained using frequency splitting.

Compared to conventional filter-based-algorithms, the proposed algorithm's predictive capability enables it to anticipate future vehicle motions, thereby enhancing specific force tracking, which is absent in filter-based algorithms. For instance, in Figure 3.9 and Figure 3.11, during the onset of a step signal or a lane change maneuver, the adaptive washout algorithm generates false cues. This occurs because one component successfully tracks its reference while the other can not. On the other hand, in the proposed algorithm, the total specific force is tracked desirably.

The proposed frequency splitting MPC algorithm includes adaptive washout weights and dynamic constraints to enhance workspace utilisation (see Subsection 3.3.2). The adaptive weights allow for a single setting applicable to various simulation scenarios, eliminating the need for re-tuning washout weights. Dynamic constraints can play a crucial role in mitigating abrupt platform motion, thereby reducing false cues induced by such movements. The parameters used for the dynamic constraints are consistent with those reported in [73]. While adjusting these parameters may yield a more responsive platform trajectory, the experimental validation was conducted using the original configuration. Therefore, the results are reported based on the implemented setup to ensure consistency and reproducibility.

Additionally, the integration of high-pass and low-pass filters for distinct references to tilt coordination and translational accelerations guides platform movements. This integration prevents the motion cueing algorithm from generating excessive motion or false cues, promoting better workspace utilisation triggering motion only when necessary.

To enhance computation and real-time performance, jerk penalisation is implemented, penalising the change in acceleration with time. This eliminates the need to add jerk as an additional system state, thereby reducing the computational complexity.

In the human-in-the-loop validation, 60.5% of participants rated the proposed algorithm higher, and 15.8% rated it equal to the adaptive washout in terms of realism. Although these results indicate that the proposed algorithm outperforms the adaptive washout, several limitations were noticed. While tilting was generally not noticed by the participants, it is perceivedin instances when the tilt is not coherent with the motion. In the adaptive washout algorithm, this is predominantly noticed after the completion of a maneuver, when the algorithm slowly returns the platform to its neutral position. This is perceived as a drifting sensation as visually the maneuver has ended, but the platform motion continues. In contrast, the proposed algorithm does not exhibit this issue as strongly, with a lower magnitude of false cues at the end of maneuvers. However, as the algorithm pre-positions the platform for the upcoming maneuvers, the platform tilts before the corner starts, and the specific force is compensated by the translation in the opposite direction.

The false cues reported by the participants showed that 40 instances were observed with the proposed algorithm compared to 76 instances with adaptive washout. However, the issue of pre-positioning before the corners was only noticed with the proposed algorithm. This phenomenon is also reported in some other works (described using "velocity buffering") [31], [84]. However, no comment is made on its effect on the subjective evaluation or perception of this anomaly. In our experiment however, this anomaly was perceived by seven participants (18%).

3.8. CONCLUSION

This study presents a novel motion cueing algorithm developed for enhancing motion perception in driving simulators. It integrates elements from motion cueing algorithms using adaptive washout and model predictive control. Hence, the proposed algorithm capitalises on the strengths of both approaches.

Despite the inherent advantages of optimal motion cueing algorithms in specific

force tracking and predictive capability, our investigation illuminated challenges associated with sub-optimal workspace utilisation. The inclusion of the high-pass and low-pass filters within the model predictive framework, coupled with dynamic constraints aids in smarter workspace utilisation. Additionally, to address computational efficiency concerns, our algorithm incorporates a novel technique for jerk penalisation. By penalising the change rate in acceleration, we eliminate the inclusion of jerk in the state space of the prediction model. The algorithm is also guided for the total specific force through references for translational acceleration and tilt coordination, resulting in faster convergence.

An experimental evaluation is conducted for the proposed algorithm comparing it with an adaptive washout MCA, which is widely used in the industry. The experimental results underscore the effectiveness of the proposed algorithm in providing a more immersive driving experience compared to adaptive washout. 76.3% of participants indicated that the proposed algorithm was equally (15.8%) or more realistic (60.5%) than the adaptive washout, while 23.7% participants preferred the simulation obtained through the adaptive washout. The experimental evaluation also depicts that the proposed algorithm can replicate the aggressiveness of the drive better compared to adaptive washout, with 68.4% participants rating it to be more aggressive.

The analysis of the reported instances of false cues indicated that the proposed algorithm generated a low amount of false cues for acceleration and deceleration. For lateral motion, the adaptive washout produced higher instances of false cue while exiting a corner, creating a drifting sensation. On the other hand, the proposed algorithm produces an additional false cue, pre-positioning the platform before approaching the corners, due to the usage of the model predictive framework. This pre-positioning will be a focus of future work to enhance simulation realism.

4

AUTOSCALING: MINIMIZING IMMERSION DISRUPTION IN MOTION CUEING USING MODEL PREDICTIVE CONTROL

I find inspiration in every moment;
life is full of beautiful melodies.

Worakls

You have to sacrifice something
in order to achieve something greater.

David Brooks

This chapter has been published in **V. Jain**, A. Lazcano, R. Happee, B. Shyrokau "Autoscaling: Minimizing Immersion Disruption in Motion Cueing Using Model Predictive Control". In Proceedings of the Driving Simulation Conference 2025 Europe, Stuttgart, Germany. 2025.

4

ABSTRACT

Driving simulators aim to replicate real-world vehicle experiences by recreating accelerations acting on occupants using a combination of translational accelerations and tilt-coordination. Due to space constraints, translational accelerations alone are insufficient, and platform tilting generates additional gravitational forces to enhance realism. However, ensuring the tilt motion remains imperceptible is critical to maintaining immersion.

Model Predictive Control-based motion cueing algorithms demonstrate superior specific force tracking and platform workspace utilization. Despite these benefits, MPC algorithms can exhibit pre-positioning, a phenomenon where the platform tilts prematurely in anticipation of future motion, causing perceptible false cues that disrupt immersion. This phenomenon is particularly noticeable in tilt-coordination due to sustained specific forces.

This work proposes a solution to mitigate pre-positioning by introducing a dynamic scaling factor for tilt-coordination. By scaling down the reference signal for tilt coordination, it stays within the simulator's tilt angle and tilt-rate capabilities, and platform tilt rates are kept below human perception thresholds. The scaling factor is derived from two key parameters: the maximum specific force generated by platform tilt and the tilt rate perception threshold. The reference for specific force is unscaled to optimally use the translational workspace.

This approach enhances driving simulator realism by minimizing the perceptibility of pre-positioning while optimizing specific force recreation. Subjective evaluations also indicate improved immersion, illustrating the effectiveness of the scenario-adaptive Autoscaling MCA.

4.1. INTRODUCTION

DRIVING simulators play a crucial role in replicating real-world driving experiences by providing visual, auditory, vestibular, and haptic cues [16]. A key aspect of realism in driving simulation is motion cueing, which is achieved through reproduction of specific forces. Motion cueing algorithms (MCAs) synchronize platform motion with visual stimuli, ensuring a coherent, immersive experience.

MCAs simulate the vehicle dynamics by replicating the accelerations and forces experienced by occupants. However, due to the physical constraints of simulators such as limited motion space, realistic accelerations cannot be generated through translational movement alone. Thus, simulators employ a combination of translational accelerations and tilt-coordination, where platform tilting induces additional gravitational forces. This technique helps recreate the specific forces acting on an occupant's head, mimicking the perception of real-world driving. The classical approach uses tilt-coordination for low-frequency accelerations and platform translation for high-frequency accelerations [14], [15].

A key challenge is keeping platform rotations imperceptible, as exceeding human perception thresholds disrupts immersion and makes specific forces feel unnatural. Thus, tilt rates must remain below perceptible limits.

Recent advancements in motion cueing, particularly through model predictive control (MPC)-based algorithms, have improved the fidelity of driving simulations [19]–[21]. These algorithms predict future platform motion and optimise specific force tracking while accounting for platform workspace constraints. Despite their advantages, MPC-based algorithms are not flawless. The predictive nature of these algorithms can lead to pre-positioning, where the platform moves prematurely in anticipation of future motion. This is particularly disturbing in transitions from steady state driving to dynamic manoeuvres where in steady state the slightest motion is noticeable. While the specific force can remain zero, the constituent components of the specific force arising from translational acceleration and tilt-coordination can be non-zero, resulting in perceptible platform motion. In a subjective assessment of a frequency-splitting MPC-based cueing algorithm [67], 7 out of 38 participants reported these premature movements as false cues. This phenomenon is also reported in some other works (described as "velocity buffering") [31], [84]. However, due to the objective nature of these studies, no comment on subjective feedback is made in these works.

In moving-base driving simulators, it is a common trend to scale down the reference accelerations by a factor of 0.2 to 0.6 to better fit the available workspace [21], [82]. Scenario-specific scaling factors are typically used to precondition the reference signal and optimise tracking within the simulator's physical limits. The quality of the driving simulation heavily depends on this factor. In MPC-based MCAs, the scaling factor is generally kept constant throughout the simulation, requiring a conservative choice that suits the entire scenario rather than optimizing for different sections. This paper addresses the challenge of pre-positioning by proposing a method to dynamically adjust the scaling factor for tilt-coordination based on the simulator capabilities. By ensuring that platform tilt remains within human perception thresholds, pre-positioning is minimized, enhancing the realism and immersion of the driving experience, while eliminating the need for scaling factor tuning for every scenario.

4.2. METHODOLOGY

Figure 4.1 presents the proposed algorithm's structure, where the MPC receives two separate references: for tilt coordination and for total specific force. This ensures that a reproducible component of the specific force is provided to tilt coordination as a reference, preventing premature platform movements.

The MPC controls four degrees of freedom (DoFs) of the platform motion, with vehicular roll and pitch assumed to be negligible for the vehicle dynamics. Hence the applied platform pitch and roll serve only to recreate vehicle acceleration through tilt coordination. However, if available, vehicle pitch and roll data can be directly incorporated into the rotational channels as additional input. Additionally, since yaw does not affect the specific force generation, the yaw controller can be decoupled from the MPC. Thus, the yaw motion is managed separately using a simple washout filter to avoid additional computational expense.

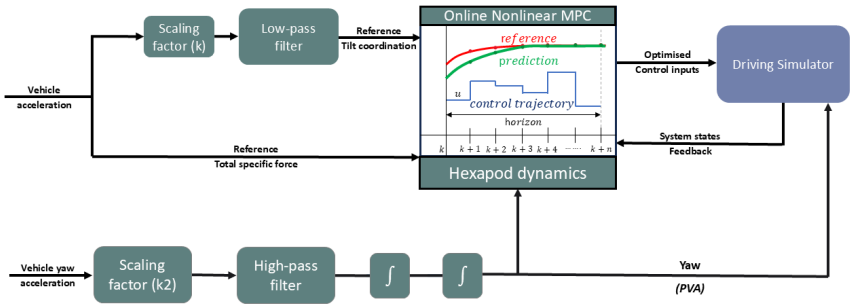

Figure 4.1: Structure of the five-DoF Autoscaling MCA

4.2.1. REFERENCES FOR THE ALGORITHM

REFERENCE FOR TILT COORDINATION

The algorithm aims to prevent platform pre-positioning by addressing its root cause in MPC: anticipatory motion triggered when required accelerations exceed what can be achieved within tilt rate limits. Unable to generate the desired force in time, the platform moves early, resulting in unrealistic specific force cues. This issue is mitigated by providing the tilt coordination with a reference signal that can be accurately followed while staying within the tilt-rate limit. Thus, the tilt-coordination receives a scaled-down low-pass vehicle acceleration data as a reference.

To enforce strict reference tracking, a high penalty is applied to the tilt coordination term in the objective function, preventing tilt components from compromising the accurate recreation of the total specific force.

DYNAMIC SCALING FACTOR DESIGN

To ensure accurate reference signal recreation, the required specific force and its rate of change must be less than or equal to the simulator's potential. Two scaling factors are derived, based on maximum achievable tilt angle and maximum rate change of tilt angle.

The first scaling factor, k_θ, is based on the maximum tilt angle, ensuring the reference specific force remains within the platform's tilt coordination capability:

$$\max|f_{spec,ref}| \quad \leq max|g\ sin(\theta_{tilt})| \tag{4.1}$$

$$k_\theta \quad = |\frac{g\ sin(\theta_{lim}|)}{\max|f_{spec,ref}}| \tag{4.2}$$

where 'θ_{lim}' is the maximum platform tilt angle.

The second scaling factor, k_ω , is derived from the tilt rate constraint to prevent false cues.

$$\max|\dot{f}spec,ref| \quad \leq \max|\omega_{tilt} g\cos(\theta_{tilt})| \tag{4.3}$$

here, the maximum value of '$cos(\theta_{tilt})$' is 1, and the tilt rate is limited to the perception threshold, ω_{thd}, $(3°/s)$. The scaling factor is thus given by:

$$k_\omega \leq \omega_{thd} \frac{g}{\max \dot{f}_{spec,ref}} \tag{4.4}$$

$$k = min(k_\theta, k_\omega, 1) \tag{4.5}$$

where k is the dynamic scaling factor that scales down the reference signal for the tilt coordination. In this work, for the choice of scaling factor the reference signal within the MPC prediction horizon is considered.

REFERENCE FOR TOTAL SPECIFIC FORCE

In this work, unscaled vehicular accelerations are used as the reference for total specific force. Given that tilt coordination has a separate reference, the MPC reproduces the remaining specific force solely through translational accelerations. This ensures optimal use of translational space while employing tilt coordination to enhance realism by complementing specific force reproduction through translational motion.

4.2.2. HEXAPOD DYNAMICS

The motion of the hexapod platform is defined in a state space form to facilitate implementation in the MPC. The base states include hexapod position (s_{hex}) and angular orientation (θ_{hex}). These base states are added to the state-space model with the relation

$$\dot{x}_{hex} = A_{hex} x_{hex} + B_{hex} u_{hex} \tag{4.6}$$

where the state vector, x_{hex}, comprises of the position, s_{hex}, translational velocity, v_{hex}, angular orientation, θ_{hex}, and angular velocity, ω_{hex}, of the hexapod and the input vector, u_{hex}, comprises of translational acceleration, a_{hex} and angular acceleration, α_{hex}. The matrix A_{hex} and B_{hex} represent the double integrator system of the inputs, adapted from [78].

As the algorithm is designed for both longitudinal and lateral degrees of freedom, each state comprises of components in x and y directions (roll and pitch for orientation). In this study, positive values correspond to forward, left, and upward orientations along the x, y, and z axes, with counterclockwise rotations indicated as positive.

4.2.3. OBJECTIVE FUNCTION

The objective function structure is similar to that of the frequency-splitting algorithm in Equation 3.4, but with changes in output terms and references. Instead of using translational motion, total specific force, and tilt coordination as output terms, this algorithm includes only tilt coordination and total specific force.

$$\begin{aligned} J_c = \quad & [\underbrace{(Y(x_k,u_k)-\hat{Y}_k)^T W_Y (Y(x_k,u_k)-\hat{Y}_k)}_{output\ terms} \\ & + \underbrace{(X_k-\hat{X}_k)^T W_X (X_k-\hat{X}_k)}_{state\ terms} + \underbrace{J_k^T W_J J_k}_{jerk\ terms} \\ & + \underbrace{(U_k)^T W_U (U_k)}_{input\ terms} + \underbrace{\delta^T w_\delta \delta}_{slack\ term} \ ] \end{aligned} \tag{4.7}$$

$$Y(x_k,u_k) = [f_{spec}\ G_{loc}] \tag{4.8}$$

$$W_Y = [w_{f,spec}\ w_{G,loc}] \tag{4.9}$$

$$J_k = [j_{trans}\ j_{ang}] \quad W_J = [w_{j,trans}\ w_{j,ang}] \tag{4.10}$$

Penalising jerk in the cost function of an MPC-based MCA is a well established practice to reduce oscillations in the specific force. We approximate jerk using the acceleration change over time-steps divided by the time-step $j(k) = \frac{a(k)-a(k-1)}{Ts}$. This approach avoids the need to add jerk as a system state, reducing computational complexity. The state term $(x_k - \hat{x}_k)$ introduces 'washout' by bringing the platform back to its neutral position $\hat{x}_k$. The input term (U_k) penalises high input values.

In Equation 4.7, the user defined (tunable) parameters are the weighting matrices W_Y, W_U, W_X and w_δ. W_X is a diagonal matrix with weights corresponding to the states being its diagonal elements. The washout weights w_s and w_θ are time varying and are defined in a later subsection.

The slack variable, δ, represents the deviation of the tilt-rate from the soft constraint limit (perception threshold).

PLATFORM CONSTRAINTS

Unlike a real vehicle, a driving simulator is restricted to a maximum displacement and maximum tilt angle, specific to the simulator used. This work uses the workspace limitations of Delft Advanced Vehicle Simulator (DAVSi).

DAVSi is a 6-DoF moving-based driving simulator [20], capable of generating acceleration up to 1 g in all directions and can simulate motions up to the frequency of 10 Hz. The considered limits of the platform motion are given in Table 4.1. As the algorithm includes yaw washout as a separate controller, conservative limits are chosen for translational and rotational displacement. Additionally, the soft constraint used to define the tilt-rate perception limit is formulated as

$$\begin{aligned} -\omega_{thd} &\leq \omega_{hex} + \delta \\ \omega_{hex} - \delta &\leq \omega_{thd} \\ 0 &\leq \delta \end{aligned} \tag{4.11}$$

Table 4.1: Limits for the simulator and the used MPC limits

Quantity	Platform physical limit	Defined MPC limit
θ_{hex}	$\pm 30deg$	$\pm 20deg$
v_{hex}	$\pm 7.2m/s$	$\pm 7.2m/s$
a_{hex}	$\pm 9.81m/s^2$	$\pm 9.81m/s^2$
s_{hex}	$\pm 0.5m$	$\pm 0.3m$

where ω_{thd} is the perception threshold limit (3 deg/s). δ is a positive slack variable which is penalised in the cost function to keep its value low. Hence, the tilt-rate soft constraint limit is allowed to be violated, however, any violation of the constraint is penalised, to minimise it.

WORKSPACE MANAGEMENT

The simulator platform has the maximum potential of recreating the specific forces at its neutral position. To ensure the platform remains near its neutral position, we penalize its states in the cost function. In this work, we use non-linear weights (based on the platform orientation and position) for the washout instead of constant weights. This allows a single non-linear setting for all scenarios rather than tuning the washout weights for each scenario.
The non-linear weights are defined as

$$w_s = \frac{k_1}{k_2 * (|s_{hex}| - s_{lim})^2 + \Delta} \tag{4.12}$$

$$w_\theta = \frac{k_3}{k_2 * (|\theta_{hex}| - \theta_{lim})^2 + \Delta} \tag{4.13}$$

where k_1, k_2 and k_3 define the shape of the weight function, s_{lim} and θ_{lim} are the defined limits for the platform for displacement and tilt angle. Δ (here 0.01) is a small value added to the denominator to avoid singularity. The selected values are $k_1 = 1$, $k_2 = 50$ and $k_3 = 0.1$, these values were manually tuned to ensure that the penalisation is low near the neutral position, while high, close to the platform limits.

4.2.4. YAW CHANNEL

The fifth DoF, yaw, is controlled separately using a parallel washout channel, ensuring reduced computational complexity. The first-order high-pass filter used for this purpose is given as

$$HP = \frac{s}{s + 2\pi v_{yaw}} \tag{4.14}$$

where v_{yaw} is the cutoff frequency for the high pass filter. In this work, we use the value of 0.0159 Hz for this cutoff frequency.

4.2.5. WEIGHT SETTINGS

To ensure a fair comparison the penalisation weights on tilt angle, translational displacement, translational jerk, angular jerk and slack variable are kept the same as used in Sub-

section 3.3.2. Additionally the time step and prediction horizon length is also kept the same as in Chapter 3. As the output terms vary in the cost terms of the two MCAs, the weights for these terms also change. In the autoscaling MCA priority is given to the tilt-coordination to follow its reference accurately, hence the weight for tilt-coordination reference tracking is selected to be 5 times higher than for specific force tracking (the weight used for specific force tracking is unity). However, as the tilt-coordination is forced to begin at the onset of the manoeuvres, pre-positioning in the translational workspace can be observed by the occupant of the simulator. To resolve this, the translational velocity of the platform is penalised. Varying the velocity penalty from 0 to 1 shows an insignificant difference. However, a penalty of 10 resulted in an improved solution, with reduced pre-positioning and limited adverse effect on the rendered profile.

YAW WASHOUT

The tuning parameter for the yaw washout was the cut-off frequency of the washout filter. The cut-off frequency for the yaw washout was varied between 0.0159 Hz (0.1 rad/s) to 0.1592 Hz (1 rad/s).

Since human perception is primarily sensitive to rotational velocities, the selection of the cut-off frequency is chosen based on desirable rotational velocity tracking. It is also essential to ensure that the yaw angle remains within acceptable limits (20 deg for this work). Based on these considerations, a cut-off frequency of 0.0159 Hz is chosen for this study.

4.2.6. BENCHMARKING

As pre-positioning was identified to occur with the subjective validation of the frequency splitting algorithm Chapter 3, it is chosen as the benchmark for this study.

SCENARIO DESCRIPTION

To compare the realism and immersion of the algorithm in the driving simulator, real-vehicle driving data from an experiment conducted by our group at the Valkenburg track was utilised [81]. Given the experiment's duration, specific sections were chosen for this study, including multi-turns with acceleration and braking, a slalom maneuver, and a lane-change maneuver, capturing a variety of naturalistic driving scenarios.

The total scenario duration was deliberately limited to 110 seconds to minimize the risk of simulator sickness and potential bias in the study.

4.2.7. FIDELITY CRITERIA

In this work, the algorithm is evaluated both subjectively and objectively. For the objective comparison, the shape similarity, root mean squared of the specific force and the timing of the initiation of the tilt-coordination compared to the onset of the vehicle maneuvers is considered. On the other hand, for subjective assessment the participants were asked to rate the realism of the ride based on realism of cornering and braking, the amount of unnatural instances/false cues observed during the ride and are asked for any instance of pre-positioning observed.

4.3. HUMAN-IN-THE-LOOP EVALUATION

This section describes the human-in-the-loop driving simulator experiment and its subjective evaluation. Perceived driving simulator fidelity was evaluated from the perspective of passive users, representative of users of automated vehicles. In pilot studies, we even aimed to evaluate perceived fidelity with the eyes off the road using a tablet for a non-driving task. However, with vision limited to the vehicle interior, the MCAs were not perceived as representative of driving. This was resolved by adding exterior vision and instructing participants to observe the road.

4.3.1. EXPERIMENTAL PROCEDURE

All participants gave their informed consent prior to participating. The Human Research Ethics Committee of TU Delft, The Netherlands, approved the experiment protocol under application number 3965.

In total, 8 participants from the pool of students and employees of TU Delft participated in the study (mean age: 25.5, std: 2.5 years, 3 females, 5 males). All participants were subjected to both the proposed algorithm and frequency splitting drives sequentially within one session, to compare the subjective evaluation of the realism and feel of the MCAs.

Before the experiment, the participants underwent a concise briefing session to familiarise themselves with the questionnaire and to understand the objective of the experiment. During the experiment, two-way communication was established between the experimenter and the participant via bluetooth headphones and microphones.

The visualisation was projected onto a screen in front of the simulator, with side windows and windshield partially covered to block peripheral views and eliminate cues revealing platform motion. Dynamic visual compensation adjusted the projection to match the platform's movements, ensuring the visuals stayed aligned with the motion felt by the participants despite the screen being outside the cockpit.

Following the briefing, participants underwent a series of six two-minute drives in fully automated mode with minimal time between drives to facilitate a clear comparison. After each drive, participants completed an absolute grading questionnaire to assess various aspects of the driving experience. These questions can be found in Table 4.4. To ensure fair comparison, the sequence of algorithms was varied for different participants, maintaining either the pattern (A B A B A B) or (B A B A B A), where A represents the frequency-splitting and B represents autoscaling MCA respectively.

The first round for each algorithm aimed to immerse participants in the simulation environment and was not graded. Participants provided ratings in a 5-point scale for the second and third rounds based on the provided questionnaire. At the end of the experiment, the participants were asked to fill in a comparative questionnaire.

RESULTS AND DISCUSSION

This section presents the results of both objective and subjective evaluations of the two algorithms, followed by an analysis of the findings.

4.3.2. OBJECTIVE EVALUATION

SPECIFIC FORCE TRACKING

The comparison between the profiles rendered through the autoscaling MCA and the benchmarking frequency-splitting algorithm for real driving data is presented in Figure 4.2 and Figure 4.3.

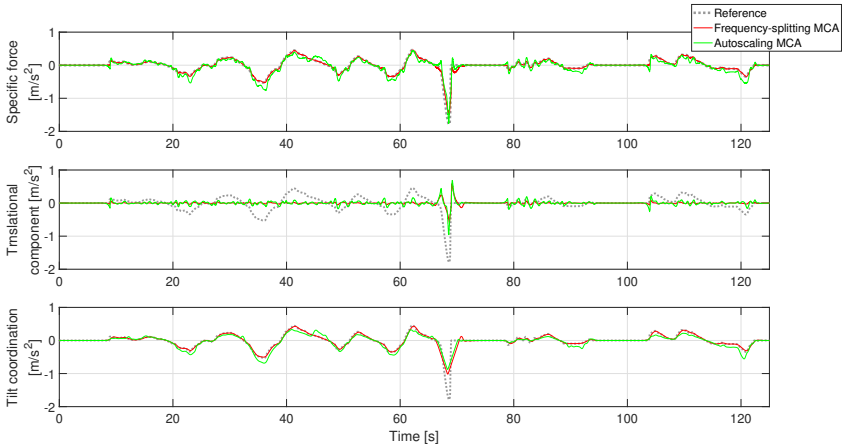

Figure 4.2: Comparison of the response of Autoscaling and Frequency-splitting MCAs: longitudinal acceleration.

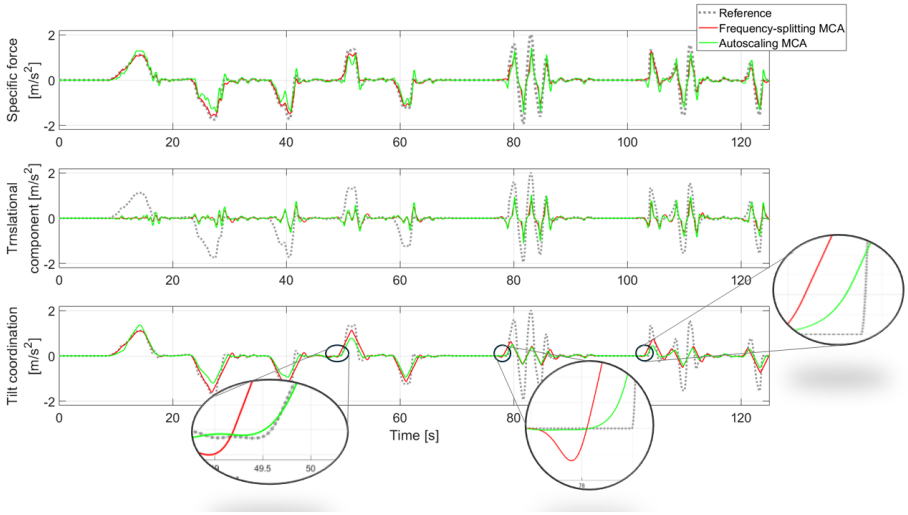

Figure 4.3: Comparison of the response of Autoscaling and Frequency-splitting MCAs: lateral acceleration.

It is worth mentioning that the autoscaling MCA receives unscaled vehicle accelerations, whereas the frequency-splitting algorithm used a reference scaled down by a factor of 0.3 for longitudinal acceleration and 0.4 for lateral acceleration. The reference signal presented in Figure 4.2 and Figure 4.3 corresponds to the reference chosen for the frequency splitting algorithm, where coincidentally, the rendered profiles via the two algorithms have a similar magnitude.

For the frequency-splitting algorithm, the RMSE of the longitudinal specific force tracking is 0.0466 while for the lateral tracking it is 0.1943. On the other hand, for the autoscaling MCA the RMSEs for longitudinal and lateral specific force tracking are 0.1210 and 0.2459 respectively.

Additionally, the shape similarity factors for the rendered profiles were analysed. For the longitudinal direction, the shape similarity factor is 0.9787 for the frequency-splitting algorithm and 0.9312 for the autoscaling MCA. Similarly, for the lateral direction, the frequency-splitting algorithm achieves a shape similarity coefficient of 0.9519, whereas the autoscaling MCA yields 0.9208.

Table 4.2: Tracking Performance for the two algorithms

Algorithm	Performance				
	Specific force tracking			Shape similarity factor	
	RMSE long. [m/s^2]	RMSE lat. [m/s^2]	RMSE tot. [m/s^2]	long. [-]	lat. [-]
Autoscaling MCA	0.1210	0.2459	0.2740	0.9312	0.9208
Frequency-splitting MCA	0.0466	0.1943	0.1998	0.9787	0.9519

WORKSPACE UTILISATION

A comparison of workspace utilisation, based on profiles generated by the autoscaling MCA and the benchmarking frequency-splitting algorithm, is presented in Table 4.3. The autoscaling MCA utilises the translational workspace more, while the frequency-splitting algorithm exhibits higher usage of the rotational workspace. Although both algorithms respect the tilt-rate perception threshold, the FS MCA achieves higher platform tilts by initiating tilt earlier, causing pre-positioning, whereas autoscaling MCA avoids this by reducing the reference specific force, eliminating the need for early motion.

Table 4.3: Workspace utilisation for the two algorithms

Algorithm	Workspace utilisation			
	RMS displacement [m]	RMS velocity [m/s]	RMS angular displacement [deg]	RMS angular velocity [deg/s]
Autoscaling MCA	0.0423	0.0770	2.2339	1.8113
Frequency-splitting MCA	0.0334	0.0682	2.6181	2.0091

PRE-POSITIONING

In Figure 4.2, it can be observed that, for the autoscaling MCA the translational accelerations generate a higher component of specific force compared to the frequency

splitting MCA. Additionally, the onsets of the manoeuvres are also at the correct instances, however, due to the gradually varying and continuous nature of longitudinal acceleration, this difference is not distinctly observed. On the other hand, it can be observed in Figure 4.3, that for lateral motion, the frequency-splitting algorithm exhibits pre-positioning within the rotational workspace at various instances to prepare for future motion. In contrast, the autoscaling MCA significantly reduces pre-positioning. The motion onset in the autoscaling MCA occurs at the correct instances, with a higher contribution from translational motion compared to the frequency-splitting algorithm.

SUBJECTIVE EVALUATION

This subsection compares the two algorithms based on the conducted experiment. Table 4.4 presents the obtained responses in detail, including their statistical significance.

Table 4.4: Subjective evaluation and statistical analysis (on a scale from 0-5)

Criterion	Algorithm	All data				
		mean	std.	median	p-value	significance
How closely did the ride's motion correspond to the video?	AU	3.75	0.71	4	0.0796	No
	FS	3.38	0.52	3		
How close did the cornering feel compared to a real car?	AU	4	0.76	4	0.0072	Yes
	FS	3	0.53	3		
How realistic did the deceleration feel compared to a real vehicle drive?	AU	3.5	0.53	3.5	0.1705	No
	FS	3.75	0.46	4		
Aggressiveness of Section 1 : multi-turn	AU	3.75	0.46	4	0.0750	No
	FS	3.125	0.64	3		
Aggressiveness of Section 2 : slalom	AU	2.5	0.76	2	0.5983	No
	FS	2.625	0.52	3		
Aggressiveness of Section 3 : lane change	AU	2.75	0.46	3	0.0112	Yes
	FS	2.125	0.35	2		
Was the ride disorienting or sickening?	AU	2	0.89	2	0.3506	No
	FS	1.75	0.76	2		
Were there any unnatural motions that did not match real driving?	AU	2.25	0.46	2	0.0025	Yes
	FS	3	0.76	3		

COHERENCE OF THE MOTION WITH THE VIDEO

The autoscaling MCA received an average rating of 3.75 out of 5 (75% realism), while the frequency-splitting algorithm scored 3.25 (65% realism). Both algorithms provided a coherent ride experience relative to the video, with no statistically significant difference between them.

Post-experiment verbal feedback indicated that the limiting factor in perceived coherence was the video quality, rather than the platform's motion.

CORNERING REALISM

The autoscaling MCA received an average rating of 4.0 out of 5, with a median of 4.0, whereas the frequency-splitting algorithm was rated 3.0 on average, with a median of 3.0. A statistically significant difference was observed between the ratings, indicating a preference for the autoscaling MCA in terms of cornering realism.

Participants reported instances of pre-positioning in the frequency-splitting algorithm during post-experiment verbal feedback, which may have influenced its lower realism rating.

REALISM OF BRAKING

The autoscaling MCA received an average rating of 3.5 (median: 3.5), while the frequency-splitting algorithm scored 3.75 (median: 4). However, the difference was not statistically significant. In post-experiment feedback, participants found the frequency-splitting algorithm more comfortable, whereas the autoscaling MCA felt abrupt during acceleration and braking.

OVERALL REALISM

In the comparative questionnaire, 7 out of 8 participants found the autoscaling MCA more realistic overall, showing a clear preference for its motion cueing.

AGGRESSIVENESS

The autoscaling MCA was rated more aggressive in the first and third sections, while the second section scored higher for the frequency-splitting algorithm. However, statistical significance was found only in the third section, preventing a general conclusion on the autoscaling MCA's aggressiveness, especially given its dynamic scaling. Detailed statistics are provided in Table 4.4.

Despite this, 6 out of 8 participants in the comparative questionnaire perceived the autoscaling MCA as more aggressive overall.

SICKNESS

After the 2-minute ride, participants rated the algorithms on their sickening or disorienting effects. The autoscaling MCA received an average rating of 2, while the frequency-splitting MCA scored 1.75, with both medians at 2. This indicates no significant difference in the motion profiles' sickening effects.

UNNATURAL MOTION/ FALSE CUES

The autoscaling MCA received an average rating of 2.25 (median: 2), while the frequency-splitting MCA scored 3.0 (median: 3). This statistically significant difference suggests that the autoscaling MCA generates fewer false cues.

In the comparative questionnaire, seven participants reported more false cues with the frequency-splitting MCA, while one found the autoscaling MCA to produce higher unnatural motions. Additionally, six out of eight participants observed pre-positioning in the frequency-splitting algorithm, whereas only one reported it in the autoscaling MCA, occurring during a single corner.

DISCUSSION

The autoscaling MCA aims at eliminating two major issues encountered in MPC-based MCAs, one being pre-positioning, where the platform prepares itself for the future motion, moving prematurely. The second issue being the necessity to scale down the reference signal to precondition it for desirable recreation of specific scenarios. The performance of traditional MCAs depends highly on the preconditioning (scaling) parameters. In this work, we present the autoscaling MCA which automatically derives a time varying scaling factor for the tilt coordination reference.

As shown in Figure 4.3, the autoscaling MCA reduces roll pre-positioning in lateral motion, though it does not eliminate it entirely. This is due to total specific force error minimization in the objective function. A higher penalty on tilt coordination improves adherence to the reference, leading to reduced pre-positioning, as the platform produces dynamically scaled-down accelerations via tilt coordination.

The scaling factor is determined based on the platform's capability to reproduce the maximum specific force via tilt coordination, while ensuring that the resulting rotational velocity remains within human perception thresholds. In this context, the maximum allowable tilt rate governs the maximum rate of change of specific force, thereby playing a critical role in defining the scaling factor. This ensures the simulator always has the potential to generate the scaled-down reference for tilt coordination, maximising the simulator's potential in recreating specific forces. Since the platform can always achieve its reference tilt coordination, premature tilting is avoided, reducing pre-positioning.

Referencing tilt coordination and total specific force ensures that the algorithm tracks the scaled-down tilt reference while using translational motion to recreate the remaining specific force. This is evident in workspace utilization, where the autoscaling MCA relies less on tilt workspace and more on translational workspace compared to the frequency-splitting algorithm. As a result, tilt coordination serves as a supporting mechanism for generating higher specific forces rather than being the primary contributor. Studies have shown that translational motion has a greater impact on realism than tilt coordination [85], [86].

Based on the objective performance indicators, however close, the frequency splitting algorithm showed a better performance, with higher shape similarity and lower RMSE for the specific force tracking. Both the algorithms achieved high values for their performance, however the objective KPIs indicated frequency splitting algorithm to perform better. However, these KPIs are based on the total specific force, combining tilt coordination and translational accelerations. Thus, conflicting motions in translational workspace and tilt coordination may create a motion that does not correspond to the actual specific force. One such case is when the tilt and translational components cancel each other to create a zero net specific force. This corresponds to the no motion case, however, the opposite motions of tilt and translation can still be picked up by the participant.

Hence, in this work, the tilt coordination is treated as a separate reference with higher penalisation, and the rest of the specific force is left for the translational motion to generate. The reference on tilt coordination is scaled down rather than that on the translation motion, as tilt produces sustained forces on the occupant's head, thus a premature motion creates a sustained acceleration perception which is probable to be perceived more than a pre-positioning motion in translational workspace.

4.4. CONCLUSION

In this work, an autoscaling framework for a model predictive control-based cueing algorithm is developed. The developed algorithm is capable of scaling the vehicular accelerations on itself without the need to precondition the vehicular accelerations or the reference specific force.

The dynamic scaling factor ensures that the reference can be tracked without the need to prematurely tilt the platform to obtain the demanded specific force. As the dynamic scaling factor reduces the demanded acceleration to an achievable reference, the problem of pre-positioning reduces.

In the conducted experimental validation, 87.5% of participants (7 out of 8) indicated autoscaling algorithm renders a more realistic ride. Additionally, only one participant indicated having observed pre-positioning in the simulation generated via the autoscaling algorithm, compared to 6 participants for the frequency-splitting algorithm.

Even when the objective metrics like RMSE specific force and shape correlation factors are higher for the frequency splitting algorithm, the autoscaling algorithm is rated to be more realistic by human participants. This indicates that while specific force RMSE and shape correlation factor are essential and good metrics to evaluate the performance of the cueing algorithms. Additional considerations must be taken into account to ensure satisfactory recreation of a driving scenario. The difference between the onset of the platform motion and the onset of the manoeuvre is one of them.

Additionally, the autoscaling algorithm utilises the translational workspace more than the frequency-splitting algorithm while relying less on tilt coordination. As a result, a higher proportion of specific force is recreated through translational motion compared to the frequency-splitting algorithm, making it closer to an actual vehicle ride, which primarily consists of translational accelerations.

5

Towards Sickness-Free Driving Simulation: Optimising Motion Cueing for Human Comfort

Success is a journey, not a destination

Ayrton Senna

This chapter will serve as basis for a future publication: **V. Jain**, V. Kotian, A. Lazcano, D.M. Pool, R. Happee, B. Shyrokau "Towards Sickness-Free Simulation: Optimising Motion Cueing for Human Comfort".

ABSTRACT

The utilisation of driving simulators in the automotive industry is on the rise, serving as an invaluable tool for evaluating vehicle comfort and user acceptance of emerging technologies. While driving simulators aim to replicate the real-world driving experience, disparities in motion between the simulator platform and actual vehicles can lead to varying degrees of motion sickness. This paper presents a Motion Cueing Algorithm that explicitly and uniquely incorporates motion sickness mitigation into a model predictive control formulation. A 6-DoF subjective vertical conflict model is used within the motion cueing algorithm's cost function to penalise predicted sensory conflict directly, alongside platform-specific force error. This enables the algorithm to optimise for both accurate motion reproduction and reduced motion sickness

Objective evaluations show that increasing the weight on predicted sensory conflict in the motion cueing algorithm cost function leads to a reduction in predicted sickness levels by up to 70%, when transitioning from a configuration focused solely on specific force tracking to one prioritising sickness mitigation. This improvement comes at the cost of reduced specific force tracking accuracy. The lowest sickness levels were predicted with negligible mechanical motion.

To balance motion fidelity and sickness reduction, a compromise weighting was selected based on pilot studies, with a 1:9 ratio between specific force tracking and motion sickness mitigation. In the objective analysis, this compromise weighting achieved a 33% reduction in predicted motion sickness (from MISC 3 to 2) while increasing specific force error from $0.0272\,m/s^2$ *to* $0.2157\,m/s^2$*, where shape similarity was reduced from* 0.9990 *to* 0.9705*.*

Human-in-the-loop driving simulator experiments with a realistic automated driving scenario were conducted using four algorithm configurations: adaptive washout (industry benchmark), No Motion, and two novel optimisation-based algorithm variants (optimal specific force tracking and compromise weighting, which accounts for both specific force fidelity and motion sickness mitigation). Participants reported motion sickness levels every 30 seconds. Optimal specific force tracking and adaptive washout achieved similar motion sickness and perceived realism ratings. Compared to these, the compromise weighting resulted in over 50% reduction (average MISC level 3 *to* 1.5*) in reported sickness without a statistically significant reduction in perceived realism. As predicted, the no-motion condition provided the lowest sickness level, which came at the cost of a lower perceived realism.*

The proposed algorithm thus offers a significant advancement in achieving an optimal balance between comfort and realism in driving simulator motion cueing, supporting simulators' expanded use in vehicle development.

5

5.1. INTRODUCTION

SINCE the inception of driving simulator technology, a key challenge has been to bring the driving simulator experience closer to the real vehicle experience.

One such challenge is an escalated risk of motion sickness in the driving simulator environment. Motion sickness is a malady characterised by symptoms such as nausea, dizziness, and discomfort. It can be experienced by regular travellers, astronauts, and simulator users alike. Around 60% of the population experiences motion sickness symptoms and about a third of the population has suffered from nausea at least once by car travel before the age of 12 [87].

Various theories have been proposed to explain the underlying cause of motion sickness [8], [10], [88]. Among these, the most widely accepted explanation is the Sensory Conflict Theory [8], which posits that motion sickness arises when there is a mismatch between the motion perceived by the sensory systems and the motion expected to be sensed by the brain. In essence, any discrepancy between sensed and expected motion contributes to the onset and severity of motion sickness.

In the context of driving simulators, the problem of motion sickness is amplified due to the intricate interplay of visual, vestibular, and proprioceptive cues. When the motion experienced in the simulator diverges from the expectation of a real vehicle, it triggers a sensory conflict that can lead to motion sickness.

The issue is further exacerbated by variations in visual fidelity and motion cueing strategies. A recent meta-analysis demonstrated that the development of simulator sickness is influenced by the visual fidelity of the simulated environment [32]. In another comparative study [33], three motion cueing strategies were assessed against a fixed-base setup. While motion-enhanced simulations improved perceived realism, they were also associated with increased sickness incidence, highlighting a trade-off between immersion and physiological comfort.

This paper addresses the critical issue of motion sickness in driving simulators and presents an innovative solution, a motion cueing algorithm crafted to reduce motion sickness while preserving a realistic perception of motion. The algorithm integrates a 6-Degree of Freedom (6-DoF) Sensory Conflict (SVC) model, a predictive framework capable of assessing motion sickness [89].

Recent developments in motion cueing increasingly rely on Model Predictive Control (MPC)-based strategies, owing to their ability to generate high-fidelity motion cues while respecting the physical workspace limitations of the simulator. By incorporating a predictive horizon, these methods anticipate future motion demands, enabling smoother and more perceptually accurate platform behaviour. The algorithm proposed in this study builds on this optimisation-based approach, extending it to directly account for motion sickness through an integrated cost formulation.

Various machine learning models have been proposed for motion sickness prediction[90]–[92]. However, they typically rely on physiological data which has to be collected with human in the loop experiments. Such models may become valuable when it is proven that they accurately predict the MISC. This would enable replacing the distracting collection of MISC data by collecting physiological data. The SVC model only uses the motion stimuli experienced by occupants, making it particularly suitable for mitigating motion sickness through motion cueing. Its simplicity is especially advantageous in

this context, as future physiological states cannot be predicted, whereas future motion profiles are explicitly determined within the MPC optimization, which incorporates the motion sickness prediction model.

The MCA minimises the sensory conflict predicted based on the motion data generated by the simulator platform. Machine learning models would not have such an intermediate measure as sensory conflict and thus would not fit this approach. To minimise the sensory conflict, the MCA incorporates a cost function that simultaneously accounts for specific force errors as well as sensory conflict errors. By doing so, the balance between optimised motion perception (specific force tracking) and reduced likelihood of inducing motion sickness (sensory conflict minimisation) can be actively controlled.

This research represents a pivotal step toward enhancing the utility and overall safety of driving simulators, both by improving user comfort and by enabling safe, controlled testing of automated driving systems. The motion cueing algorithm presented herein offers a flexible solution for balancing motion perception and user comfort, enabling the simulator to maintain perceptual credibility while reducing motion sickness. However, this comes at the cost of real-time feasibility — the algorithm operates with a real-time factor of approximately 2.1, requiring offline execution. In this pursuit, we explore the intricate relationship between human perception, motion simulation, and motion sickness.

The contributions of the work are outlined below:

- Incorporated a six-degree-of-freedom Subjective Vertical Conflict motion sickness model, for the first time, directly into a motion cueing algorithm as part of its cost function.
- Formulated a multi-objective optimisation framework that jointly considers motion sickness reduction and reproduction of motion perception compared to real-world driving.
- Demonstrated that the inclusion of the motion sickness model allows for an adjustable trade-off between motion fidelity and predicted motion sickness, enabling the algorithm to prioritise either physical realism or passenger comfort based on application-specific requirements.
- Conducted Human-in-the-loop experiments, which confirm that the proposed algorithm effectively mitigates motion sickness symptoms, while having minimal impact on motion perception.

The chapter is organised as follows: Section 5.2 discusses existing work in the domain of motion cueing and driving simulator experiments related to motion sickness. The proposed algorithm and the formulation of the optimal control problem (OCP) are detailed in Section 5.3, followed by the algorithm configuration in Section 5.4. The benchmark used for the study is described in Section 5.5. Objective evaluation is presented in Section 5.6, while the experimental procedure and subjective assessment are addressed in Section 5.7. The results are analysed and discussed in Section 5.8, and the conclusions are presented in Section 5.9.

5.2. RELEVANT STUDIES

In the field of motion cueing, recent research primarily focuses on Model Predictive Control (MPC)-based strategies, aiming to reduce false cues while improving computational efficiency.

To address computational cost, explicit MPC techniques precompute control solutions for offline storage in look-up tables [23]. This significantly reduces online computation but presents challenges in terms of memory requirements and scalability, particularly for large prediction horizons and fast sampling rates due to exponential increases in control region complexity.

A hybrid MPC approach was proposed to balance these trade-offs by combining explicit (offline) and implicit (online) MPCs [24]. In this method, a 4 DoF explicit MPC provides an initial guess to the implicit MPC, facilitating faster convergence.

Further, performance improvements have been realised by efficiently splitting acceleration references within the MPC framework [67]. This method separates vehicle accelerations into high-frequency and low-frequency components using filters, then applies them to translational acceleration and tilt coordination, respectively. This enhances specific force tracking and convergence speed.

Although these approaches improve motion fidelity and computational efficiency, they do not explicitly aim to reduce simulator sickness. In contrast, research on motion planning in real vehicles has investigated motion sickness mitigation more directly. These studies focus on modifying trajectories to reduce discomfort from accelerations and jerks.

To reduce motion sickness in trajectory planning, several studies incorporated the Motion Sickness Dose Value (MSDV) into optimisation criteria [34], [38], [39], [93]. While effective in real vehicles, such methods inherently alter the drive experience by modifying the vehicle's dynamics, an approach unsuitable for simulators where maintaining perceived fidelity is critical.

A recent meta-analysis on simulator sickness [32] reviewed 41 studies and reported modest sickness levels across different simulator configurations. It found that visual fidelity significantly reduced sickness in motion-base simulators but not in fixed-base systems. Mechanical motion had a minor, non-significant effect on sickness (SS=0.077 for motion base vs. SS=0.096 for fixed base; p=0.105). Active driving reduced sickness compared to passive driving (SS=0.073 vs. SS=0.117; p=0.073), although these comparisons were across different studies. Notably, active driving rarely induces sickness in real vehicles, highlighting a gap between simulation and reality.

Romano et al. [33] compared fixed-base and three motion-cueing strategies, finding that motion improved perceived fidelity but did not significantly affect sickness levels. Similarly, while motion cueing research often targets perceptual fidelity, there is a lack of approaches explicitly designed to reduce simulator sickness.

Several studies suggest that driving simulators hold potential for motion comfort and sickness research. Bellem et al. [82] showed strong correlation in comfort ratings between real and simulated driving using appropriate MCA scaling. Works in[94] and [95] emphasised that moving-base simulators can effectively evoke motion sickness when tuned correctly. However, none of these studies propose an algorithm to mitigate motion sickness in driving simulators.

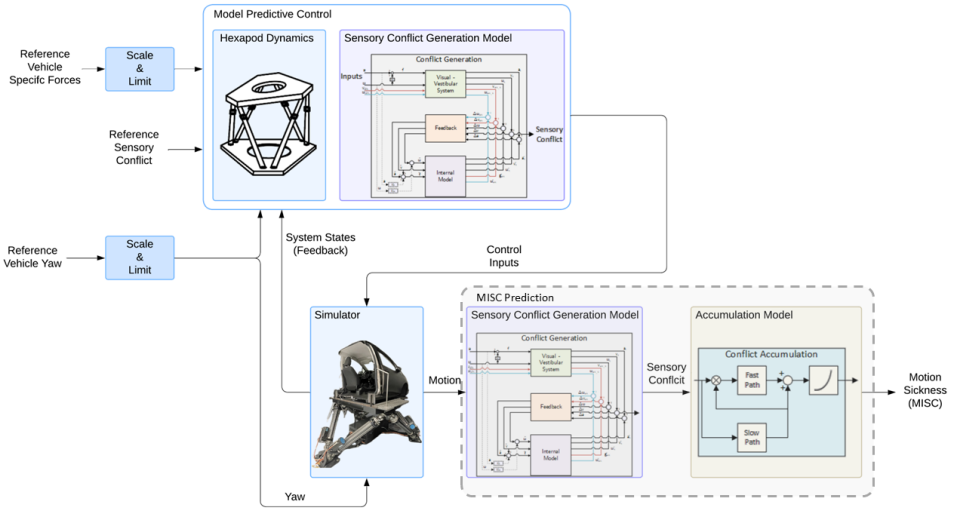

Figure 5.1: Structure of the SVC MCA; the two blocks at the bottom right, highlighted by the dashed gray box, are not part of the MCA and are only used to predict the actual resulting Motion Sickness over the whole experiment duration.

To the best of the authors' knowledge, no prior work has established a motion cueing strategy explicitly aimed at reproducing or reducing motion sickness in a simulator environment. This work tackles the mitigation of sickening stimuli arising from the platform motion stimuli of the driving simulator.

5.3. MOTION CUEING STRATEGY

Figure 5.1 illustrates the structure of the proposed MPC-based motion cueing algorithm. The MPC receives two reference inputs: one for motion sickness and one for vehicle specific forces. The reference sensory conflict is chosen to be zero in this paper, aiming to minimise motion sickness. However, this framework can also be used to reproduce sickness as occurring in real vehicles. This can be achieved adding another SVC block which derives the conflict occurring in vehicles.

In this work, the proposed algorithm explicitly optimises the trade-off between motion sickness mitigation and motion perception fidelity. The corresponding optimal control problem cost function is introduced later in the chapter (see Equation 5.17).

5.3.1. MOTION SICKNESS MODEL

The MPC-based algorithm needs a motion sickness prediction model to calculate a motion sickness metric (J_{MS}) for the cost function (J_c). For this, we use the Subjective Vertical Conflict with Visual Rotational velocity (SVC-VR) as described by [96]. The model was first introduced by [97] and later validated and found to be favourable for motion sickness predictions in vehicles for a population by [98]. This model ([97]) gave Motion

Sickness Incidence (MSI) as output a group-averaged metric giving the percentage of people who will get motion sick. This is not suitable as we need a scale based on the severity of motion sickness in an individual. This way we will have better control on how much the severity of sickness varies with different algorithms. For this, we used the model by [96], which adapted the model by [97] to predict motion sickness for an individual in MIsery SCale (MISC). This model accepts specific forces, angular rotations and visual flow (visual angular rotation) as inputs and gives motion sickness in MISC as output.

It is important to mention that the platform's motion is different from the visual cues. In this study we simulate conditions with out of the window view. Thus, the vehicle angular velocities are given for the vision angular velocity input to the SVC model, while the vestibular system is provided with the platform motion.

The motion sickness score output from the accumulation model has a large time constant due to the slow dynamics of the accumulation model. The high time constant of the accumulation model implies that a long prediction horizon would be required for it to function effectively. However, as demonstrated in Chapter 2, optimising for motion sickness over a short horizon can still lead to effective reduction of accumulated sickness over longer durations, provided that an appropriate short-term proxy, such as instantaneous sensory conflict, is used. As we optimise the motion at each time instant, we want to calculate the instantaneous response to the motion stimuli which drives motion sickness. This is the sensory conflict that can be obtained by the first half part of the model, often termed the 'sensory conflict generation' model shown in Figure 5.1.

We converted a Simulink implementation of the SVC-VR model into ordinary differential equations, which our MPC solver can use. The ordinary differential equations for the SVC-VR model are given below:

$$\dot{v}_s = \frac{f_{spec} - v_s}{\tau} - \omega_s \times v_s \tag{5.1}$$

$$\dot{\omega}_s = \dot{\omega} - \frac{\omega_s}{\tau_d} \tag{5.2}$$

$$\dot{\hat{v}}_s = \frac{\hat{f}_s - \hat{v}_s}{\tau} - \hat{\omega}_s \times \hat{v}_s \tag{5.3}$$

$$\dot{\hat{\omega}}_s = \frac{(K_{\omega,c} + K_\omega)\dot{\omega} + K_{\omega,vis}\dot{\omega}_{vis} - \frac{K_{\omega,c}}{\tau_d}(\omega_s - \hat{\omega}_s)}{1 + K_{\omega,vis} + K_{\omega,c}} - \frac{\hat{\omega}_s}{\tau_d} \tag{5.4}$$

$$\dot{\tilde{v}} = K_{vc}(v_s - \hat{v}_s) + K_{g,vis}(v_{vis} - \tilde{v}) \tag{5.5}$$

$$\dot{\hat{f}}_s = K_{vc}(v_s - \hat{v}_s) + K_{g,vis}(v_{vis} - \tilde{v}) + K_{ac}(f_s - v_s - \hat{f}_s + \hat{v}_s) + K_a \dot{a} \tag{5.6}$$

where $\hat{f}_s$ represents the estimated specific force vector, v_s and $\hat{v}_s$ are the sensed subjective vertical and estimated subjective vertical, respectively. ω_s and $\hat{\omega}_s$ are the sensed angular velocity and estimated angular velocity respectively. $\tau = 5\ s$, $\tau_d = 7\ s$, $K_{\omega,c} = 10$, $K_{a,c} = 1$, $K_{v,c} = 5$, $K_a = 0$, $K_\omega = 0$, $K_{\omega,vis} = 10$, $K_{g,vis} = 0$ are the parameters used for the SVC model taken from [89]. Here, τ and τ_d are the time constants corresponding to the

otoliths and the semicircular canals respectively. $K_{\omega,c}$, $K_{a,c}$, and $K_{v,c}$ are the vestibular feedback gains, K_a and K_ω are the anticipatory gains, $K_{\omega,\text{vis}}$ and $K_{g,\text{vis}}$ are the visual feedback gains.

The sensory conflict is derived by calculating the Euclidean norm or 2-norm of the difference between the sensed subjective vertical and estimated subjective vertical:

$$c_v = \|v_s - \hat{v}_s\|_2 = \left(\sum_{i=1}^{3}(v_{s_i} - \hat{v}_{s_i})^2\right)^{1/2} \tag{5.7}$$

$$J_{MS} = w_{con} \quad {c_v}^2 \tag{5.8}$$

where, w_{con} is the weight on the conflict, c_v, to create the sensory conflict term quantifying motion sickness (J_{MS}) used in the objective function in Equation 5.14.

The sensory conflict is one-dimensional. The accumulation of this sensory conflict drives the overall motion sickness scores. Minimising this sensory conflict over the MPC time horizon will result in a reduction of motion sickness.

However, for the weight selection of the cost function, it is better to calculate the motion sickness score in MISC over the full experiment duration to better understand the difference it makes in symptoms. Also, it is interesting to compare the calculated MISC at the end of the experimental session between the different weights. Hence, we use the entire model framework by [96], including the 'conflict accumulation' model as shown in the bottom right in Figure 5.1. To predict the variance in MISC across a population we simulate the MISC for 1000 individuals with varying motion susceptibilities. These parameters are sampled from the parameter distribution described in [89]. In that work, a 3-component probability distribution of parameter sets was generated for the model by [96], which can be sampled according to the desired motion sickness susceptibility. These parameter sets have been shown to generalise well for MISC predictions in new driving scenarios [89]. This makes it ideal to use for testing and selecting algorithms.

5.3.2. HEXAPOD/DRIVING SIMULATOR DYNAMICS

The motion of the hexapod platform is defined in a state-space form to facilitate implementation in the MPC. The base states include hexapod position (s_{hex}) and angular orientation (θ_{hex}). These base states are added to the state-space model with the relation

$$\dot{x}_{hex} = A_{hex}x_{hex} + B_{hex}u_{hex} \tag{5.9}$$

where the state vector, x_{hex}, comprises of the position, s_{hex}, translational velocity, v_{hex}, angular orientation, θ_{hex}, and angular velocity, ω_{hex}, of the hexapod and the input vector, u_{hex}, comprises of translational acceleration, a_{hex} and angular acceleration of each euler angle, α_{hex}. The matrices A_{hex} and B_{hex} represent the double integrator system of the inputs, adapted from [78].

As the algorithm is designed for both longitudinal and lateral degrees of freedom, each state comprises of components in x and y directions (roll and pitch for orientation). In this study, positive values correspond to forward, left, and upward orientations along the x, y, and z axes, with counterclockwise rotations indicated as positive.

5.3.3. MPC FORMULATION

To achieve realistic motion perception (one of the primary objective of the algorithm), vehicular accelerations are tracked using specific forces generated by the driving simulator. The specific force consists of two components that arise through translational accelerations and gravity. This specific force encapsulates the combined effects of accelerations and gravity as perceived by the human via the otoliths (part of the vestibular system). Therefore, the specific force is calculated at the estimated head coordinate system, thereby incorporating the effects of platform rotation.

The translational component is the acceleration of the platform. The gravitational force vector at the estimated head location, G_{loc}, is defined by the relation:

$$G_{loc} = R^T [0\ 0\ g]' \tag{5.10}$$

Here R is the transformation matrix that resolves gravitational force to the vectors corresponding to longitudinal, lateral and vertical body reference frame directions and g is the acceleration due to gravity, acting in the inertial vertical direction.

The total specific force is defined as:

$$f_{spec} = a_{hex} - G_{loc} \tag{5.11}$$

where a is the translational acceleration of the platform. The tilt component, G_{loc}, provides an additional pseudo acceleration to the occupant of the simulator. The specific force is the quantity to be tracked to achieve realistic motion perception.

This shapes our cost function term for the MCA defining the motion perception term (J_{MP}), which is given by:

$$J_{MP} = (f_{spec} - f_{ref})\ w_{spec}\ (f_{spec} - f_{ref})^T \tag{5.12}$$

To reduce motion sickness stimuli (the secondary objective of the algorithm), sensory conflict (Equation 5.7) needs to be minimised. Thus, the MPC includes the hexapod dynamics and the 6-DOF SVC model to predict the development of motion sickness over the prediction horizon.

Thus the complete analytical description of the dynamics of motion sickness development, through the platform motion, includes the following states:

$$x = [\theta_{hex}, \omega_{hex}, s_{hex}, v_{hex}, f_{tilt}, f_{all}, \hat{f}_{all}, \hat{v}_s, \omega_s, \hat{\omega}_s, v_s] \tag{5.13}$$

Here, f_{all} denotes the vector of specific forces in all three directions (x, y, z); $\hat{f}_{all}$ represents the estimated specific forces in those directions; and f_{tilt} corresponds to the tilt-generated specific force, which is equal to the local gravitational vector G_{loc}.

Having outlined the essential states for modeling motion sickness, we now delve into the objective function, a critical component guiding the optimization process.

OBJECTIVE/ COST FUNCTION

The objective of the algorithm is to reduce motion sickness through sensory conflict minimization, while maintaining a similar motion perception, via specific force tracking, these are the primary objectives of the algorithm.

In addition to the primary objectives, several auxiliary penalty terms are incorporated into the cost function. These terms support the performance of the Model Predictive Control (MPC) framework, particularly in the absence of an infinite horizon. Specifically, they assist in achieving the washout effect (see Subsection 3.3.2) and in enforcing input constraints. Together, these components contribute to a more robust and effective control strategy over the prediction horizon. The structure of the cost function can be given as:

$$
\begin{aligned}
J_c = \quad & J_{MS} + J_{MP} + J_{penalty} \\
J_c = \quad & [\underbrace{(Y(x_k,u_k) - \hat{Y}_k)^T W_Y (Y(x_k,u_k) - \hat{Y}_k)}_{objective\ terms} \\
& + \underbrace{(X_k - \hat{X}_k)^T W_X (X_k - \hat{X}_k) + J_k^T W_J J_k + (U_k)^T W_U (U_k) + \delta^T w_\delta \delta}_{penalty\ term}] \quad (5.14) \\
Y(x_k,u_k) \quad & = [f_{spec}\ c_v] \\
W_Y \quad & = [w_{spec}\ w_{con}] \\
X \quad & = [\theta_{hex}\ \omega_{hex}\ s_{hex}\ j_{hex}\ j_{ang,hex}\ \delta] \quad (5.15) \\
W_X \quad & = [w_\theta\ w_\omega\ w_s\ w_j\ w_{ang,j}\ w_\delta] \quad (5.16) \\
J_k \quad & = [j_{trans}\ j_{ang}] \quad W_J = [w_{j,trans}\ w_{j,ang}]
\end{aligned}
$$

The output terms (Y) consist of the sensory conflict (c_v) and specific force (f), Y_{ref} defines the reference for the sensory conflict and specific force, w_Y is the weight vector corresponding to the components of the output vector; X is the vector consisting of platform states that are penalised in this work, W_X is the weight vector corresponding to the platform state being penalised (for washout effect), and u and w_u correspond to the inputs and the weight penalisation for the inputs to restrict it. δ is the slack variable and w_δ is the weight for the slack variable in the cost function.

Penalising jerks in the cost function of an MPC-based MCA is a well established practice to mitigate oscillations in specific force. We approximate jerk using the acceleration change over timesteps divided by the timestep ($j(k) = \frac{a(k)-a(k-1)}{Ts}$). This approach avoids the need to add jerk as a system state, thereby decreasing the computational complexity of the optimal control problem (OCP).

$$
\begin{aligned}
\min_{u \in U} \quad & J_c && (5.17) \\
s.t. \quad & x_v' = f_v(x_v, u) && (5.18) \\
& \phi(x_v, u) \leq 0 && (5.19) \\
& b\left(x\left(s_0\right), x\left(s_f\right)\right) = 0 && (5.20)
\end{aligned}
$$

The dynamics of the system states, as defined in Section 5.3, are used as equality constraints in Equation 5.18. The parameter ϕ in Equation 5.19 represents the constraints on the system as defined in Equation 5.3.3. Lastly, function $b(x(s_0), x(s_f))$ in Equation 5.20 defines the boundary conditions for the platform i.e. the initial and final state of the platform.

CONSTRAINTS

Unlike a real vehicle, in a driving simulator movements are restricted to a maximum displacement and maximum tilt angle. These quantities are specific to the simulator being used. For defining such constraints, the workspace limits of Delft Advanced Vehicle Simulator (DAVSi) are used (Table 5.1).

Table 5.1: Workspace limits of the DAVSi

Quantity	Limit
θ_{hex}	$\pm 30 deg$
v_{hex}	$\pm 7.2 m/s$
a_{hex}	$\pm 9.81 m/s^2$
$\sqrt{s_{hex,long}^2 + s_{hex,lat}^2}$	$0.5m$
a_{cmd}	$\pm 5 m/s^2$

Additionally, to minimise the perception of platform motion and avoid introducing false cues, it is essential to limit platform rotation rates below the human perception threshold. This threshold is typically considered to lie between 2–4°/s [20], [21], [79]. In this work, a value of $3°/s$ was selected based on subjective feedback from participants during a pilot study.

Rather than enforcing this as a hard constraint, we model it as a soft constraint to allow occasional violations when necessary to improve specific force tracking performance. This approach enables flexibility in generating higher specific forces without introducing excessive perceived motion. The tilt-rate constraint is therefore defined as:

$$-\omega_{thd} \leq \omega_{hex} + \delta\, \omega_{hex} - \delta \leq \omega_{thd} \tag{5.21}$$

Here, ω_{thd} is the selected perception threshold (3°/s for both pitch and roll rates), and δ is a positive slack variable included in the cost function. While violations of the threshold are permitted, they are penalized to encourage minimal deviation, balancing perceptual fidelity with motion cueing performance.

WORKSPACE MANAGEMENT

For proper workspace management we use non-linear weights (based on the platform orientation and position) for the washout instead of constant weights. This strategy remains consistent with the frequency splitting algorithm and is described in Subsection 3.3.2.

5.3.4. YAW CHANNEL

The fifth DoF (yaw) is controlled separately using a parallel washout channel, ensuring reduced computational complexity. For the simulator used in this work (DAVSi), the control commands we require to provide are yaw position velocity and acceleration. This is done by passing the acceleration through a high-pass filter to obtain the desired platform yaw acceleration. To ensure that the yaw angle returns back to it's neutral position

at the end of the simulation, we use a second order high pass filter instead of a first order filter. The second-order high-pass filter used for this purpose is given as

$$HP(s) = \frac{s^2}{s^2 + 2 * \nu_{yaw} * s + \nu_{yaw}^2} \tag{5.22}$$

Here, ν_{yaw} denotes the cut-off frequency of the high-pass filter. A value of 0.0159 Hz is used, consistent with the configuration described in Chapter 3. Additionally, for simplicity, the damping ratio is kept to be 1 (critically damped).

As yaw motion also affects motion sickness, the yaw prediction for the future should also be communicated to the MPC. As the yaw washout is highly computationally efficient, it can calculate the solution to the reference yaw for the prediction horizon almost instantly. In our implementation, we include yaw information as online data for communication with the MPC.

5.4. MPC ALGORITHM CONFIGURATION

In this section, the simulation settings used for the results presented in this chapter are outlined. The MPC algorithm and settings, including the penalty terms in Equation 5.14 are detailed in Section D.1, Appendix D for completeness. As in Chapter 3, the MPC time horizon was 3 seconds (60 steps of 0.05s).

In this work, we consider two major contribution terms that define the primary objective of the algorithm, along with several minor terms that help guide the Model Predictive Control (MPC) problem toward the desired performance. The two primary objective terms should have the highest contribution in the cost function.

Since the cost terms have different units, their relative contributions cannot be directly determined by the weights alone. To address this, we normalise the cost terms in the cost function. This is done by running a sample simulation and recording the maximum values attained by each error term. The cost terms are then scaled by dividing them by their corresponding maximum error values. The motivation for the selection of weight parameters can be found in Section D.1. The selected weights are tabulated in Table 5.2

Table 5.2: Penalization weights for the objective function terms, where I_n corresponds to identity matrix of order n

Penalisation weight	used Value
w_θ (angular orientation)	$1e-4 * I_2$
w_ω (angular velocity)	$1e-1 * I_2$
w_s (displacement)	$1e-2 * I_2$
w_j (translational jerk)	$1e-4 * I_2$
$w_{ang,j}$ (angular jerk)	$1e-4 * I_2$
w_δ (slack variable)	1e-4

The w_s and w_θ, correspond to the parameters k1 and k3 respectively, in Section 3.3.2, that affect the shape of the non-linear weight function. w_ω, w_j, $w_{ang,j}$ and w_δ are the

penalisation weights for angular velocity, translational jerk, angular jerk and the slack variable. Note that all weights are represented as 2×2 diagonal matrices to apply separate penalties in the longitudinal and lateral directions, except for the slack variable weight w_δ , which remains scalar since it does not relate to spatial dimensions.

5.5. ADAPTIVE WASHOUT REFERENCE MCA

In the results below we compare the MPC-based MCA to an adaptive washout (AW) MCA introduced in [76], with MPC-based direct workspace management. The configuration of the AW MCA is kept consistent with that described in Chapter 3. We use this adaptive washout as it is a widely used MCA in industrial applications. Thus it serves as the industrial standard to which we can compare our results.

5.6. OBJECTIVE EVALUATION

This subsection evaluates the performance of the algorithms objectively. Based on the objective evaluation, suitable MCA conditions are selected for the experimental evaluation. Here we already use the driving conditions defined in Subsection 5.7.2.

VARIATION OF CONFLICT WEIGHT

The algorithm under consideration addresses two primary objectives: accurate specific force tracking and minimisation of sensory conflict. To comprehensively explore the trade-off between these competing goals, we vary the ratio between the specific force tracking weight and the sensory conflict weight across the entire range, from pure conflict minimisation to pure force tracking. This is done by varying the sensory conflict weight, w_{con}, between 0 to 1 while maintaining the relation $w_{con} + w_{spec} = 1$.

Figure 5.2 illustrates the resulting performance metrics for different values of w_{con}. This variation is then checked for its effect on workspace utilisation and motion sickness development as opposed to the specific force tracking. The analysed metrics consider root mean square of specific force tracking error, sensory conflict, platform displacement, platform velocity, platform tilt, and the tilt rate. MISC is also checked against specific force tracking.

The green triangle represents the no motion case, which practically coincides with the conflict weight of unity in our algorithm. Thus, the algorithm indicates the reduction of motion sickness to be the most when the simulator platform does not move at all.

For the experimental evaluation, it is important to ensure a clear distinction between the MISC levels of the different algorithm configurations. Therefore, a minimum difference of at least one MISC level is desired. As shown in Figure 5.2, the profiles corresponding to $MPCw_{con0}$, $MPCw_{con0.9}$, and NM exhibit a difference of one MISC level, namely, $MPCw_{con0}$: 3, $MPCw_{con0.9}$: 2, and NM: 0.9.

FIDELITY CRITERIA

For objective comparison, shape similarity and the RMSE of specific force are considered.

Shape similarity ensures the effectiveness of the algorithm. A maneuver with a similar shape to its obtained specific force results in a similar experience. Despite magnitude scaling, a higher shape similarity provides a better recreation of the maneuver.

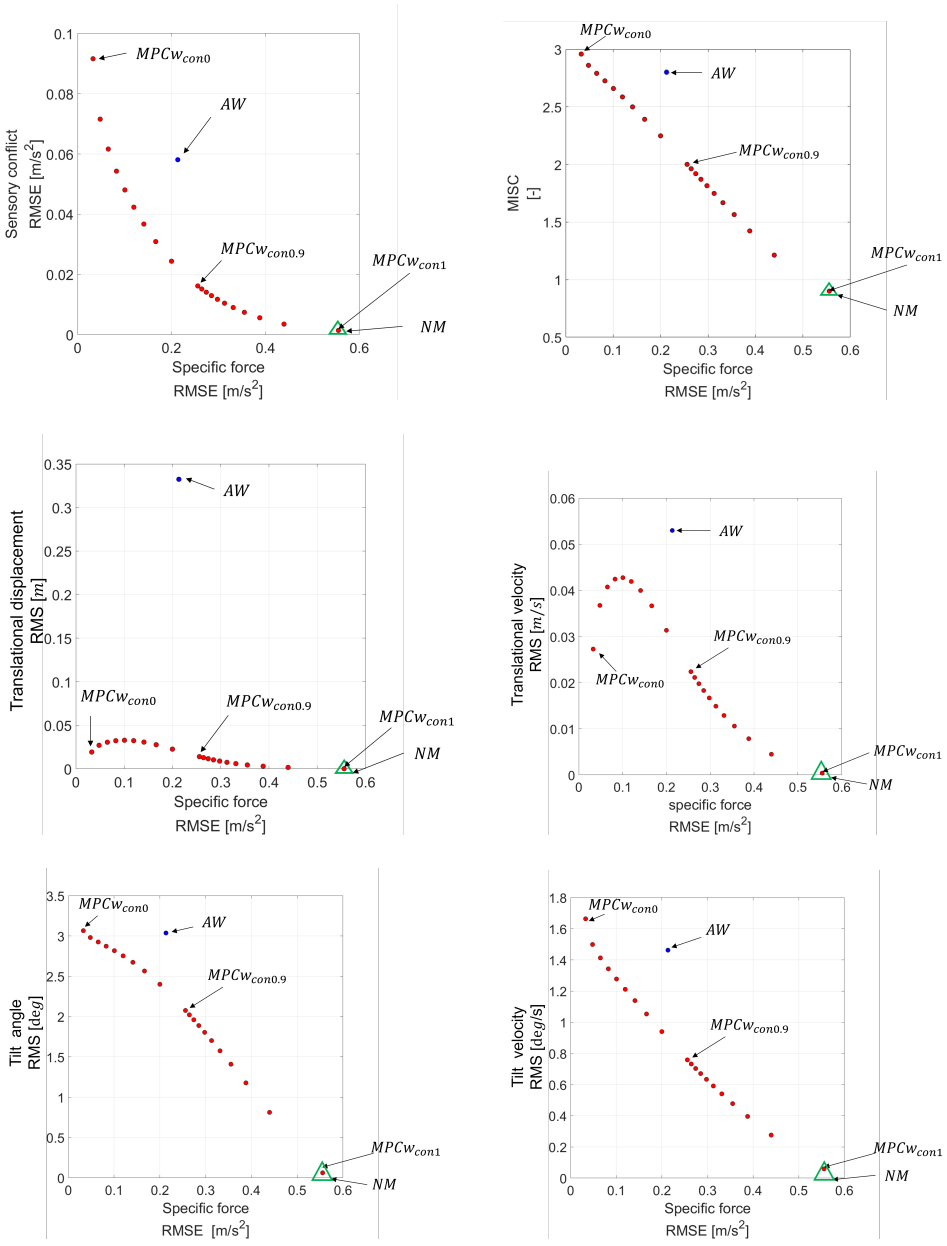

Figure 5.2: Effect of varying the specific force tracking to sensory conflict weight ratio on sensory conflict tracking accuracy and workspace utilisation. The specific force tracking error is computed as the square root of the sum of the longitudinal and lateral root-mean-square errors (RMSE) of specific force. MISC development is evaluated over 5 laps; all other metrics are calculated based on the response over a single lap.

Additionally, the RMSE between the reference and obtained specific force response portrays how closely the magnitudes of the reference and generated profile match/align.

SPECIFIC FORCE PROFILES

The selected MCA configurations were further analysed based on the rendered specific force profiles and shape similarity.

Figure 5.3 presents the specific force profiles produced by each configuration. For comparability, the reference signals were scaled—longitudinal acceleration by a factor of 0.3 and lateral acceleration by 0.4. The results show that the AW algorithm and the $MPCw_{con0}$ configuration yield very similar profiles, whereas the $MPCw_{con0.9}$ configuration results in noticeably lower specific force magnitudes.

SPECIFIC FORCE TRACKING

The root mean square error (RMSE) values quantify these differences. For the AW method, the RMSE is 0.0632 in the longitudinal direction and 0.0732 in the lateral direction. The $MPCw_{con0}$ configuration achieves lower RMSE values of 0.0256 (longitudinal) and 0.0092 (lateral), indicating a closer match to the reference. In contrast, the $MPCw_{con0.9}$ configuration results in higher RMSE values of 0.1562 (longitudinal) and 0.1488 (lateral), reflecting the reduced motion magnitudes.

SHAPE SIMILARITY

In addition to RMSE, the shape similarity between the rendered profiles and the reference signals was assessed. The AW method achieved shape similarity scores of 0.8377 (longitudinal) and 0.9432 (lateral). The $MPCw_{con0}$ configuration yielded higher shape similarity scores of 0.9981 (longitudinal) and 1.0000 (lateral), indicating near-perfect alignment. The $MPCw_{con0.9}$ configuration also performed well, with scores of 0.9648 (longitudinal) and 0.9762 (lateral).

Table 5.3: Performance of the selected MCAs along with their descriptions. The algorithm configuration marked with '*' is excluded from the experiment, as pilot tests with three participants revealed that, for a significant portion of the simulation, it closely resembled the no-motion condition.

Algorithm	Specific force RMSE $[m/s^2]$ $\left[\sqrt{long.^2 + lat.^2}\right]$	Shape similarity $\left[\frac{long.+lat.}{2}\right]$	End MISC (predicted)	Description
NM	0.5364	0	0.9	No motion of platform coincides with $MPCw_{con1}$
$MPCw_{con0.97}$*	0.3551	0.8960	1.5	MPC based MCA with $w_{con} = 0.97$
$MPCw_{con0.9}$	0.2157	0.9705	2.0	MPC based MCA with $w_{con} = 0.9$
$MPCw_{con0}$	0.0272	0.9990	3.0	MPC based MCA with $w_{con} = 0$
AW	0.0967	0.8904	2.8	Widely accepted motion cueing in industry

WORKSPACE UTILISATION

The workspace utilisation for each algorithm, including RMS displacement, RMS velocity, RMS angular displacement, and RMS angular velocity is presented in Table 5.4. These quantities reflect how much of the simulator's translational and rotational workspace is engaged during motion cueing.

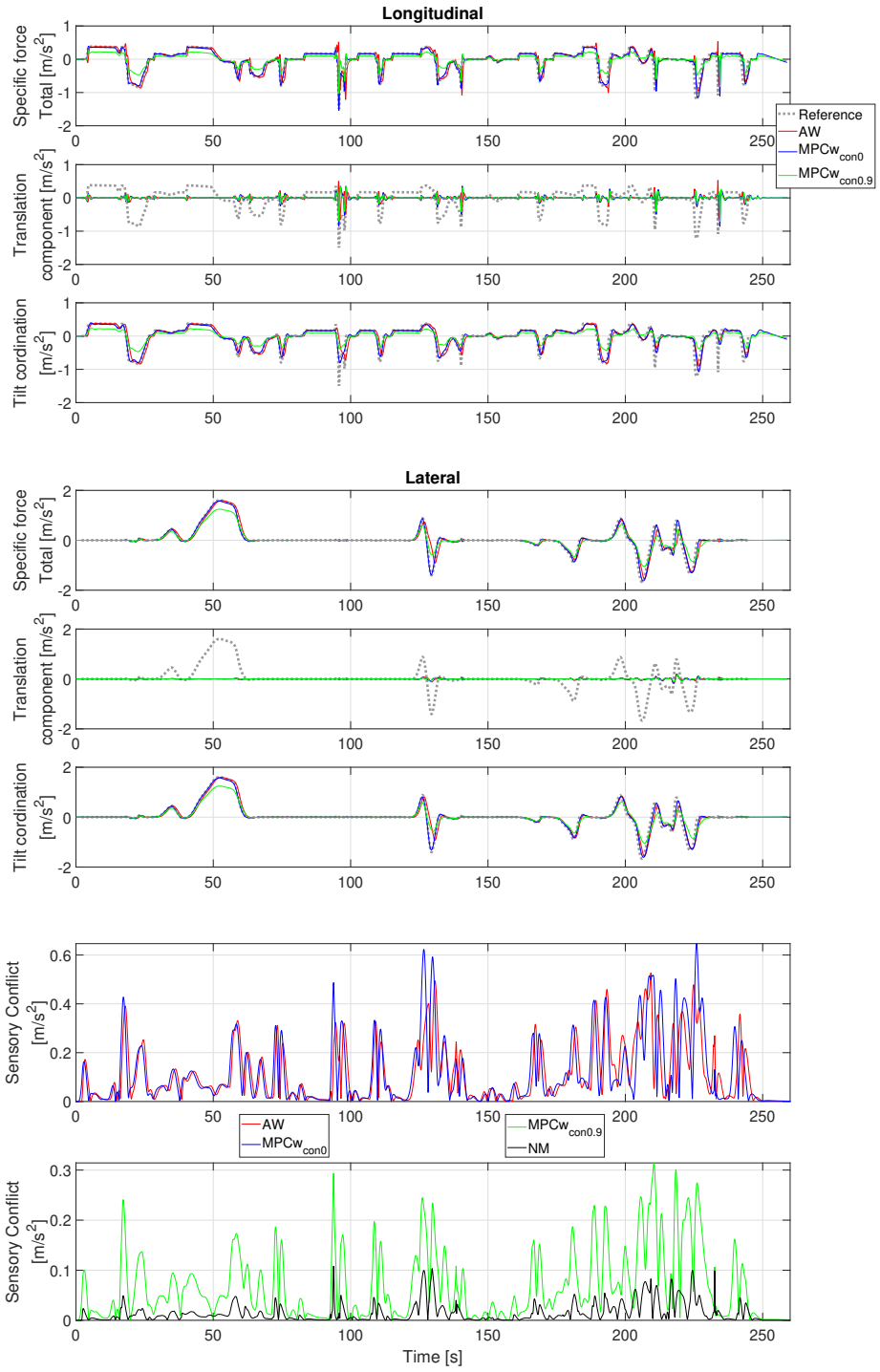

Figure 5.3: Specific force and its components, along with the sensory conflict generated over one lap of the simulation, shown for different algorithm configurations

The variation of the workspace utilisation along with the variation of the conflict weight can also be seen in Figure 5.2.

Table 5.4: Workspace utilisation for the algorithms tested experimentally

Algorithm	Workspace utilisation			
	RMS displacement [m]	RMS velocity [m/s]	RMS angular displacement [deg]	RMS angular velocity [deg/s]
$MPCw_{con0}$	0.0273	0.0193	3.0661	1.6636
$MPCw_{con0.9}$	0.0224	0.0140	2.0761	0.7587
AW MCA	0.3477	0.0518	3.0281	1.4229
No motion	0	0	0	0

5.7. HUMAN-IN-THE-LOOP EVALUATION

This section describes the human-in-the-loop driving simulator experiment and its subjective evaluation method. Perceived driving simulator fidelity and motion sickness was evaluated from the perspective of passive users, representative of users of automated vehicles. This work utilises the Delft Advanced Vehicle Simulator (DAVSi) for the experiment conduction. DAVSi is a 6-DoF moving-based driving simulator [20], capable of generating acceleration up to 1 g in all directions and can simulate motions up to the frequency of 10 Hz.

5.7.1. EXPERIMENTAL PROCEDURE

All participants provided informed consent before participating in the study. The Human Research Ethics Committee of TU Delft, The Netherlands, approved the experimental protocol (application number 4819).

In total, 20 participants from the pool of students and employees of TU Delft participated in the study (mean age: 27.70 years, std: 3.42 years, 6 females, 14 males).

Individuals with no prior history of motion sickness were excluded from the study. The Motion Sickness Susceptibility Questionnaire-Short (MSSQ-Short) was administered to the participants of the experiments, as described by [99]. The participants had a mean MSSQ-Short score of 49.6 (SD = 24.9), substantially higher than the population mean of 12.9 reported in [99], indicating a high level of motion sickness susceptibility.

Each participant experienced all four selected motion cueing algorithm (MCA) configurations, in a randomised order. To minimize carry-over effects and mitigate motion sickness influence from previous exposures, sessions were spaced at least 48 hours apart for each participant.

It is important to mention that, since the MPC algorithm is not capable of real-time execution (real-time factor ≈ 2.0), the MCA first renders the motion profile for the entire scenario. This rendered profile is then replayed in the driving simulator in an offline mode. Such an approach is particularly suitable for passive driving scenarios, where the driver does not actively control the vehicle. In these cases, online generation of motion cues is not required.

Before the experiment, the participants underwent a concise briefing session to familiarise themselves with the questionnaire and to understand the objective of the ex-

periment. During the experiment, two-way communication was established between the experimenter and the participant via blutooth headphones and microphones.

Measures were taken to ensure that the driving scene remained their sole visual focus, including blocking side window views and part of the windshield to eliminate external cues indicating platform tilt (same as presented in Figure 3.12, Chapter 3).

During each session, participants reported their motion sickness levels every 30 seconds using the Misery Scale (MISC) [100], prompted by an auditory beep in the headphones. After completing a session, participants filled out an absolute grading questionnaire (listed below) assessing different aspects of the driving experience.

To ensure a fair comparison, the sequence of algorithm exposures varied across participants. A Latin square design was employed to balance the experimental testing order. Participants could withdraw from the experiment at any time.

QUESTIONNAIRE

Participants rated realism on a 5-point Likert scale with the following questions:

- How closely did the ride's motion correspond to the video?
  [0 = Not at all, 5 = Completely coherent]
- How close did the cornering feel compared to a real car?
  [0 = Not at all, 5 = Exactly like a real car]
- How realistic did the acceleration and deceleration feel compared to a real car?
  [0 = Not at all, 5 = Exactly like a real car]
- Were there any unnatural motions that did not match real driving?
  [0 = Not at all, 5 = A lot of them]

5.7.2. SCENARIO

The aim of this study is to investigate simulator sickness in relation to motion cueing in driving simulators. To this end, a virtual driving scenario was designed to simulate a naturalistic urban drive that would not typically induce motion sickness in real-world driving, but may do so in a simulator due to sensory mismatch.

Since the ultimate goal is to develop strategies to mitigate simulator sickness, the experiment must first ensure a sufficiently high likelihood of inducing sickness. Given the naturalistic and non-aggressive nature of the driving scenario, participants need to be exposed to it for an extended period to allow the gradual onset of sickness symptoms. Based on this consideration, the total session duration was set to approximately 30 minutes.

The driving scenario consists of 240-second laps, followed by a 10-second pause, repeated six times per session. This structure provides consistency across participants while maintaining manageable session length and data segmentation for analysis.

The urban driving scenario includes vehicle speeds ranging from 0 to 70 km/h and consists of a diverse set of maneuvers: stop-and-go sequences at traffic lights and pedestrian crossings, moderate cornering, a tunnel section, and a double lane-change maneuver due to a road diversion caused by an accident. These dynamic events are chosen to

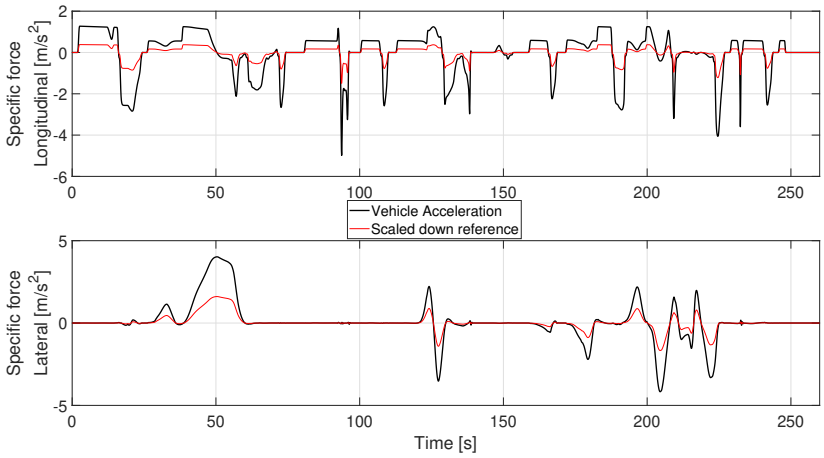

Figure 5.4: Vehicle accelerations along with their scaled down references

replicate realistic driving conditions while introducing sufficient variations in acceleration to challenge the simulator's motion rendering capabilities.

The scenario was created using IPG CarMaker, which provides a realistic virtual environment and high-fidelity vehicle dynamics simulation. CarMaker's vehicle models are experimentally validated, ensuring that the generated accelerations are representative of actual driving conditions. These acceleration signals serve as the reference specific forces for the motion cueing algorithm that drives the simulator platform.

Figure 5.4 presents the acceleration profiles generated by the vehicle model for one lap of the defined scenario. The reference provided to the MPC is scaled down by a factor of 0.3 and 0.4 for the longitudinal and lateral vehicle accelerations, respectively. The choice of the scaling factor is coherent with the selected values in Chapter 3. The resulting data shows lateral accelerations within the range of approximately $\pm 4 m/s^2$, longitudinal accelerations up to 1.25 m/s^2, and decelerations reaching $-5 m/s^2$. These dynamic variations are used to evaluate the simulator's motion cueing effectiveness and its relationship with simulator sickness development.

5.7.3. RESULTS

SUBJECTIVE REALISM RATINGS

Based on participant realism scores collected during the experiment, a subjective evaluation of the motion cueing algorithms was conducted. Figure 5.5 presents a summarised boxplot of the ratings for the different motion cueing configurations. The results indicate that the three platform motion configurations—$MPCw_{con0.9}$, $MPCw_{con0}$, and AW—received closely clustered ratings across all realism criteria. In contrast, the NM (no motion) configuration consistently received the lowest scores, suggesting that participants perceived it as the least realistic.

These findings imply that the absence of motion cues in the *NM* configuration significantly reduced the sense of immersion, making it feel less like a real vehicle drive. Conversely, the other configurations were perceived to deliver comparable levels of realism and immersion, reinforcing the value of motion-based cues in enhancing perceived driving authenticity.

Furthermore, Figure 5.5 highlights statistically significant differences between the configurations using asterisks ('*'). These markers indicate that each motion-based configuration exhibits a statistically significant difference in perceived realism when compared to the *NM* configuration. However, no significant difference is observed among the motion-based configurations themselves, further supporting the conclusion that they provide a comparable level of immersive experience.

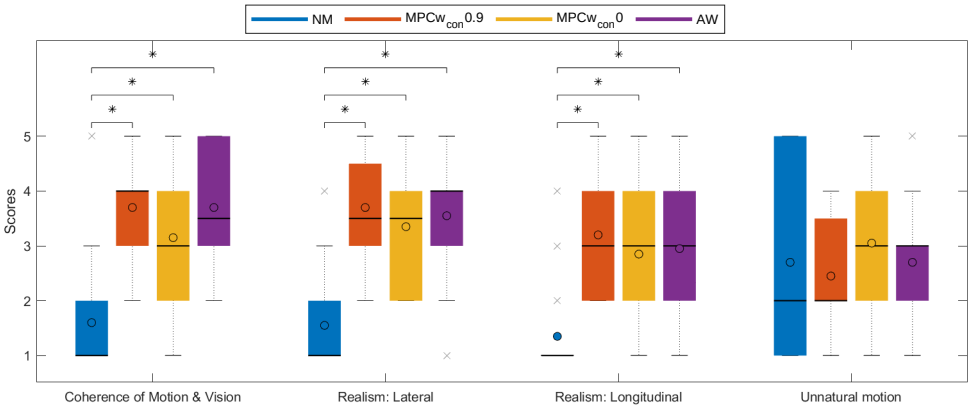

Figure 5.5: Realism scores obtained for the different algorithm configurations during the human-in-the-loop validation experiments. '*' represent significant differences, circles represent the mean, solid lines represent the median, boxes represent 25th and 75th percentile, with '×' capturing the full range including outliers.

MOTION SICKNESS RATINGS

Figure 5.6 presents the experimental motion sickness results alongside the predictions from the model framework by [96] as described in Subsection 5.3.1. It can be observed that the *NM* configuration results in the lowest levels of motion sickness. Slightly higher levels are seen with the $MPCw_{con0.9}$ configuration, followed by *AW*, and the highest levels are recorded for $MPCw_{con0}$. This trend confirms that increasing the weight on sensory conflict leads to reduction in motion sickness, as expected from the offline analysis in Figure 5.2. Additionally, only one participant dropout occurred in the $MPCw_{con0.9}$ condition, compared to six in $MPCw_{con0}$ and four in the *AW* condition. This confirms that SVC MCA is capable of extending the exposure time in the simulator.

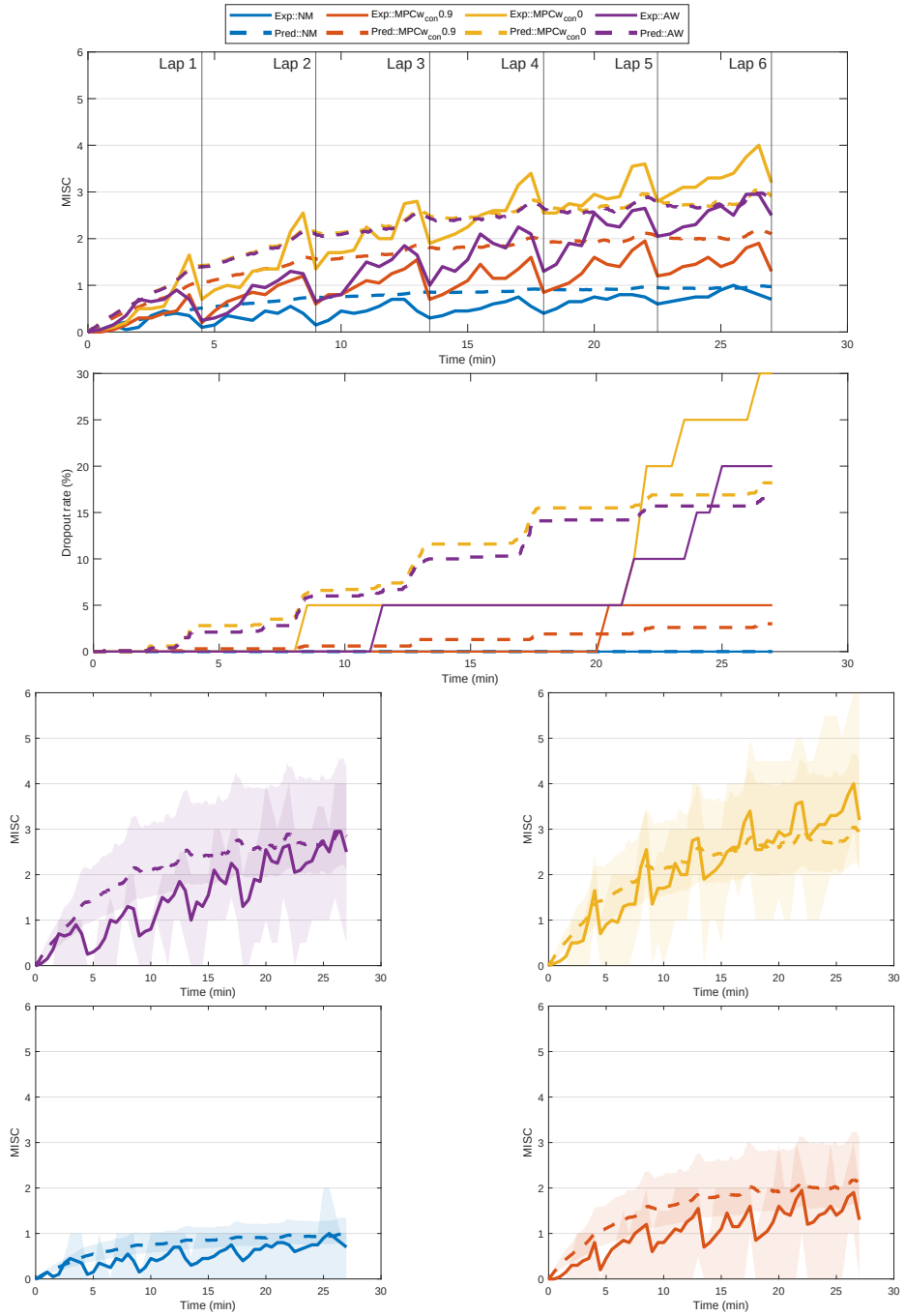

Figure 5.6: Experimental MISC responses along with model predictions for all scenarios considered in the experiment. The solid lines represent the data collected during the experiment, the dashed lines represent the predictions coming from the SVC model. Mean response (upper graph), dropout rates (second graph) and variance (four separate graphs) where the shaded region spans from 25th to 75th percentile.

Furthermore, the experimental data aligns with the predicted MISC levels predicted by the model framework. Although the predicted values do not exactly match the experimental outcomes, they follow a similar trend across configurations (see Figure 5.6). The SVC model generally overestimates MISC levels relative to the observed data, with the exception of the $MPCw_{con0}$ configuration, where the predictions are lower than the measured values at the end of the experiment.

Table 5.5: Analysis of the experimental MISC data using ANOVA

Session Order effects
(Overall p-value = 0.4569)

pairs		p-value
S1	S2	0.9146
S1	S3	0.5717
S1	S4	0.4727
S2	S3	0.9183
S2	S4	0.8537
S3	S4	0.9985

MCA Condition effects
(Overall p-value = 6.3897e-08)

pairs		p-value
NM	$MPCw_{con0.9}$	0.2624
NM	$MPCw_{con0}$	9.6973e-08
NM	AW	1.9748e-04
$MPCw_{con0.9}$	$MPCw_{con0}$	8.9266e-05
$MPCw_{con0.9}$	AW	0.0497
$MPCw_{con0}$	AW	0.1732

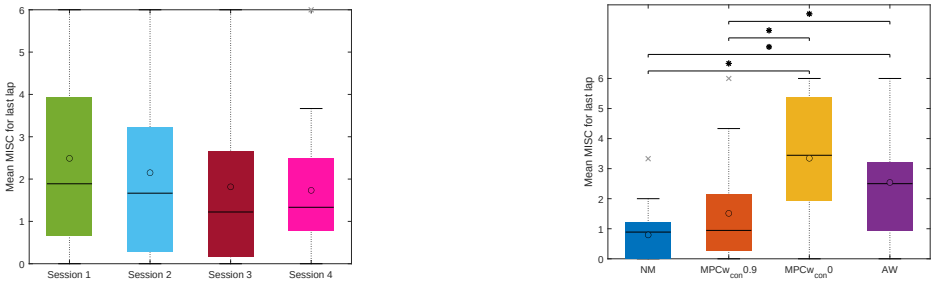

Figure 5.7: Order effect (left) and MCA effect for mean MISC at the end of the last lap in the experiment with '*' representing significant difference between the algorithm configurations.

The experimental data was also checked for condition effects and order effects based on the mean of the collected MISC data levels obtained for the participants. For this analysis, participants who dropped out had their MISC level assumed to be 6 from the point of dropout until the end of the experiment. The analysis for the statistical significance is tabulated in Table 5.5 and the boxplots are shown in Figure 5.7. The table indicates that there were no significant differences because of order effects i.e. the order with which the participant was subjected to the algorithms did not have a significant effect on the output of the experiment. However, there was a significant effect of conditions on the mean MISC in the last lap. It also indicates that there was a significant difference in the motion sickness levels between the pairs (a) NM and $MPCw_{con0}$ (b) NM and AW (c)

$MPCw_{con0.9}$ and AW (d) $MPCw_{con0.9}$ and $MPCw_{con0}$. Whereas, no significant difference were found between (a) NM and $MPCw_{con0.9}$ and (b) AW and $MPCw_{con0}$.

In Figure 5.8, we compare the histogram of MISC levels at the end of the experiment, as predicted by the model framework and as observed in the experimental data.

While there are some deviations in the exact occurrence percentages across MISC levels, the overall trend is reasonably well captured by the motion sickness model.

The most notable discrepancy occurs at MISC level zero, where the model underestimates the proportion of participants reporting no motion sickness, failing to predict a MISC of zero for a substantial segment of the population.

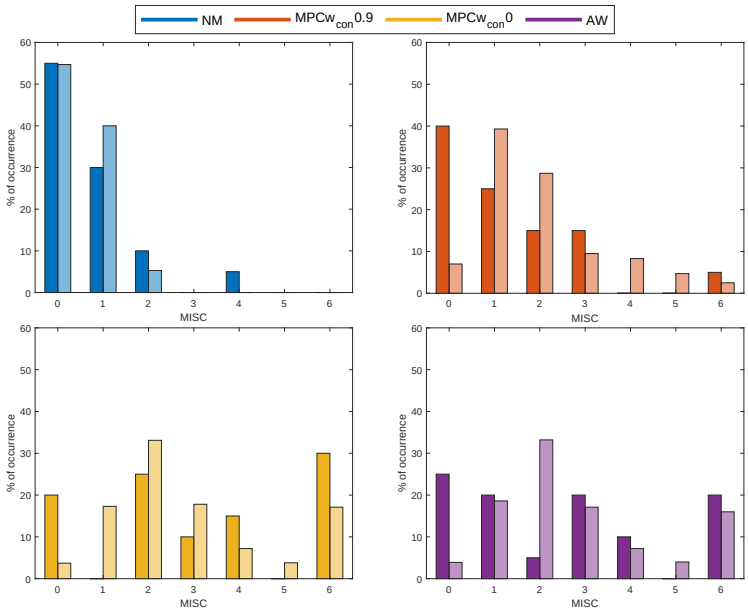

Figure 5.8: Histogram of MISC at the end of the experiment. Experimentally observed MISC in dark colours and predicted MISC in lighter colours.

5.8. DISCUSSION

This work addresses a pivotal gap in the domain of motion cueing algorithms by directly integrating motion sickness mitigation as an explicit control objective. Historically, the development of MCAs has emphasised fidelity in motion perception, often overlooking the physiological consequences of simulator use, especially motion sickness. While prior works have explored high-fidelity motion rendering through MPC (also in Chapter 3 and Chapter 4), to the best of the authors' knowledge, no work has incorporated advanced physiological models, specifically the 6-DoF Sensory Conflict model (SVC) to anticipate and suppress motion sickness.

The algorithm introduced here not only balances the perceptual accuracy of motion (via specific force tracking), but also integrates a predictive layer that quantifies human discomfort through sensory conflict. This dual-objective formulation represents a sig-

nificant methodological advancement, transcending traditional MPC frameworks that focused solely on mechanical accuracy or visual congruence.

A notable strength of this work is the comprehensive validation strategy. Through simulation, objective metrics (like RMSE and shape similarity), and human-in-the-loop evaluations, the proposed solution is shown to be robust across both technical and perceptual domains. The experimental results confirm the hypothesis that sensory conflict minimisation, even at the expense of reductions in specific force magnitude, can lead to a statistically significant improvement in user comfort without degrading immersion and realism. The successful prediction of MISC levels using a population-based SVC and sickness accumulation model further emphasizes the algorithm's predictive validity and practical utility.

5.8.1. ERROR TERM NORMALISATION FOR MULTI-OBJECTIVE TRADE-OFFS

Given the presence of multiple primary objectives in the algorithm, it is important to control the relative contributions of the different cost terms. Normalisation facilitates this by simplifying the assignment of weights, enabling them to be adjusted according to the priority of each objective. In this work, normalisation is achieved through a preliminary simulation used to estimate the maximum expected values of each variable. Each error term in the cost function is then divided by its corresponding maximum value, ensuring that all normalised errors lie within a comparable range. This normalisation process also enabled us to explore the full spectrum or Pareto front between the objectives of motion perception and motion sickness, represented respectively by specific force tracking and RMS sensory conflict. While this method does not yield exact or universal scaling, the estimated maxima, derived from a representative set of scenario and weight configuration, it provides a practical and sufficiently robust basis for comparative analysis across different trade-offs. If future scenarios deviate significantly from those used during normalisation, the bounds can be re-evaluated and updated accordingly.

5.8.2. WORKSPACE UTILISATION

By analysing the explored spectrum between sensory conflict and specific force tracking as competing objectives—achieved by varying the ratio between their respective weights from 0 to infinity (see Figure 5.2)—we observe that increasing the weight on the sensory conflict term leads to a general reduction in the overall motion of the platform.

More interestingly, when evaluating translational and rotational workspace utilisation separately, distinct trends emerge. In the rotational workspace, both rotational velocity and rotational angle utilisation consistently decrease as the weight on the sensory conflict term increases.

However, the trend differs in the translational workspace. Initially, as the sensory conflict weight increases, translational workspace utilisation slightly increases before eventually showing reduced utilisation (see Figure 5.2). This suggests that when the specific force tracking objective still holds significant weight, and the motion sickness term is only weakly weighted, the MPC attempts to balance both objectives. It does so by generating solutions that maintain fidelity in specific force tracking while modestly reducing motion sickness.

Overall, as the weight on sensory conflict increases, translational motion initially

rises before declining, while rotational motion consistently decreases. This suggests that rotational movement contributes more significantly to motion sickness. To reduce conflict early on, the controller limits rotational motion while allowing slight increases in translation. However, substantial mitigation of motion sickness ultimately requires reducing both rotational and translational motion.

5.8.3. MISC PREDICTION

In a novel contribution to the field, this work presents the first-ever quantitative prediction of absolute motion sickness levels using the SVC model in combination with a sickness accumulation model in driving simulator motion cueing. Here we build on our recent papers where we combine the SVC model with an accumulation model and estimated individual parameters to capture experimental MISC values in vehicle and driving simulator experiments [89], [96]. Prior research has predominantly focused on relative trends or qualitative sickness development; in contrast, our approach enables the prediction of absolute MISC scores. Although motion sickness is inherently subjective and often requires individual calibration parameters, we generalise our model using population-representative parameters. As a result, we provide predicted average MISC responses, accompanied by the standard deviation to capture inter-individual variability. This methodology offers a new standard for objective, model-based evaluation of motion sickness in simulator contexts.

As shown in Figure 5.6, the predictions (represented by dotted lines) follow a similar trend to the experimental data (represented by solid lines). Additionally, the predicted MISC levels remain close to the actual values recorded at the end of the experiment.

Interestingly, the adaptive washout and the configuration $MPCw_{con0}$ yield very similar MISC predictions. However, this similarity is not reflected in the experimental data, providing scope to enhance the SVC and accumulation models and their parameters. Likewise the experimental MISC fluctuates more across time whereas the experimental MISC increased more gradually providing scope to enhance the accumulation model and its parameters. Certain instances of false cues may have a higher/bigger impact on motion sickness than others, which the model may not be able to discern/quantify (such as prepositioning or coupled of the translational and rotational motion). Thus, the SVC may have similar predictions for the AW and $MOCw_{con0}$, whereas in the experiment the outcome was slightly different; however, even with these discrepancies, the trend of prediction of motion sickness holds for the SVC model. This is evident by the outcomes of the MCAs $MPCw_{con0}$, $MPCw_{con0.9}$ and NM where the experimental results follow the trend predicted by the SVC model.

The discrepancies between the predicted and experimental results may be partially attributed to the use of generalised rather than individual-specific parameters in the MCA. Nevertheless, the use of generalised parameters still proves valuable for reducing motion sickness. This is because it is more important to lower the sickening stimuli than to precisely predict their impact on MISC levels. For this reason, minimising instantaneous sensory conflict is often sufficient, as it ultimately contributes to reducing the accumulation of sensory conflict over time.

In the developed algorithm, sensory conflict is minimised instead of directly minimising the motion sickness rating. Within the optimisation process, it is the accumu-

lated error that is minimised rather than the instantaneous error at a single point in time. Since the accumulation of sensory conflict increases over time, its contribution to the cost function grows accordingly, starting with a minimal impact and becoming more dominant as time progresses.

5.8.4. REALISM

This work evaluates realism through both subjective and objective measures. The objective metrics include specific force tracking and the shape similarity factor.

While RMSE is a useful metric for assessing how accurately a reference signal is tracked, shape similarity is arguably more important in this context. This is because the vehicle accelerations are scaled down before being used as reference inputs in MCAs. As a result, the primary objective shifts from matching the exact magnitude to preserving the overall shape of the motion profile. In this context, the aggressiveness of the ride is more closely associated with acceleration magnitude, whereas perceived realism is more accurately conveyed through similarity in the motion shape.

It is important to note that shape similarity is assessed based on the total specific force vector, rather than its individual components.

Additional data is needed to determine whether realism remains consistent across the entire weight spectrum, particularly in the range $w_{con} = 0$ to 0.9.

5.8.5. MOTION SICKNESS MANIPULATION

Although this work specifically targets the reduction of motion sickness, the same algorithm can also be configured to recreate motion sickness if desired. To minimise motion sickness, the sensory conflict is given a reference of zero. However, by feeding the actual sensory conflict—calculated from real vehicle data—into the MPC as the reference, motion sickness can be intentionally reproduced. This feature could prove valuable for assessing how sick an occupant might feel when exposed to specific automated driving styles, and for conducting human-acceptance or behavioural studies within a simulated environment, especially in cases where real vehicle and simulator responses are directly compared.

A key finding is that the algorithm is capable of significantly reducing motion sickness while preserving the perception of motion. Subjective results revealed that a conflict weight of $w_{con} = 0.9$ resulted in an average end MISC level of 2 across participants. In contrast, both the adaptive washout and the MPC configuration with only specific force tracking yielded an average MISC level of 3. This reflects a 33% reduction in motion sickness without substantially compromising scenario realism. Additionally, the experimental validation also showed that the no motion case resulted in the least amount of sickness, which was also observed in the predictions obtained through the SVC model. Indicating the SVC model's capability in predicting motion sickening. The perceived fidelity for this case however, reduced significantly. This aligns with the finding in [33], where the percieved fidelity improved with the addition of motion to the simulator platform, accompanied by an increase in motion sickness. However, this does not align with the findings of [32], where enhanced visual fidelity reduced motion sickness in for moving base but not for fixed base, indicating that increasing the visual fidelity may be responsible for additional sickness induction.

It is worth noting that for the experiment, the frontal view was the main focus, thus, the peripheral vision was blocked (see Figure 3.12). This blocking of peripheral vision might have subdued the sickness levels in the occupants. A similar study should be conducted to further explore the role of peripheral vision in motion sickness development in simulators.

Finally, in this study, yaw motion was controlled via a traditional washout algorithm, which does not consider motion sickness in its design. This decision was made to simplify the MPC computation. Future work may explore integrating yaw dynamics into the MPC framework to potentially improve sickness mitigation and deliver more precise rotational cueing.

5.9. CONCLUSION

The developed motion cueing algorithm demonstrates a strong capability to reduce motion sickness while maintaining a realistic perception of vehicle motion. Experimental results show that increasing the weight for sensory conflict within the model predictive control framework leads to a noticeable reduction in motion sickness experienced by participants. This confirms the effectiveness of penalising sensory conflict as a control objective in motion cueing design.

Although the configuration with a high sensory conflict weight (compromise configuration; $MPCw_{con0.9}$) produces specific force profiles with reduced magnitude, resulting in a higher root mean square error (RMSE) in specific force tracking, the shape similarity of these profiles to the reference signal remains high. Notably, this high shape similarity is consistent across all considered configurations except for the no-motion condition (see Table 5.3). This pattern corresponds well with the relatively uniform subjective realism ratings observed across these configurations, where realism scores for all configurations except the no-motion condition were similar. Consequently, shape similarity may serve as a more meaningful performance metric than the RMSE of scaled specific force, as it appears to better capture participants' perceived realism and, by extension, the perceptual fidelity of the motion cues.

Subjective evaluations further reinforce the findings, with participants rating motion-based configurations significantly higher in realism compared to the no-motion baseline. Additionally, statistical analysis confirms that these improvements are not due to order effects, and there are significant differences in motion sickness levels between key configuration pairs.

Our findings align with those of [32] and [33], where even low-amplitude motion was shown to significantly enhance perceived motion fidelity compared to no-motion conditions. However, in contrast to [32], where the fixed-base simulator was associated with slightly higher motion sickness, our study observed the lowest sickness levels in the no-motion configuration. It is important to note, however, that the differences in sickness levels reported by [32] were not statistically significant. This discrepancy may be attributed to differences in visual fidelity, as highlighted in their study, suggesting that visual rendering quality could play a critical role in motion sickness development.

In summary, this work marks a significant advancement in motion cueing design by successfully integrating a perceptually-informed motion sickness model directly into the control framework. The algorithm not only proves effective in reducing motion sick-

ness through both simulation and human-subject validation, but also demonstrates that motion fidelity can be preserved while optimising for comfort. This achievement paves the way for more immersive and tolerable long-duration driving simulation experiences, setting a new benchmark for future motion cueing algorithms.

6

COMPUTATIONALLY-EFFICIENT MOTION CUEING ALGORITHM VIA MODEL PREDICTIVE CONTROL

The journey of a thousand miles begins with a single step.

Lao Tzu

Youth is wasted on the young,
don't let the wisdom of age waste upon you.

Ted Lasso

This chapter is based on *A. Chadha, **V. Jain**, A. M. R. Lazcano, and B. Shyrokau, "Computationally-efficient motion cueing algorithm via model predictive control." in 2023 IEEE International Conference on Mechatronics (ICM), 1-6. [34].*

6

ABSTRACT

Driving simulators have been used in the automotive industry for many years because of their ability to perform tests in a safe, reproducible and controlled immersive virtual environment. The improved performance of the simulator and its ability to recreate in-vehicle experience for the user is established through motion cueing algorithms. Such algorithms have constantly been developed with model predictive control acting as the main control technique. Currently, available model predictive control-based methods either compute the optimal controller online or derive an explicit control law offline. These approaches limit the applicability of the cueing algorithms for real-time applications due to online computational costs and/or offline memory storage issues. This research presents a solution to deal with issues of offline and online solving through a hybrid approach. For this, an explicit model predictive controller is used to generate a look-up table to provide an initial guess as a warm-start for the implicit model predictive control-based algorithm. From the simulations, it is observed that the presented hybrid approach is able to reduce online computation load by shifting it offline using the explicit controller. Further, the algorithm demonstrates a good tracking performance with a significant reduction of computation time in a complex driving scenario using an emulator environment of a driving simulator.

6.1. INTRODUCTION

DRIVING simulators are frequently used for development and testing in the automotive domain [16]. The virtual environment of the simulator helps to recreate the in-vehicle experience without any damage dealt to the real vehicle. To achieve this, an MCA is used acting as the control technique for the driving simulator's movements. It governs the process allowing the simulator to function properly so that a similar feeling of motion is experienced by the user and to maximise the workspace utilization[101].

In motion cueing, driver input is sent to the vehicle model which generates the reference signal to be tracked. The MCA computes the desired platform motion to follow these reference signals and commands it to the platform as specific forces and rotational accelerations. The notion of specific force is exploited for the recreation of in-vehicle experience. The sensed specific force $f_{spec,s}$ comprises two components: platform translational acceleration, $a_{tran,p}$ and the gravitational acceleration, which allows us to study the human body's movement in space during the cueing process. This is compared with the actual specific force value $f_{spec,a}$ obtained from the real vehicle. The computed error is then fed back into the MCA to improve results for the next time step. Based on this, several kinds of MCAs have been developed, which differ in terms of control techniques used.

Conventional filter-based algorithms use the concept of high and low pass filters to reproduce the on-road experience within the virtual environment [14]. They operate using three main channels. The first is the translational channel which takes in translational accelerations as input. It uses a high pass filter to filter out sustained low-frequency accelerations, which can drive the simulator to its physical limits [14], [15], [20], [102]. These filtered low-frequency accelerations are then recreated using tilt-coordination in the tilt channel [103]. Lastly, a rotational channel is present, which is similar to the translational channel.

Based on the same principle, other kinds of conventional algorithms have been developed such as the optimal and adaptive washout algorithms. The main drawback of such algorithms is their inability to take explicit constraints into account, leading to poor workspace utilization. Furthermore, some of these approaches like the classical washout algorithm are feed-forward techniques which result in poor performance. To overcome these problems, MPC-based MCAs are commonly used.

MPC has been used in MCAs for over a decade considering two different approaches. The first approach is the implicit controller, which solves the optimization problem online at each time step. Initially, linear MPC-based MCAs were developed [68], [103]. They outperformed the conventional methods but provided sub-optimal results, as the nonlinear dynamics were not taken into account. Further, they employed constraints in the driver reference frame, to keep the problem linear, resulting in difficulties in realizing the available workspace. To solve these issues, nonlinear MCAs have been proposed [19], constraining the actuator lengths and showing performance improvement compared with the linear MPC-based MCA. A nonlinear MPC-based MCA with actuator constraints was also developed in [20]. Perception thresholds were applied to reduce false cues, additionally, adaptive weights were introduced for washout effect, which improved tracking performance. A similar algorithm has been developed involving perception thresholds, which uses a separate optimal control problem to predict future driver behaviour

[21]. Such MPC-based MCAs provide better performance compared to conventional and linear MPC-based algorithms; however, they suffer from high online computation costs resulting in these algorithms not being real-time implementable.

To reduce computational costs, an alternative approach of MPC-based cueing has been proposed. Explicit MPC has been developed, which pre-computes the solution and then uses it in the form of a look-up table online. This method significantly reduces online computation time [23]. A 2 DoF MCA was developed which was later extended by incorporating a vestibular model in [73]. Although this technique reduces online computation time, it suffers from memory storage issues along with restrictions in using large prediction horizons N_p with fast sampling rates. This is due to the exponential increase in control region computation time with an increase in the complexity and scope of the problem.[1]

To overcome issues faced by implicit and explicit MPCs, a hybrid approach has been developed by Zeilinger [104]. An explicit controller provides an initial guess for the online optimization problem. The guess acts as a warm-start resulting in faster computation of the optimal control input. Since its inception, this technique has been used in applications such as curve tilting [105] and lateral motion stabilisation [106].

The main contribution of the paper is a hybrid motion cueing approach using explicit and implicit MPCs. The proposed algorithm increases the computational efficiency without degradation of the tracking performance. The algorithm outperforms the state-of-the-art MPC-based MCA described in Subsection 6.3.1, in terms of computational performance.

The paper is structured as follows. In Section 6.2, the controller design is explained including information about both MPCs in the hybrid scheme. The test setup and simulations performed are presented in Section 6.3. Conclusions and recommendations are listed in Section 6.4.

6.2. METHODOLOGY

6.2.1. HYBRID SCHEME

The design of the hybrid MPC-based MCA comprises two main components: initialisation using explicit MPC and online computation using the implicit controller. A general scheme of the MCA is shown in Figure 6.1. As the first step, the initial states and reference values are sent to the explicit MPC. This block searches for the corresponding control region related to the states and reference values, the associated control inputs are then provided to the online nonlinear solver (implicit MPC), as the initial guess. With the information of the initial guess along with the current states and the reference signals, the implicit controller computes the optimised control inputs. These inputs are fed to the plant model and the states are updated for the next time step. Once the state update is complete, the entire process is repeated.

[1] Deep learning has been applied to derive explicit MPC formulations [74]. A Gaussian radial basis function–based neural network (RBF-NN) was developed in [75]; however, the resulting explicit MPC formulation exhibited degraded performance compared to conventional approaches.

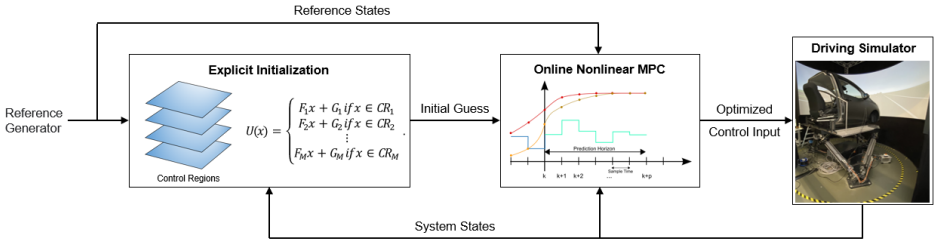

Figure 6.1: Hybrid MPC scheme for the proposed motion cueing algorithm

6.2.2. EXPLICIT MPC

The explicit MPC is used to compute a look-up table that provides the online solver's initial guess. This comprises states and reference values stored in the form of control regions. Each control region corresponds to a particular control input value generated as follows [107], [108]:

$$U(x) = F_i x + G_i \text{ if } x \in \mathscr{CR}_i. \tag{6.1}$$

where, $\mathscr{CR}_i$ are the control regions, to which the vectors F_i and G_i correspond.

To generate the look-up table, an MCA is designed considering 4 DoFs of the driving simulator using the Multi Parametric Toolbox (MPT). The algorithm is a simplified version of the online implicit controller to provide an educated guess for the warm-start strategy. Eight states are used in the model considering the platform displacement s_p, platform velocity v_p, tilt angle θ_p and tilt rate ω_p for pitch-surge and sway-roll DoFs. The state space equations are shown in (6.2):

$$\dot{x}(k) = \begin{cases} \dot{\omega}_{p,long} = a_{p,long,rot} \\ \dot{\theta}_{p,long} = \omega_{p,long} \\ \dot{v}_{p,long} = a_{p,long,tran} \\ \dot{s}_{p,long} = v_{p,long} \\ \dot{\omega}_{p,lat} = a_{p,lat,rot} \\ \dot{\theta}_{p,lat} = \omega_p \\ \dot{v}_{p,lat} = a_{p,lat,tran} \\ \dot{s}_{p,lat} = v_{p,lat} \end{cases} \tag{6.2}$$

Here, the subscripts $'long'$ and $'lat'$ refer to the pitch-surge (longitudinal) and sway-roll (lateral) DoFs respectively. Also, this problem contains four control inputs $u(k)$, comprising translational and rotational accelerations acting in both longitudinal and lateral directions:

$$u(k) = [a_{p,long,rot}, a_{p,long,tran}, a_{p,lat,rot}, a_{p,lat,tran}] \tag{6.3}$$

Thus, the combined system can be represented as follows:

$$\dot{x}(k) = f(x(k), u(k)) \tag{6.4}$$

Constraints are applied in the MCA to limit the movements of the motion platform, according to the driving simulator's capabilities. Firstly, the tilt rate is constrained according to the perception thresholds of pitch and roll movements, to ensure that the driver does not perceive the tilting action. Generally, a lower value in the range of 2-4 deg/s is used [20], [21], [79] and for the proposed MCA, 3 and 2.6 deg/s were chosen for pitch and roll tilt rates respectively.

Secondly, constraints are applied to the platform displacement to limit the platform within the workspace envelope. Since 4 DoFs are considered, the workspace envelope can be represented by $\sqrt{s_{p,long}^2 + s_{p,lat}^2} \leq s_{max}^2$. The explicit MPC is defined using the MPT toolbox where non-linear constraints can not be added. Thus, the constraint described above is only applied in implicit MPC. For the explicit MPC, the platform displacement limits are imposed separately with a value of $\sqrt{s_{max}^2/2}$ in both the longitudinal and lateral directions. As the explicit controller only provides the initial guess for the actual solution, using a marginally different constraint for the displacement does not affect the final solution. The implicit controller produces the final solution. The constraints used in the problem are summarised below:

$$\begin{aligned} -3deg/s \leq \omega_{p,long} \leq 3deg/s \\ -2.6deg/s \leq \omega_{p,lat} \leq 2.6deg/s \\ -30deg \leq \theta_p \leq 30deg \\ -7.2m/s \leq v_p \leq 7.2m/s \\ -0.35m \leq s_p \leq 0.35m \\ -9.81m/s^2 \leq a_p \leq 9.81m/s^2 \end{aligned} \tag{6.5}$$

Here, subscript $'p'$ alone (without $'long'$ or $'lat'$) represents that both longitudinal and lateral counterparts have the same constraint limit. The goal of this MCA is to track the reference specific force defined by the two vector components: translational and gravitational tilt accelerations. Rotations with respect to the x and y axis are used in deriving the gravitational tilt components which are as follows:

$$g_{tilt} = \begin{cases} g_{long} = g\sin\theta_{p,long} \\ g_{lat} = -g\cos\theta_{p,long}\sin\theta_{p,lat} \end{cases} \tag{6.6}$$

Taking the translational accelerations into account, the specific force is given by:

$$y(k) = \begin{cases} f_{spec,long} = a_{p,long,tran} + g\sin\theta_{p,long} \\ f_{spec,lat} = a_{p,lat,tran} - g\cos\theta_{p,long}\sin\theta_{p,lat} \end{cases} \tag{6.7}$$

Furthermore, the objective function consists of weighted states, specific forces and control inputs. As the states are already constrained, a value of 0 is assigned to allow freedom of movement in the available workspace. Further, the highest weights are given

to the specific forces to achieve their tracking. Thus for the objective function, a weight of 1 is selected for specific force (output), and the inputs namely translational and angular accelerations are penalised with a weight of $1e-3$. The cost function can be defined as:

$$J_{ex} = \sum_{i=0}^{N_c} [y_k - y_{ref}]^T \, w_f [y_k - y_{ref}] + x_p^T \; w_x \; x_p + u^T \; w_u \; u \tag{6.8}$$

where y_{ref} is the reference specific force, w_f is the weight for specific force tracking, x_p are the states of the motion platform, w_x are weights on the states to obtain washout effect. Lastly, u are the control inputs and w_u corresponds to the weights on the inputs to restrict them.

6.2.3. IMPLICIT MPC

The second part of the hybrid approach is the online implicit MPC-based algorithm. This algorithm is able to take nonlinear constraints into account and is designed using `ACADO` optimisation toolbox in `MATLAB`. The formulation of the implicit MCA is as follows:

$$\begin{aligned} \min_{u_{N_p}} \quad & J(x_0, u) \\ \text{s.t.,} \quad & x(k+1) = f(x(k), u(k)) \\ & x \in \chi_i \\ & x(N) \in \mathbb{X}_f \end{aligned} \tag{6.9}$$

The cost function in Equation 6.9 is defined as:

$$J_{im} = \sum_{i=0}^{N_c} [y_k - y_{ref}]^T \, w_f [y_k - y_{ref}] + x_p^T \; w_x \; x_p + u^T \; w_u \; u \tag{6.10}$$

The cost function of the implicit MPC is similar to explicit MPC, apart from the addition of a few extra states corresponding to commanded inputs. The states $x(k)$ of the cueing algorithm are also updated by adding the platform accelerations, previously used as the control inputs. Commanded acceleration values that include a first-order time delay are now employed as control inputs. The state space model is presented in Equation 6.11:

$$\dot{x}(k) = \begin{cases} \dot{\omega}_{p,long} = a_{p,long,rot} \\ \dot{\theta}_{p,long} = \omega_{p,long} \\ \dot{v}_{p,long} = a_{p,long,tran} \\ \dot{s}_{p,long} = v_{p,long} \\ \dot{\omega}_{p,lat} = a_{p,lat,rot} \\ \dot{\theta}_{p,lat} = \omega_p \\ \dot{v}_{p,lat} = a_{p,lat,tran} \\ \dot{s}_{p,lat} = v_{p,lat} \\ \dot{a}_{p,long,tran} = \dfrac{a_{cmd,long,tran} - a_{p,long,tran}}{T_s} \\ \dot{a}_{p,long,rot} = \dfrac{a_{cmd,long,rot} - a_{p,long,rot}}{T_s} \\ \dot{a}_{p,lat,tran} = \dfrac{a_{cmd,lat,tran} - a_{p,lat,tran}}{T_s} \\ \dot{a}_{p,lat,rot} = \dfrac{a_{cmd,lat,rot} - a_{p,lat,rot}}{T_s} \end{cases} \tag{6.11}$$

The implicit controller allows us to consider the constraints of the working envelope directly. Apart from this, additional braking constraints are incorporated [23]. As the workspace limits approach, braking constraints help in slowing down the platform velocity and tilt rate. Two sets of constraints are used: one for platform displacement and the other for the tilt angle as follows:

$$s_{p,min} \leq s_p + c_v v_p T_{brk,p} + 0.5 c_u a_{p,tran} T_{brk,p}^2 \leq s_{p,max} \tag{6.12}$$

$$\theta_{p,min} \leq \theta_p + c_w \omega_p T_{brk,\theta} + 0.5 c_u a_{p,rot} T_{brk,\theta}^2 \leq \theta_{p,max} \tag{6.13}$$

where, $c_v = 1, c_w = 1, c_u = 0.45, T_{brk,\theta} = 0.5,\ T_{brk,p} = 2.5$ and s_p, θ_p thresholds are 0.5m and 30 deg respectively.

The constraints used in the model are presented in Table 6.1

Table 6.1: Constraints applied to the implicit MPC

Quantity	Limit
$\omega_{p,long}$	$\pm 3 deg/s$
$\omega_{p,lat}$	$\pm 2.6 deg/s$
$\theta_{p,long,lat}$	$\pm 30 deg$
$v_{p,long,lat}$	$\pm 7.2 m/s$
$a_{p,long,lat,tran}$	$\pm 9.81 m/s^2$
$\sqrt{s_{br,long}^2 + s_{br,lat}^2}$	$\pm 0.5 m$
$\theta_{br,lat,long}$	$\pm 30 deg$
$a_{cmd,long,lat,tran}$	$\pm 5 m/s^2$

where

$$\begin{aligned} s_{br,long} = \quad & s_{p,long} + c_v v_{p,long} T_{brk,p} \\ & + 0.5 c_u a_{p,long,tran} T_{brk,p}^2 \\ s_{br,lat} = \quad & s_{p,lat} + c_v v_{p,lat} T_{brk,p} \\ & + 0.5 c_u a_{p,lat,tran} T_{brk,p}^2 \\ \theta_{br,long} = \quad & \theta_{p,long} + c_w \omega_{p,long} T_{brk,\theta} \\ & + 0.5 c_u a_{p,long,rot} T_{brk,\theta}^2 \\ \theta_{br,lat} = \quad & \theta_{p,lat} + c_w \omega_{p,lat} T_{brk,\theta} \\ & + 0.5 c_u a_{p,lat,rot} T_{brk,\theta}^2 \end{aligned}$$

Finally, washout effect is introduced. The usage of constant weight penalisation requires weight re-tuning for different scenarios to obtain desirable performance. On the other hand, the application of adaptive weights allows a unique configuration for various driving scenarios. The formulation of the adaptive weight for these two states can be seen in (6.14) and (6.15). Figure 6.2 shows how the weight changes based on the platform's position. A high weight is applied when the platform is close to its limit, and a low weight when it is near the neutral position, allowing a washout effect to take place.

$$\begin{aligned} W_{s_p} = & w_{s,1} + w_{s,2} \left(\frac{abs(s_{p,i})}{w_{s,5}} \right) + w_{s,3} \left(\frac{abs(s_{p,i})}{w_{s,5}} \right)^2 \\ & + w_{s,4} \left(\frac{abs(s_{p,i})}{w_{s,5}} \right)^4 \end{aligned} \tag{6.14}$$

$$\begin{aligned} W_{\omega_p} = & w_{\omega,1} + w_{\omega,2} \left(\frac{abs(\omega_{p,i})}{w_{\omega,5}} \right) + w_{\omega,3} \left(\frac{abs(\omega_{p,i})}{w_{\omega,5}} \right)^2 \\ & + w_{\omega,4} \left(\frac{abs(\omega_{p,i})}{w_{\omega,5}} \right)^4 \end{aligned} \tag{6.15}$$

where, the parameters are $w_{s,1} = 0.01$, $w_{s,2} = 20$, $w_{s,3} = 20$, $w_{s,4} = 20$, $w_{s,5} = 0.5$, $w_{\omega,1} = 0.0001$, $w_{\omega,2} = 0.7$, $w_{\omega,3} = 0.7$, $w_{\omega,4} = 0.7$, and $w_{\omega,5} = 3$. The parameter selection is heuristic and based on the analysis of various driving scenarios.
The weighting for the objective function remains consistent with the explicit MPC, apart from the added adaptive washout weights. A more detailed description of the weight selection is in [109].

6.3. SIMULATION RESULTS

6.3.1. SIMULATION SETUP

To analyse the effectiveness of the algorithm in reducing computational costs, a general set of test conditions is taken into account. This includes specific force signals to be tracked in the form of sine waves and step signals along with multiple event waves (step signal + sine wave), for a range of amplitude ($0.5 - 2$ m/s^2) and frequency ($0.1 - 0.8$ Hz) values. Only the latter scenario is shown in Figure 6.3 and Figure 6.4).

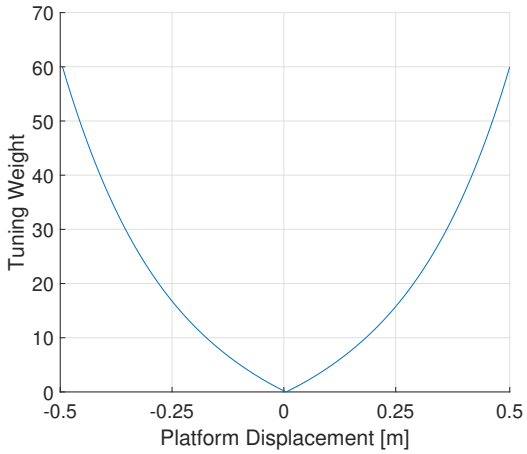

Figure 6.2: Adaptive weights for platform displacement r_p

While computing the explicit solution, a N_p of 2 is selected with a sampling time of 0.25 s to ensure the look-ahead time of 0.5 s. A higher N_p with a faster sampling time cannot be achieved due to the exponential increase in the computation time of the explicit solution. The online version of the MCA (implicit MPC) is able to operate at a faster sampling time and higher prediction horizon N_p. Thus, N_p of 50 with a T_s of 0.01 s is used to maintain the same look-ahead time as used in the explicit controller. It is to be noted that explicit MPC only gives the initial guess for the hybrid MPC setup. Thus, the numerical stability of the method is ensured by selecting a time step of 0.01s for the implicit MPC.

Different MCA algorithms were analysed to compare their performance and listed as follows:

- Implicit MPC without any initial guess.
- Implicit MPC with the first control input. The first control input from the trajectory prediction is applied for the entire horizon as the initial guess for the next optimisation step.
- Hybrid MCA with the first explicit MPC control input. The first control input from the explicit MPC is applied for the entire prediction horizon.
- Hybrid MCA with all explicit MPC control inputs. All control inputs obtained from the explicit MPC controller are used for the entire horizon. Since the sampling time is different in both controllers, the explicit MPC inputs are applied in equal intervals throughout the larger prediction horizon of the implicit MPC. For e.g. with a $N_{p,eMPC}$ of 5, the five control inputs are applied ten times each (1^{st} from 1-10, 2^{nd} from 11-20 and so on) for a $N_{p,iMPC}$ of 50.

Simplified actuator dynamics of the motion platform were considered for the comparison of the algorithms shown in the next section. The extended description of the simulation parameters can be found in [109].

6.3.2. MOTION CUEING PERFORMANCE

Using the defined reference signals, the comparison has been conducted focusing on specific force tracking and online computation time. In Figure 6.3 and Figure 6.4 the specific force tracking performance for a multiple event wave is shown. This comprises an initial step signal followed by a sine wave, both of amplitude 0.5 m/s^2. From the results, it can be observed that the MCA is able to track the reference signal.

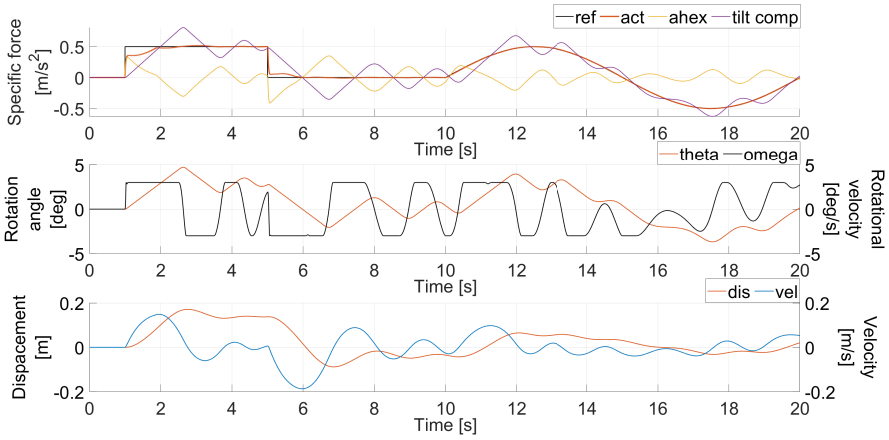

Figure 6.3: Specific force tracking for longitudinal motion for multiple event wave

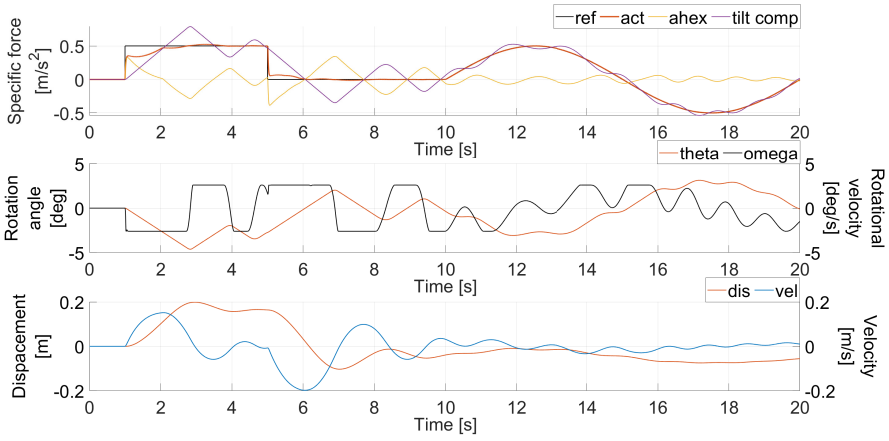

Figure 6.4: Specific force tracking for lateral motion for multiple event wave

Furthermore, the cueing algorithms were evaluated from the point of computational costs across different reference signal scenarios mentioned earlier. All the hybrid models were compared with the implicit MPC-based cueing algorithm, which is the current state-of-the-art MCA. The obtained results are presented in Figure 6.5. The average tracking performance in both longitudinal and lateral directions for all scenarios is also shown in Figure 6.5. It can be observed that the developed hybrid models need less time to compute the optimized control input. The hybrid model with all explicit MPC control inputs performs best amongst all the models analysed. The highest improvement in mean iterations from the implicit algorithm is by 30% while keeping similar tracking performance in both longitudinal and lateral directions. Also, while performing the simulations the maximum iterations are set to 200. This ensures faster computation with marginal sub-optimal results (< 0.3%).

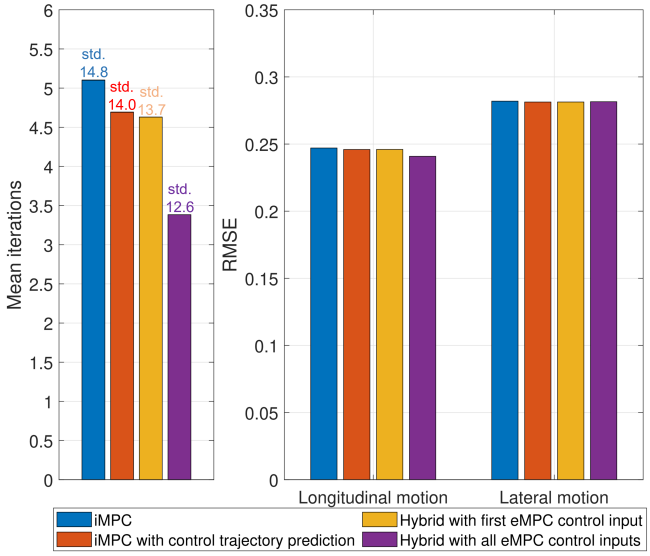

Figure 6.5: Mean iterations along with respective standard deviation and tracking performance for all scenarios

6.3.3. EMULATOR TRACK PERFORMANCE

To evaluate the performance and computational costs, the software emulator has been used developed by the motion platform supplier E2M Technologies B.V. The multibody modeling and the coordinate system are described in [110].

This emulator represents the actual dynamics of the Delft Advanced Vehicle Simulator (DAVSi). The DAVSi is a 6 DoF driving simulator and using its emulator interface, tests can be performed without imparting any damage to the real system.

Full-track simulation tests were performed using this virtual environment. First, IPG CarMaker (a high-fidelity virtual vehicle simulation environment) was used to simulate a

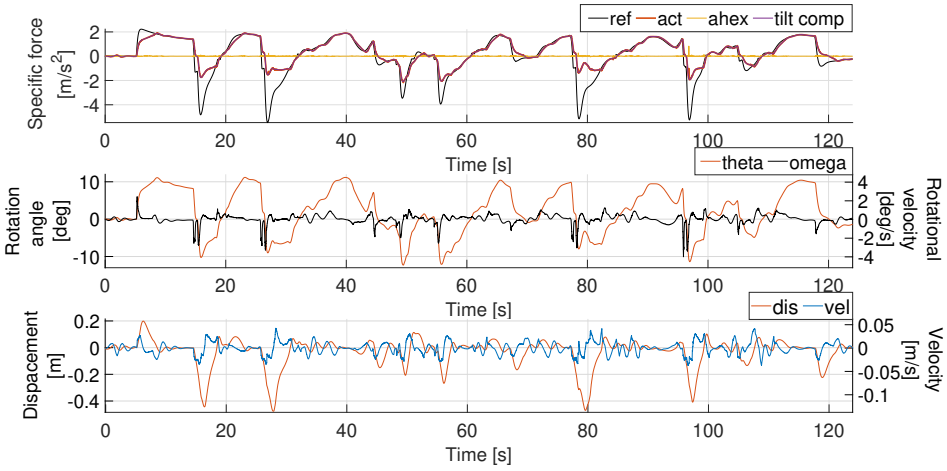

Figure 6.6: Specific force tracking for longitudinal motion results for Hockenheim track simulation

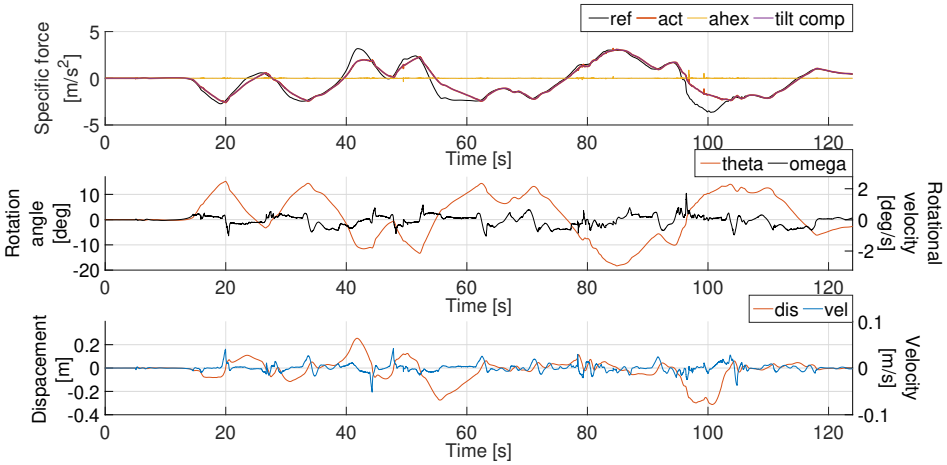

Figure 6.7: Specific force tracking for lateral motion results for Hockenheim track simulation

vehicle driving around the Hockenheim race track, limited to a speed of 120 km/h. Then, acceleration values were extracted and passed through the perception model [79] before using them as reference signals. This was done to ensure that only the perceived acceleration values are sent to the MCA for performing the simulations with the emulator interface. Additionally, the perception model also scaled down the accelerations which makes the signals fit to be recreated in the driving simulator. Figure 6.6 and Figure 6.7 show that the MCA is capable of tracking the reference signal in a desirable manner. An

RMSE of 0.42, 0.21 is observed in both directions respectively. Further, a similar trend in mean iterations is observed with the hybrid MCA improving online computation time performance. An improvement of 9% can be observed with the hybrid model using all control inputs, whereas the other hybrid and implicit models show an improvement of 5.9% and 5.1% respectively. Thus, the developed algorithm can be implemented and used with real track data in motion-based driving simulators.

6.4. CONCLUSION

In this study, a hybrid MCA is proposed using a combination of explicit and implicit MPC techniques. The explicit MPC provides an initial guess used by the implicit MPC to warm-start the algorithm and computes the optimised control input. Amongst the considered state-of-the-art motion cueing algorithms, the best computation time performance is observed from the proposed algorithm, taking all explicit MPC control inputs as the initial guess. Moreover, to improve motion cueing, braking constraints are used for workspace management of the simulator when it is about to reach its physical displacement limits. Adaptive washout weights are also implemented to reduce false cues by bringing the simulator to its neutral position. Overall, the proposed algorithm maintains similar tracking performance across the considered state-of-the-art motion cueing algorithms, but it helps to reduce online computation time by 30%. The performance of the proposed algorithm has been demonstrated in complex track driving. Future work focuses on human-in-the-loop experiments for subjective assessment of the proposed algorithm.

For better results/performance of the adaptive weights law, feasibility analysis of the adaptive weight should be conducted. This is considered as the scope for future work in this paper.

7

Discussion and Conclusion

Nothing, just an inchident,
on the race

Charles Leclerc

This chapter synthesises the thesis findings, which focused on mitigating motion sickness in the context of automated driving and driving simulator motion cueing. A trajectory planning algorithm was developed for automated vehicles, using a model predictive control (MPC) framework to jointly minimise motion sickness dose value (MSDV) and time efficiency. Given the safety and practicality constraints of real-world testing, this algorithm was validated using a high-fidelity 6-DoF driving simulator. The remainder of the thesis concentrated on the development of motion cueing algorithms (MCAs) tailored to improve perceptual fidelity and reduce simulator-induced motion sickness. These MCAs were designed to operate within the physical constraints of the motion platform while explicitly addressing key sources of false cues and sensory conflict. The following discussion critically examines the effectiveness and limitations of the developed strategies, compares them to existing methods, and explores their implications for future automated mobility and simulation technologies.

7.1. DISCUSSION

This dissertation presents a multi-faceted exploration of strategies to reduce motion sickness in the context of automated vehicles (AVs) and driving simulators. The central hypothesis across the chapters is that improving the perceptual realism of motion, while accounting for physiological comfort, can enhance passenger comfort and the effectiveness of simulator-based development. By integrating principles from control systems, vehicle dynamics, and human perception, this work develops a suite of algorithms for trajectory planning and motion cueing that target motion sickness reduction while maintaining high simulation fidelity.

More precisely, the thesis revolved around the following research objectives:

- Developing trajectory planning algorithms for AVs that minimise motion sickness by optimising velocity and curvature profiles.
- Designing motion cueing algorithms for simulators that balance motion fidelity, workspace limitations, and computational efficiency.
- Integrating 6-DoF sensory conflict models into control frameworks to predict and reduce motion sickness.
- Validating the effectiveness of these control strategies using both simulation tools and human-in-the-loop experiments.

While doing so, we also developed algorithms tackling some of the issues faced in the realm of driving simulation. More precisely, to bring the experience in a driving simulator closer to reality and to reduce the computational efficiency of the MCAs.

It is important to note that, as the thesis focuses on automated driving, where the driver becomes the passenger, the MCAs developed herein are tailored to passive driving conditions. Unlike active driving scenarios, in which the user directly controls the virtual vehicle (and, by extension, the simulator platform), the algorithms in this work are designed for cases where the motion is externally controlled and the occupant is a passenger.

INTERCONNECTED GOALS: MOTION COMFORT, REALISM, AND COMPUTATIONAL EFFICIENCY

Across all chapters, the tension between realism, comfort, and real-time performance surfaces repeatedly. While each chapter focuses on a different aspect, whether trajectory optimisation, motion cueing fidelity, computational scalability, or sickness modelling, these goals are fundamentally connected through their shared aim- to support the development of AVs and reduce motion sickness. This is achieved either by designing motion planning algorithms for automated vehicles or by developing motion cueing strategies that enhance simulator realism without increasing discomfort or even decreasing it.

For instance, the trajectory planning algorithm presented in Chapter 2 enhances passenger comfort by modifying vehicle motion to reduce sickness-inducing accelerations. A similar principle guides the motion cueing approaches introduced in Chapter 3, Chapter 4, Chapter 5 and Chapter 6, which strive to recreate realistic vehicle dynamics on limited simulator platforms. Chapter 5 uniquely combines optimization to recreate realistic motion perception while also minimising perceptual conflicts leading to motion sickness. Across these chapters, predictive optimization serves as a unifying tool, enabling anticipatory control that balances realism, comfort, and computational efficiency.

7.1.1. TRAJECTORY PLANNING AND MOTION SICKNESS MITIGATION

This thesis began by addressing the frequently overlooked aspect of passenger comfort in automated vehicle (AV) motion planning. While prior works have proposed comfort-focused strategies—such as bounding vehicle acceleration and jerk [44], or generating smooth paths using geometric curves like clothoids and Bezier curves [37]–[39], these often apply to fixed paths or rely on overly simplified vehicle models. Velocity profile optimization for motion sickness reduction, such as those using MSDV minimization along predefined routes [52]–[54], provides a valuable foundation but similarly suffers from limited model fidelity and constrained trajectory flexibility.

The foundation of the thesis is laid in Chapter 2, where an optimal control-based trajectory planner is developed to minimise motion sickness, using the MSDV as the primary cost metric. The study's use of a 3-DoF non-linear bicycle model allows for more nuanced control compared to traditional point-mass models. Furthermore, human-in-the-loop experiments substantiate the algorithm's benefits in reducing motion sickness.

Importantly, the proposed algorithm modifies not only the velocity profile but also subtly alters the route to further reduce motion sickness—an approach that diverges from the fixed-path optimisations in the aforementioned literature. By incorporating a secondary cost on journey time, the planner introduces a tunable trade-off between comfort and efficiency, which can be modulated through the weight ratio w_m/w_t. As shown in Figure 2.4, reducing the emphasis on MSDV leads to higher sickness exposure but shorter routes. In exploring the ratio between the penalisation weights for MSDV and travel time, w_m/w_t (see Figure 2.4), it was observed that, for a fixed travel time, variations in this ratio affected both the route distance and the resulting MSDV. Specifically, as the weight on MSDV was reduced (i.e., lowering w_m/w_t), the MSDV increased.

For the selected scenario, a reduction in MSDV from $72 m/s^{1.5}$ (corresponding to the REF drive; benchmark) to $34 m/s^{1.5}$ (MSM drive; optimal configuration), showing an approximate reduction of 62%. During the experimental validation in the driving simula-

tor, this translated into an average 65% reduction in reported discomfort, highlighting the effectiveness of the algorithm in mitigating motion sickness. However, this improvement came at the cost of increased travel time—up to 50% longer for the same route.

Thus, while motion sickness was significantly reduced, this improvement came with a clear trade-off in journey duration. Additionally, the algorithm demonstrated real-time capability, achieving a real-time factor of 0.32, which indicates that the trajectory planner is suitable for real-time implementation in actual vehicles. However, practical deployment would require addressing additional considerations, such as collision avoidance and integration with other safety-critical systems.

7.1.2. MOTION CUEING IN DRIVING SIMULATORS

Chapter 2 applied the industry-standard adaptive washout (AW) algorithm, tuned to elicit motion sickness via parameter adaptation (see Table 2.3). However, in Chapter 2, no explicit evaluation of perceived realism or specific force reproduction was conducted. The subsequent chapters address this by introducing an enhanced motion cueing approach based on MPC, with the aim of improving simulator fidelity and realism.

FREQUENCY-SPLITTING MCA: ENHANCING REALISM WHILE MANAGING PLATFORM CONSTRAINTS

MPC-based MCAs are well-regarded for their superior motion fidelity compared to traditional filter-based methods [20], [25], [31], primarily due to their predictive capability and optimisation over a defined horizon. This allows improved specific force tracking and better compliance with platform constraints. However, a key limitation of MPC-based approaches lies in their substantial computational demands, which often hinder real-time implementation.

In Chapter 3, a state of the MPC-based MCA was implemented, demonstrating satisfactory motion cueing performance but also revealing opportunities for further improvement. As expected, the computational load associated with this approach proved to be a significant bottleneck, limiting its practicality for real-time use.

To overcome these challenges, the FS MCA was developed as a hybrid solution, integrating elements from both filter-based and MPC-based strategies. The FS-MCA aims to preserve the perceptual advantages of MPC-based cueing, such as high motion fidelity, while reducing the computational overhead to a level suitable for real-time operation.

This is achieved by providing three separate reference inputs to the MPC:

- The high-frequency component of the vehicle acceleration, used to generate translational platform accelerations.
- The low-frequency component of the vehicle acceleration, used for tilt coordination.
- The complete vehicle acceleration, used to match the total specific force, with the highest penalisation applied in the cost function.

This tri-channel architecture introduces two additional reference signals—namely, the high- and low-frequency components of vehicle acceleration, which are not present

in traditional MPC-based MCAs. While this increases the complexity of the algorithm, it improves convergence by guiding the optimization more effectively. As a result, the RTF improves, enabling more practical real-time implementation without sacrificing perceptual realism.

Objective comparison against two baseline cueing strategies, the AW MCA and the benchmark MPC-based MCA from Chapter 3 showed that the FS-MCA achieves improved specific force tracking compared to the AW approach, while matching the tracking performance of the MPC-based MCA.

In addition, the FS-MCA showed enhanced computational efficiency compared to the benchmark MPC-based MCA, achieving a real-time factor of 0.85 and demonstrating real-time capability. In contrast, the benchmark MPC-based MCA did not meet the requirements for real-time execution with a real-time factor of 1.12.

Subjective evaluations indicated that the FS-MCA provided a more realistic driving experience compared to the AW baseline. However, some participants reported instances of pre-positioning, where platform motion occurred prior to the corresponding visual cue. These instances involved a cancellation between tilt and translational components, resulting in a net-zero specific force but with noticeable simulator movement. This phenomenon, often referred to as velocity buffering in the literature [31], [84], has typically been viewed positively in objective evaluations, as it enables higher specific force magnitudes by anticipating future motion. In contrast, our experiments revealed that such anticipatory behaviour, while characteristic of the predictive nature of MPC, was occasionally perceived as a false cue, diminishing overall realism.

This finding highlighted a critical perceptual trade-off: although FS-MCA improved realism over AW MCA, it introduced temporal inconsistencies that compromised motion realism. These insights directly informed the design of the autoscaling MCA, described in the next chapter.

AUTOSCALING MCA: BALANCING WORKSPACE USE AND CUE FIDELITY

The autoscaling MCA in Chapter 4 builds directly upon the limitations identified in the FS-MCA, particularly the issue of platform pre-positioning, a phenomenon where the simulator initiates motion before any corresponding visual cue. This anticipatory behaviour, although considered to be a positive phenomenon during objective evaluation (described by 'velocity buffering') [31], [84], arises from the mismatch between the predictive demands of the reference trajectory and the physical tilt-rate constraints of the simulator. The autoscaling MCA proposes a novel solution to this problem by dynamically scaling the tilt coordination signal through a time-varying gain.

The autoscaling MCA introduces a time-varying gain that dynamically attenuates the tilt coordination reference signal, ensuring that the resulting tilt rate remains below the perceptual threshold of $3^{\circ}/s$. This constraint is critical to prevent premature or unnatural tilt motions that could disrupt the realism of the driving experience. Unlike fixed scaling approaches, which often distort the signal shape and compromise perceptual coherence, the autoscaling MCA preserves the shape similarity of the specific force signal, a key determinant of perceived vehicle dynamics. This adaptive approach maintains the integrity of motion cues while satisfying sensory and platform constraints, making it a perceptually and computationally efficient solution.

Autoscaling MCA's core innovation lies in its redefinition of cueing fidelity. While traditional MCAs focus on errors in specific force tracking, autoscaling MCA targets temporal coherence: the alignment of translational and rotational motion onsets with visual cues. By focusing on this temporal alignment of motion with visual cues, this approach tackles a previously overlooked but perceptually important issue - false cues resulting from visually incongruent platform behaviour.

Another major design shift in autoscaling MCA is its prioritisation of translational motion for force reproduction. Tilt coordination plays only a supporting role in recreating low-frequency components of the desired force. This philosophy mirrors real-world driving dynamics, where the majority of perceived forces stem from linear accelerations rather than prolonged rotational movement.

The algorithm also preserves computational efficiency, achieving a real-time factor of 0.71, making it suitable for online applications. Compared to the AW MCA, the autoscaling MCA demonstrated superior shape similarity.

By incorporating a dynamic scaling factor, the algorithm eliminates the need for manual tuning of vehicle acceleration scaling across different driving scenarios, requiring only minimal parameter adjustment. Unlike any other MPC-based algortihms that uses a fixed scaling factor, this algorithm promotes shape similarity dynamically tweaking the scaling factor (refer Table 7.1) maintaining motion realism and minimising undesirable pre-positioning.

Subjective evaluations confirmed the success of this approach: 87.5% of participants preferred autoscaling MCA over FS-MCA, citing a more natural and immersive experience. While some increased abruptness in longitudinal transitions was reported, attributed to the absence of frequency-splitting, this was considered a minor trade-off given the substantial improvements in perceptual coherence.

Autoscaling MCA builds upon the structural logic of FS-MCA but diverges in its key priorities. By focusing on dynamic tilt rate control and perceptual alignment rather than rigid reference tracking, autoscaling MCA addresses the limitations of FS and offers a practical, computationally efficient, and subjectively preferred cueing solution.

SENSORY CONFLICT MINIMISATION: PREDICTING AND PREVENTING MOTION SICKNESS

Most existing works on MPC-based MCAs, including those developed in Chapter 3 and Chapter 4, focus primarily on enhancing motion fidelity in driving simulators [19]–[21], [31], with no emphasis on mitigating motion sickness.

In contrast, Chapter 5 introduces a fundamentally different approach, embedding a motion sickness model directly into the MCA's cost function. This represents a deliberate shift away from traditional objectives such as motion fidelity or computational efficiency, instead targeting the perceptual root cause of motion sickness: sensory conflict, defined as the mismatch between expected and actual sensory inputs. The resulting Sensory-Conflict-based Motion Cueing Algorithm (SVC-MCA) prioritises the reduction of motion sickness, optimising cueing not just for specific force accuracy.

This transforms the cueing problem into a multi-objective optimisation that balances specific force tracking against predicted sensory conflict. The SVC-MCA is conceptually unique: its primary aim is not only to preserve realism but to reduce the occurrence of sickness.

To explore the trade-off between fidelity and sickness mitigation, the SVC-MCA was tested across a range of weighting ratios between conflict and specific force terms (w_{con} : w_{spec}). The results demonstrated a tunable balance between competing objectives, akin to a Pareto front, where improvements in one domain came at the cost of performance in another

- High w_{con} values suppressed motion cues to reduce discomfort, at the cost of specific force accuracy.
- Balanced profiles, such as $MPCw_{con0.9}$, successfully retained motion perception while mitigating sickness.
- No-motion profiles yielded the least discomfort but were found to be non-immersive.

Importantly, shape similarity, the resemblance between the desired and rendered motion cues, remained reasonably intact even when the algorithm prioritised conflict reduction. This suggests that important aspects of 'how motion feels' can still be preserved, even when the algorithm focuses on reducing motion sickness.

Subjective evaluations further validated the algorithm's effectiveness:

- Profiles with high conflict weights achieved statistically significant reductions in reported sickness.
- The no-motion condition resulted in the greatest overall mitigation of motion sickness.
- Participants consistently preferred profiles optimised for motion perception or those with balanced motion perception and motion sickness reduction over the no-motion condition.
- The proposed method contributed to a more holistic sense of realism, wherein reduced sickness enhanced perceived comfort, even in cases where objective cue fidelity was moderately compromised.

These findings are consistent with [33], which reported increased perceived fidelity with the addition of motion cues, despite a concurrent rise in motion sickness. However, they contrast with a meta study [32], which concluded that enhanced visual fidelity reduced motion sickness for moving-base simulators but had no such effect in fixed-base setups—suggesting that higher visual fidelity may, in some cases, exacerbate sickness in motion-enabled systems.

However, this benefit came at a computational cost. The real-time factor of 2.1 makes the current SVC-MCA implementation not feasible for online deployment. Future work may address this through explicit MPC reformulation or offline trajectory generation for hybrid applications.

In summary, SVC-MCA represents a paradigm shift: it moves motion cueing from a strictly perceptual optimisation problem toward a perceptually grounded framework considering motion sickness, with demonstrated benefits in subjective outcomes and future potential for controlled induction of motion sickness in driving simulators.

HYBRID MPC: TOWARDS REAL-TIME CAPABILITY

Chapter 6 further addresses computational inefficiency, a central challenge of MPC-MCAs, which limits their real-time applicability. To address this, a hybrid MPC framework was developed, combining the advantages of both explicit and implicit MPC formulations. This two-stage architecture achieved a 30% reduction in computation time without compromising the perceptual quality of the rendered motion cues, bringing high fidelity MPC-based algorithms closer to real-time deployment.

The proposed hybrid approach operates in two phases:

- Explicit MPC (offline): This stage uses a precomputed solution space (look-up table), allowing for instantaneous retrieval of suboptimal control actions with negligible computational load.
- Implicit MPC (online): The result from the explicit MPC is passed as an initial guess to the online solver. This warm start significantly accelerates the convergence of the implicit MPC, leading to faster and more efficient optimisation.

This hybrid design not only improves computational efficiency but also enables practical deployment of predictive algorithms in human-in-the-loop applications, where responsiveness and timing are critical.

This work however, was done earlier in the timeline of the PhD. One key limitation prevented us from implementing this structure in other chapters, specifically SVC-MCA. The explicit MPC used in Chapter 6 supports only linear system models, limiting its compatibility with more complex, nonlinear formulations such as the SVC-MCA, which relies on a nonlinear sensory conflict prediction model. As such, the current hybrid framework could not be directly applied to the SVC-MCA.

Nonetheless, the demonstrated success of the hybrid MPC in accelerating linear-MPC applications provides a promising foundation. With further extension to support nonlinear explicit MPC, or linearisation of the SVC, this method could bridge the gap between perceptually optimised algorithms like SVC-MCA and the demands of real-time deployment—a critical step for simulator realism and operational scalability.

7.1.3. COMPARISON OF THE DEVELOPED MCAS

The MCAs developed over the course of this thesis represent a continuous evolution of motion cueing strategies, shaped by experimental insights and an increasing emphasis on perceptual realism and user comfort. This section synthesises the key similarities and differences between the algorithms presented in Chapter 3 through Chapter 6.

PERCEPTUAL REALISM VS SPECIFIC FORCE TRACKING

A common thread across all cueing algorithms developed is the pursuit of realism and immersion, particularly through improved congruence between vestibular and visual cues. While specific force tracking is traditionally regarded as a core performance metric, this work demonstrates that accurate signal reproduction alone does not guarantee a perceptually convincing experience.

- The FS MCA enhances specific force tracking performance; however, despite this improvement, it introduces perceptually misleading cues during platform pre-positioning, a phenomenon commonly observed in MPC-based MCAs.

- The autoscaling MCA promoted shape similarity over strict magnitude matching. This approach improved the perceptual quality of the cue without introducing misleading cues or oscillations.
- The SVC-based MCA, on the other hand, shifts focus from signal fidelity to minimisation of predicted sensory conflicts, directly targeting the root cause of simulator sickness.

Thus, the progression from FS-MCA to SVC-MCA reflects a fundamental shift in motion cueing design—from prioritising accurate specific force tracking to emphasising motion sickness reduction, even if it means deviating from exact specific force replication, as long as coherent motion perception is preserved. While specific force tracking aims to match the net inertial and gravitational forces acting on the simulator occupant, it may not always be a reliable metric for perceptual fidelity. This is because specific force is a vector sum of inertial and gravitational components, which can cancel each other out, leading to a net zero specific force despite the presence of perceivable motion. Consequently, matching only the magnitude of specific force may fail to recreate a convincing experience. Instead, preserving the shape and timing of specific force profiles, in alignment with vehicle accelerations, can provide a more coherent and perceptually accurate simulation, as demonstrated in Chapter 4. The transition from FS-MCA to autoscaling MCA, and ultimately to SVC-MCA, embodies this evolving philosophy: from the common approach of specific force tracking, to promoting timely motion onsets, and finally to minimising sensory conflict as the core design objective.

TILT COORDINATION AND ONSET TIMING

Tilt coordination emerges as a key differentiator in the algorithms. All proposed strategies utilise tilt to generate low-frequency specific force cues, but their approaches to onset timing and gain control differ significantly:

- FS-MCA uses a frequency-splitting structure, where tilt is planned separately in the low-frequency domain and often causes pre-positioning, leading to false cues.
- Autoscaling MCA introduces a time-varying gain to enforce tilt-rate limits, thus preventing early tilt onsets. It prioritises translational motion while favouring tilt in cases where visual congruence can be reasonably maintained.
- The SVC-MCA doesn't explicitly redesign tilt coordination; rather, its emphasis lies on overall motion planning through conflict minimisation.

COMPUTATIONAL FEASIBILITY AND REAL-TIME IMPLEMENTATION

Another major distinction lies in the computational efficiency of each algorithm. While high-fidelity solutions often demand complex optimisation, real-time applications necessitate a balance between fidelity and feasibility:

- FS and autoscaling MCAs achieve real-time performance using deterministic, rule-based strategies (e.g., frequency-splitting, dynamic gains) that are easily implementable and efficient.

- The SVC-MCA demands substantial computational resources due to its high complexity and the need for a large prediction horizon.

- The Hybrid MPC offers an elegant compromise, reducing computation time by 30% via an offline–online dual-stage approach. It provides a pathway for real-time MPC implementation without compromising fidelity.

This comparison underscores a critical trade-off: while perceptually-driven optimisation may enhance realism, it often increases computational complexity. The Hybrid MPC stands out by demonstrating that intelligent pre-processing (via lookup tables and warm-starts) can mitigate this issue.

Table 7.1: Comparison of Developed MCAs. Flexibility refers to adaptability across vehicle types, scenarios, and simulator setups. For shape similarity, 'maintained' indicates indirect shape similarity as a result of specific force tracking, while 'prioritised' refers to cases where the algorithm incidentally preserved shape similarity more strongly than specific force tracking, despite not explicitly targeting it in the cost function.

Criteria	**AW-MCA**	**FS-MCA**	**Autoscaling-MCA**	**SVC-MCA**
Scaling factor (long.)	0.3	0.3	Automatic and dynamic	0.3
Scaling factor (lat.)	0.4	0.4	Automatic and dynamic	0.4
Real-time	✓	✓	✓	✗
Real-Time Factor	—	0.85	0.71	2.1
Subjective fidelity	Moderate	High (preferred over AW)	High (preferred over FS)	Tunable
Pre-positioning	Absent	Present	Minimal	Tunable
Sickness mitigation	✗	✗	✗	✓
Tuning effort	High	Moderate	Low	Moderate
Shape similarity	Maintained	Maintained	Prioritised	Maintained

While the research in this thesis focused on developing real-time capable algorithms, this work also demonstrates that automated driving simulations can be conducted even when an algorithm is not real-time feasible. Offline-optimized strategies enable the integration of computationally intensive perceptual models, such as SVC, while still producing valid and informative simulation outcomes.

7.1.4. APPLICATION SUITABILITY

Each algorithm exhibits strengths tailored to different use-cases:

- The trajectory planning algorithm is well-suited for automated vehicles aimed at motion sickness reduction. It can serve as a high-level motion planner, defining optimal paths while mitigating motion sickness. However, for practical deployment, it must integrate additional layers, including traffic and collision avoidance and time interpolation for smooth real-time control. The algorithm provides a foundation for motion planning, but underlying layers are essential to account for real-world dynamic interactions and safe vehicle control.

- FS-MCA and autoscaling MCA are most suitable for real-time driving simulations, where the emphasis lies on motion plausibility and visual congruence. The autoscaling MCA, in particular, eliminates the need for scenario-dependent tuning and offers the most consistently preferred experience across subjects.

- The SVC-MCA is optimal for applications requiring sickness mitigation, such as long-duration automated driving simulation or VR-based studies. It is also suitable for research on human motion perception, where inducing or suppressing conflict is a controlled variable.

- Hybrid MPC is ideal for simulators that demand high motion fidelity and responsiveness, especially when computational resources are constrained. This framework amendment integrates with existing MPC-based MCAs to significantly speed up computations without sacrificing fidelity. With further development, it can be extended to non-linear models, enabling integration with perceptually-driven cost functions like those in SVC-MCA, making it adaptable for high-fidelity simulation applications where real-time performance is critical.

7.2. CONCLUSION

This thesis presents a cohesive framework for addressing motion sickness in AVs and driving simulators through trajectory planning and motion cueing algorithms grounded in control theory and human perception. It demonstrates how tailored control strategies, ranging from path planning to optimisation-based motion cueing, can significantly enhance comfort, realism, and efficiency.

Developing trajectory planning algorithms for AVs that minimize motion sickness by optimizing velocity and curvature profiles (R1).
Chapter 2 introduced an optimal trajectory planner that outputs a comfortable reference velocity profile and generates curvature-adaptive paths through corner cutting. By lowering lateral accelerations within the allowable road area, the algorithm reduces motion-inducing stimuli. Human-in-the-loop experiments demonstrated a 65% reduction in motion sickness compared to a benchmark controller, with fewer dropouts and consistently higher comfort ratings. Although individual susceptibility to sickness varied, every participant reported an improvement, highlighting the potential of trajectory planning as a sickness-mitigation strategy while pointing to the future need for personalised comfort settings.

Designing motion cueing algorithms for driving simulators that balance motion fidelity, workspace limitations, and sickness mitigation (R2).
3, 4, and 6 advanced model predictive control (MPC)-based motion cueing algorithms.

- The frequency-splitting MCA improved specific force tracking under short prediction horizons and reduced unnecessary platform motion. Human studies confirmed its ability to reproduce aggressive driving manoeuvres more realistically than adaptive washout, though some false cues from pre-positioning were noted.

- The autoscaling MCA addressed the pre-positioning problem by dynamically scaling accelerations, ensuring feasible reference tracking without premature tilt. In experiments, 87.5% of participants rated it as more realistic than the frequency-splitting algorithm, underscoring that subjective realism may diverge from objective error metrics.

- The Hybrid MCA combined explicit and implicit MPC to reduce online computation time by 30% while maintaining comparable tracking performance to state-of-the-art algorithms.

Integrating 6-DoF sensory conflict models into control frameworks to predict and reduce human discomfort (R3).
Chapter 5 introduced the SVC MCA, which embedded a Subjective Vertical Conflict model directly into the MPC cost function. By penalising sensory conflict, the algorithm reduced motion sickness in both simulations and human-subject experiments, while maintaining realism in perceived motion. Results further revealed that shape similarity of specific force profiles aligned more closely with subjective realism than conventional RMSE measures, suggesting that perceptual congruence can be more critical than strict accuracy in motion cueing design.

Validating the effectiveness of control strategies using both simulation tools and human-in-the-loop experiments (R4).
Across all studies, human-in-the-loop evaluations confirmed the alignment between algorithm design goals and subjective experience. Participants consistently rated the developed algorithms as more realistic and less sickness-inducing compared to baseline approaches, underlining the importance of perceptually driven evaluation in addition to objective performance metrics.

Overall Contributions. While individual variability in motion sickness susceptibility remains an open challenge, this thesis demonstrates that control-theoretic methods can substantially mitigate discomfort while preserving realism. By systematically addressing trajectory planning, motion cueing design, perceptual modelling, and human validation, the research establishes a shift from system-centric to human-centric control in automated driving and simulation. The findings enrich theoretical understanding while laying practical foundations for adaptive, personalised, and sickness-free mobility solutions.

7.3. FUTURE RECOMMENDATIONS

TRAJECTORY PLANNING FOR MOTION COMFORT IN AUTOMATED VEHICLES

The proposed trajectory planner successfully reduced motion sickness stimuli in open-loop simulations. However, practical deployment in automated vehicles (AVs) requires integration of essential functionalities:

- Collision avoidance: Future iterations must embed obstacle proximity constraints into the optimization layer.

- Consensus-based multi-agent planning: With vehicle-to-vehicle communication, motion comfort optimization can be coordinated across vehicles to ensure both safety and cooperative mitigation of sickness.
- Temporal interpolation: Since the current planner operates in the spatial domain, additional layers must handle timing and control execution to ensure feasible and smooth vehicle actuation.

Additionally, extending the framework to support four-wheel steering may enhance vehicle maneuverability and introduce new trade-offs between lateral acceleration and yaw rate. While this has potential to improve motion comfort, its impact on motion sickness should be systematically assessed.

Finally, the current framework, which relies on the MSDV metric, does not account for rotational stimuli. To improve its effectiveness—especially in vehicles equipped with active suspension systems where pitch and roll become significant—a more sophisticated motion sickness model incorporating rotational dynamics such as the SVC model is necessary.

AUTOSCALING VS SVC-BASED MCA: CHOOSING FOR THE APPLICATION

Both the Autoscaling and SVC-based Motion Cueing Algorithms (MCAs) shared one thing in common: the algorithms promoted generation of scaled down specific force profiles compared to the provided reference. However, a critical distinction lies in how each method prioritises and distributes motion reduction. Autoscaling targets the tilt coordination component specifically, scaling it down only when it risks causing prepositioning errors. This ensures that the majority of specific force reproduction, particularly high-frequency translational motion, remains intact. As a result, Autoscaling preserves a sharper sense of acceleration while avoiding overt visual-motion mismatches.

In contrast, the SVC-based MCA reduces the magnitudes of both translational and rotational cues in a globally optimized manner to minimize sensory conflict. This broader attenuation allows the algorithm to more comprehensively suppress motion sickness but often at the cost of reduced motion intensity.

Moreover, SVC-based framework offer tunable control through adjustable conflict weights, enabling tailored motion intensity based on the application or user sensitivity. Autoscaling MCA, by design, automatically adapts to scenario demands and lacks this level of customization, which may limit its flexibility in specialized use cases.

In summary, Autoscaling MCA excels in scenarios where ease of tuning and perceptual coherence are key, while SVC-based MCAs are better suited for applications requiring precise sickness control, such as VR exposure therapy, long-duration simulator training, or psychophysiological studies.

The following recommendations are proposed:

- Establish psychophysical baselines for both approaches under different simulator contexts and user populations.
- Explore hybrid strategies, such as dynamically tuning SVC weights based on user sensitivity or combining Autoscaling's selective scaling with SVC's conflict-aware framework, to harness the strengths of both.

ADVANCING MOTION SICKNESS MODELING: PRECISION VS PRACTICALITY

This thesis highlights the trade-off between computational simplicity and physiological accuracy in motion sickness modeling. While the MSDV metric proved effective for trajectory optimization and real-time applications, its omission of rotational stimuli restricts its predictive fidelity. Sophisticated 6-DoF models such as the SVC model offer more accurate sickness predictions by accounting for both translational and rotational mismatches. However, their complexity currently limits real-time deployment.

Two promising directions for further research are identified to be:

- Model simplification: Derive computationally efficient approximations of 6-DoF SVC models that retain sensitivity to key rotational components.
- Computational efficiency: Improve real-time feasibility of SVC-based frameworks through algorithmic strategies such as those demonstrated in the Hybrid MPC, including pre-processing, warm-starting, and model simplifications, potentially reducing reliance on high-performance hardware.

Furthermore, a comparative study replicating the results of Chapter 2 using the SVC model would clarify how much sickness reduction potential is lost when using simplified models like MSDV.

Moreover, the SVC-MCA framework holds promise beyond mitigating sickness. With minor modifications, the same system can be employed to recreate motion sickness intentionally, for example, in motion sickness acceptance testing or evaluation studies where eliciting perceptual conflict is desirable.

SEPARATING COMFORT AND REALISM IN SUBJECTIVE EVALUATION

During the experiment, some participants verbally described one of the algorithms as being more “comfortable” than others, despite being instructed to rate only perceived realism. This indicates a potential perceptual bias, where comfort may have been conflated with realism in the subjective responses.

To improve the interpretability and reliability of such ratings, future studies should explicitly include comfort as a distinct evaluation metric alongside realism. This separation would allow researchers to differentiate between the two perceptual dimensions and determine whether comfort is inadvertently influencing judgments of realism. It would also provide deeper insights into how different cueing strategies affect both experiential comfort and perceived fidelity, two factors critical for simulator design and evaluation.

USE OF THE ALGORITHMS FOR ACTIVE DRIVING SIMULATIONS

The developed algorithms could potentially be extended to active driving scenarios by integrating driver prediction models, which estimate future accelerations and update the reference trajectory over the prediction horizon, as demonstrated in [21], [111].

However, applying such motion cueing algorithms in active driving presents additional challenges. In passive driving conditions, the MPC-based algorithms in this thesis benefited from preview information of upcoming maneuvers, whereas the adaptive washout algorithm lacks the ability to anticipate future motion. In active driving, such

preview information must be generated online. A particular challenge is the prediction of upcoming maneuvers within the prediction horizon, which can be based on driver models or extrapolation approaches. This introduces uncertainties in the prediction horizon, requiring robust control mechanisms to handle prediction errors and avoid unrecoverable platform states, such as excessively large tilt angles. Furthermore, implementing the SVC-MCA in active driving would require real-time capability or more powerful computational hardware due to its higher complexity. A detailed robustness analysis and real-time implementation strategy are beyond the scope of this work and are identified as important directions for future research.

ACKNOWLEDGEMENTS

Although mere words can hardly do justice in expressing my gratitude to everyone who has contributed to the success of this thesis, I will attempt to express it here.

First and foremost, I would like to thank my daily supervisor, **Dr. Barys Shyrokau**, without whom this PhD would never have been possible. I still vividly remember how a casual catch-up turned into an impromptu interview, which I didn't even know was happening, and the next thing I knew, I was giving a presentation to Toyota for this position. We've had our ups and downs, but this journey simply could not have happened without you. I will always remain deeply thankful to you.

To **Prof. Riender Happee**, at various stages of this PhD, you tried to understand my state of mind and adapted your supervision accordingly. I truly enjoyed our discussions, both about the thesis and beyond it. They were always intellectually stimulating, sometimes philosophical, and almost always insightful. Your consistent involvement kept me on my toes and motivated me to keep pushing for novelty. I will never forget the day I had a breakdown and I yelled at you; your golden words, "It's better to have an outburst in front of me rather than you suffering all alone," have stayed with me ever since. Thank you for your understanding, patience, and guidance throughout.

To **Dr. Daan Pool**, who although not my direct supervisor, guided me on various occasions and always provided valuable insights. To **Dr. Ksander de Winkel** and **Dr. Georgios Papaioannou**, for directly or indirectly contributing to parts of the work in this thesis.

I am grateful to Toyota Motor Europe for funding the project and ensuring the research stayed both academically rigorous and industrially relevant. Special thanks to **Xabier Carrera Akutain** for his wisdom and support in shaping the project, and to **Andrea Michelle Rios Lazcano** for maintaining smooth communication between Toyota and TU Delft, for her availability, and for testing the developed algorithms at TU Delft. Parts of this thesis were published and patented with Toyota's support, for which I am thankful.

To a few people who have been connected to me the most, who have known my mental condition at all times during the journey. **Gabriele Tombakaite**, you have been there for me as a best friend from before the PhD, you were even there at the next desk during my interview. Thank you for being part of this journey from start to finish. **Zeta**, thank you for being my pillar of support and believing in me throughout this journey. Even though we never met in person during my PhD, your presence was constant and invaluable. **Daniel**, I can finally tell you my graduation date! 18th December 2025, I made it! Thank you for your consistent faith, support, and belief in me. **Gürol**, thank you for all your belief and support, you tried to help me in every way you could and I can't express how much I appreciate it. **Chrysovalanto**, thank you for teaching me how to recognize when work is too much, you believed in me and supported me through good and bad times. **Federico**, thank you for all those "ballerina cappuccina" breaks that kept

me refreshed throughout. Your presence, both within and outside the workplace, meant a lot.

A special thanks to everyone who supported me during my leg injury. As it was during COVID, your support feels all the more important to me. **Tuğrul**, you were there from the very beginning of that painful period, the one who carried me to my bed after I broke my leg and who took me for my final surgery. Your kindness and care made an unforgettable difference. Although you were a PhD student yourself when I started, you knew the most about motion sickness. From our random chats about "putting people in misery" to you actually trying to induce motion sickness in me during the chair experiment, you guided me in more ways than one and became something of a role model. Thank you for being both a mentor and a friend. **Lotte**, thank you for being there for me during this time, I'll never forget the help you provided me or that spinach–avocado smoothie you recommended. **Rupak**, you took care of me more like a little brother than a roommate during this time, I can't thank you enough for this. **Cristian**, you were selflessly there with me during this time and even made me meals. Thank you for your support during that time and for believing in me through this whole journey.

To those who have been a joy to be around and have helped me manage my stress throughout this journey, **Robin**, talking to you has always been a delight. Thank you for your warmth, sweetness, and the support you've given me whenever I needed it. **Maxime**, thank you for all the tennis sessions, they were exactly what I needed during the more stressful phases of the PhD. You even helped make my experiment better, and I'm grateful for your support. **Alysia**, although we haven't known each other for very long, you have always trusted me blindly in everything I've done, Thank you for that. **Renate**, Your weird sense of humor was so refreshing! keep up the good work! **Marie**, thank you for all the short, fun conversations and for the amazing fresh Belgian waffles.

To those who stuck with me through thick and thin. **Vishant**, thank you for hosting me wherever you've lived and for tolerating my frequent visits. You've been a true friend through all these years. **Arsel**, your humor and point of view is always refreshing, thank you for trying to help in your own way throughout. **Arjun**, a much underappreciated friend, you literally started and ended the PhD journey a month before me, you have been a consistent support, thank you. **Akshay**, thank you for being an absolutely lovely person and providing your support in any way you could. **Yannick**, thank you for your great company at all the F1 races, all the drinks, and all the festivals we went to together. **Orçun**, my first Dutch friend, you have been like a brother to me. Thank you for your trust and belief and for bearing with me through my horrible Dutch conversations. **Jochem**, thank you for always being ready to help in any way possible and for your kindness and reliability.

A special mention goes to Socieats Thea, a small club founded and kept to four with a similar outlook towards the PhD journey, whose camaraderie and support were essential. **Alberto**, you have been there since day one of my PhD, always willing to help, and our discussions, academic or otherwise, have been priceless. **Hidde**, I always enjoyed our deep and resonating discussions, especially during coffee breaks and post drinks. **Wilbert**, as a co-founder of Socieats Thea and a former roommate, you've seen me at my best and my worst. Thank you for all those times and for your belief.

To all the people at the office who were an active part of my life during this jour-

ney. **Varun**, thank you for being the other half of the project. This journey would have been much harder without you and without our Hindi conversations. **Shiming**, thank you for your generosity, kindness, guidance to amazing Chinese food, and for enriching my Chinese vocabulary. **Andras**, I will always remember the data collection we did in my second month of PhD with the Prius, your company was as fun as that experience. **Mubariz**, my Pakistani brother, even during difficult global times, our friendship remained strong. **Xiaolin**, though not in the same office, it always felt like you belonged there. **Soyeon**, thank you for helping me improve my experiment design and for being such a delightful and kind presence. **Charlotte**, thank you for always bringing a cheerful and helpful attitude. **Ted**, a giant man with a giant heart, thank you for enriching my Dutch vocabulary. **Hanneke**, I can't thank you enough for your help with bureaucracy, you were always there like a dear friend whenever I needed assistance. **Andre**, thank you for your quick and resourceful help in setting up my experiments at short notice. **Emma**, dankjewel for all the fun Dutch lessons and for being such a joyous officemate. **Remco**, no matter how much Dutch I learn, you always find a way to make me feel like a beginner, challenge accepted! **Yanggu**, same supervisor, similar topic, and the same passion for motorsports, thank you for the great chats. **Mario**, thank you for all your PC hardware help and the constant laughter. **Ronald**, thank you for the thoughtful and engaging conversations over food and beyond. **Sandeep**, my first master's student, during your supervision I was bedridden, yet you took charge, visited me, and ensured your thesis progressed smoothly. Thank you for contributing to the early phase of this PhD.

Riccardo, someone once said, "I think you guys will get along," and they were absolutely right, thank you for your constant trust and support. **Samir**, from a master's student to a researcher to a PhD, it was great to see your growth and share this journey. **Ebrahim**, you embody the "work hard, party hard" spirit, thank you for involving me in the latter! **Mohammad**, the X-man, your energy and dedication to workout is insane, thank you for the post-workout drinks and all the good times. **Moretza**, thank you for all the coffee talks, tennis, and general conversations we had throughout the past years, they were always a little funny and a little insightful. **Gabriele Rini**, thank you for sharing not only a similar PhD topic but also a similar sense of humour and all those endless memes. **Giovanni Righetti**, (Giorgio), thank you for all the fun times and the attempted pizza during your visit to TU Delft. **Jose**, Sutrooo! you were always so much fun to be around. **Gabriele Dell'Orto**, Picasso, thank you for the karaoke nights and laughter. **Anna**, thank you for the funny coffee chats and for believing in me, I promise that if I ever get the chance to visit the Mercedes F1 factory, I'll take you along! **Ekaterina**, thank you for your wonderful company during coffee breaks, experiments, and drinks, and for helping me recruit participants.

Karan, **Nishant**, and **Mircea**, the three most intellectual friends I met during my master's, your friendship and inspiration stayed with me. Thank you for your consistent belief. **Yasir**, our friendship dates back to the bachelor's days, thank you for your consistent support and belief since then.

Ada, thank you for being such a supportive and tidy roommate, it was a joy to share a home with you for two years. **Cecile**, thank you for your warmth and for always making the house feel welcoming. **Leonor**, thank you for all the fun kitchen chats, the best part of having a nice roommate is definitely the great conversations that happen while cooking.

Ethan, thank you for bringing endless positivity into the house.

To **Ayush Gupta** and **Saksham Awasthi**, my friends from back home, every time we talk it feels like no time has passed since high school. Your belief in me has meant a lot. And to **Shahrukh**, my oldest friend, thank you for standing by me for longer than anyone else and for your unwavering support over the years.

Finally, to my family, my father **Ajay Kumar Jain**, my mother **Alpana Jain**, my sister **Shinzani**, and my cousin **Dishita**, words will never be enough. Everything I have achieved is because of your love, support, and sacrifice. Papa and Mummy, thank you for giving me everything I could ever need, emotionally, morally, and financially. Shinzani, you've always been someone I look up to, thank you for teaching me sensibility, empathy, and strength (even through our fights!). Dishita, your constant encouragement and belief kept me going through all times.

To all the participants who took part in my experiments, thank you for your time and effort. This thesis would not exist without you.

And finally, a light-hearted but sincere thank you to coffee, the silent companion of every PhD student. The countless "coffee breaks" (even when I cheated with water) kept me sane throughout this long journey.

Whether the dream you pursue succeeds or fails, what truly endures are the insights gained along the journey and the relationships forged along the way.

BIBLIOGRAPHY

[1] M. Martínez-Díaz, F. Soriguera, and I. Pérez, "Autonomous driving: A bird's eye view," *IET Intelligent Transport Systems*, vol. 13, no. 4, pp. 563–579, 2019.

[2] T. Litman, *Autonomous vehicle implementation predictions: Implications for transport planning*. Victoria Transport Policy Institute Victoria, Canada, 2020. [Online]. Available: https://www.vtpi.org/avip.pdf.

[3] C. Diels and J. E. Bos, "Self-driving carsickness," *Applied Ergonomics*, vol. 53, pp. 374–382, 2016.

[4] T. T. Team. "The bigger picture on autopilot safety," Tesla. (2024), [Online]. Available: https://www.tesla.com/blog/bigger-picture-autopilot-safety.

[5] Audi Australia. "Audi ai traffic jam pilot," Audi Magazine Australia. (2017), [Online]. Available: https://magazine.audi.com.au/article/audi-ai-traffic-jam-pilot.

[6] T. W. Team. "Waymo one is now open to everyone in san francisco," Waymo. (Jun. 2024), [Online]. Available: https://waymo.com/blog/2024/06/waymo-one-is-now-open-to-everyone-in-san-francisco/.

[7] I. Pettersson and I. M. Karlsson, "Setting the stage for autonomous cars: A pilot study of future autonomous driving experiences," *IET Intelligent Transport Systems*, vol. 9, no. 7, pp. 694–701, 2015.

[8] J. T. Reason and J. J. Brand, *Motion sickness*. Academic press, 1975.

[9] V. Harsch, "Centrifuge "therapy" for psychiatric patients in germany in the early 1800s," *Aviation, space, and environmental medicine*, vol. 77, no. 2, pp. 157–160, 2006.

[10] G. E. Riccio and T. A. Stoffregen, "An ecological theory of motion sickness and postural instability," *Ecological psychology*, vol. 3, no. 3, pp. 195–240, 1991.

[11] S. M. Ebenholtz, "Motion sickness and oculomotor systems in virtual environments," *Presence: Teleoperators & Virtual Environments*, vol. 1, no. 3, pp. 302–305, 1992.

[12] S. M. Ebenholtz, *Oculomotor systems and perception*. Cambridge University Press Cambridge, 2001, vol. 212.

[13] T. Irmak, D. M. Pool, and R. Happee, "Objective and subjective responses to motion sickness: The group and the individual," *Experimental Brain Research*, vol. 239, no. 2, pp. 515–531, 2021.

[14] A. Stratulat, V. Roussarie, J. L. Vercher, and C. Bourdin, "Improving the realism in motion-based driving simulators by adapting tilt-translation technique to human perception," in *IEEE Virtual Reality Conference*, 2011, pp. 47–50.

[15] C. Seehof, U. Durak, and H. Duda, "Objective motion cueing test-experiences of a new user," in *AIAA Modeling and Simulation Technologies Conference*, 2014, p. 2205.

[16] B. Shyrokau, J. De Winter, O. Stroosma, C. Dijksterhuis, J. Loof, R. van Paassen, and R. Happee, "The effect of steering-system linearity, simulator motion, and truck driving experience on steering of an articulated tractor-semitrailer combination," *Applied Ergonomics*, vol. 71, pp. 17–28, 2018.

[17] R. J. Telban, W. Wu, F. M. Cardullo, and J. A. Houck, "Motion cueing algorithm development: Initial investigation and redesign of the algorithms," Tech. Rep., 2000.

[18] A. Naseri and P. Grant, "An improved adaptive motion drive algorithm," in *AIAA Modeling and Simulation Technologies Conference and Exhibit*, 2005, p. 6500.

[19] M. Bruschetta, F. Maran, and A. Beghi, "A nonlinear, mpc-based motion cueing algorithm for a high-performance, nine-dof dynamic simulator platform," *IEEE Transactions on Control Systems Technology*, vol. 25, no. 2, pp. 686–694, 2016.

[20] Y. R. Khusro, Y. Zheng, M. Grottoli, and B. Shyrokau, "Mpc-based motion-cueing algorithm for a 6-dof driving simulator with actuator constraints," *Vehicles*, vol. 2, no. 4, pp. 625–647, 2020.

[21] A. Lamprecht, D. Steffen, K. Nagel, J. Haecker, and K. Graichen, "Online model predictive motion cueing with real-time driver prediction," *IEEE Transactions on Intelligent Transportation Systems*, vol. 23, no. 8, pp. 12 414–12 428, 2021.

[22] F. Ellensohn, M. Schwienbacher, J. Venrooij, and D. Rixen, "Motion cueing algorithm for a 9-dof driving simulator: Mpc with linearized actuator constraints," *SAE International Journal of Connected and Automated Vehicles*, vol. 2, no. 12-02-03-0010, pp. 145–155, 2019.

[23] Z. Fang and A. Kemeny, "Explicit mpc motion cueing algorithm for real-time driving simulator," in *International Power Electronics and Motion Control Conference*, 2012, pp. 874–878.

[24] A. Chadha, V. Jain, A. M. R. Lazcano, and B. Shyrokau, "Computationally-efficient motion cueing algorithm via model predictive control," in *IEEE International Conference on Mechatronics*, 2023, pp. 1–6.

[25] M. R. C. Qazani, H. Asadi, S. Mohamed, C. P. Lim, and S. Nahavandi, "A time-varying weight mpc-based motion cueing algorithm for motion simulation platform," *IEEE Transactions on Intelligent Transportation Systems*, vol. 23, pp. 11 767–11 778, 2021.

[26] A. Mohammadi, H. Asadi, K. Nelson, S. Mohamed, and S. Nahavandi, "Multiobjective and interactive genetic algorithms for weight tuning of a model predictive control-based motion cueing algorithm," *IEEE transactions on cybernetics*, vol. 49, no. 9, pp. 3471–3481, 2018.

[27] H. Asadi, A. Mohammadi, S. Mohamed, M. R. C. Qazani, C. P. Lim, A. Khosravi, and S. Nahavandi, "A model predictive control-based motion cueing algorithm using an optimized nonlinear scaling for driving simulators," in *2019 IEEE International Conference on Systems, Man and Cybernetics*, 2019, pp. 1245–1250.

[28] H. Scheidel, H. Asadi, T. Bellmann, A. Seefried, S. Mohamed, and S. Nahavandi, "A deep reinforcement learning based motion cueing algorithm for vehicle driving simulation," *IEEE Transactions on Vehicular Technology*, vol. 73, no. 7, pp. 9696–9705, 2024.

[29] S. Al-serri, M. R. C. Qazani, S. Mohamed, A. Arogbonlo, M. Al-ashmori, C. P. Lim, S. Nahavandi, and H. Asadi, "Optimising horizons in model predictive control for motion cueing algorithms using reinforcement learning," in *2024 IEEE International Conference on Systems, Man, and Cybernetics*, IEEE, 2024, pp. 2793–2800.

[30] R. Jacumet, S. Wagner, M. Schwienbacher, D. Wollherr, and M. Leibold, "Sequential motion cueing algorithms: Using the best algorithm in each situation," in *Proceedings of the Driving Simulation Conference 2024 Europe VR*, 2024.

[31] P. Biemelt, S. Böhm, S. Gausemeier, and A. Trächtler, "Subjective evaluation of filter- and optimization-based motion cueing algorithms for a hybrid kinematics driving simulator," in *2021 IEEE International Conference on Systems, Man, and Cybernetics (SMC)*, 2021, pp. 1619–1626.

[32] K. N. de Winkel, T. M. Talsma, and R. Happee, "A meta-analysis of simulator sickness as a function of simulator fidelity," *Experimental Brain Research*, pp. 1–17, 2022.

[33] R. A. Romano, G. D. Park, V. Paul, and R. W. Allen, "Motion cueing evaluation of off-road heavy vehicle handling," SAE Technical Paper, Tech. Rep., 2016.

[34] V. Jain, S. S. Kumar, G. Papaioannou, R. Happee, and B. Shyrokau, "Optimal trajectory planning for mitigated motion sickness: Simulator study assessment," *IEEE Transactions on Intelligent Transportation Systems*, vol. 24, no. 10, pp. 10 653–10 664, 2023.

[35] D. Paddeu, G. Parkhurst, and I. Shergold, "Passenger comfort and trust on first-time use of a shared autonomous shuttle vehicle," *Transportation Research Part C: Emerging Technologies*, vol. 115, p. 102 604, 2020.

[36] B. Paden, M. Čáp, S. Z. Yong, D. Yershov, and E. Frazzoli, "A survey of motion planning and control techniques for self-driving urban vehicles," *Transactions on Intelligent Vehicles*, vol. 1, no. 1, pp. 33–55, 2016.

[37] A. Scheuer and T. Fraichard, "Continuous-curvature path planning for car-like vehicles," in *International Conference on Intelligent Robot and Systems*, 1997, pp. 997–1003.

[38] E. Lambert, R. Romano, and D. Watling, "Optimal path planning with clothoid curves for passenger comfort," in *International Conference on Vehicle Technology and Intelligent Transport Systems*, 2019, pp. 609–615.

[39] I. Bae, J. H. Kim, J. Moon, and S. Kim, "Lane change maneuver based on bezier curve providing comfort experience for autonomous vehicle users," in *Intelligent Transportation Systems Conference*, 2019, pp. 2272–2277.

[40] D. González, V. Milanés, J. Pérez, and F. Nashashibi, "Speed profile generation based on quintic bézier curves for enhanced passenger comfort," in *Intelligent Transportation Systems Conference*, IEEE, 2016, pp. 814–819.

[41] K. N. de Winkel, T. Irmak, R. Happee, and B. Shyrokau, "Standards for passenger comfort in automated vehicles: Acceleration and jerk," *Applied Ergonomics*, vol. 106, p. 103 881, 2023.

[42] A. Artuñedo, J. Villagra, and J. Godoy, "Jerk-limited time-optimal speed planning for arbitrary paths," *Transactions on Intelligent Transportation Systems*, vol. 23, no. 7, pp. 8194–8208, 2022.

[43] M. Benko Loknar, S. Blažič, and G. Klančar, "Minimum-time velocity profile planning for planar motion considering velocity, acceleration and jerk constraints," *International Journal of Control*, vol. 96, no. 1, pp. 251–265, 2023.

[44] H. Shin, D. Kim, and S.-E. Yoon, "Kinodynamic comfort trajectory planning for car-like robots," in *International Conference on Intelligent Robots and Systems*, 2018, pp. 6532–6539.

[45] Y. Zheng, B. Shyrokau, and T. Keviczky, "Comfort and time efficiency: A roundabout case study," in *Intelligent Transportation Systems Conference*, 2021, pp. 3877–3883.

[46] F. Hegedüs, T. Bécsi, S. Aradi, and P. Gápár, "Model based trajectory planning for highly automated road vehicles," *IFAC-PapersOnLine*, vol. 50, no. 1, pp. 6958–6964, 2017.

[47] J. Ziegler, P. Bender, T. Dang, and C. Stiller, "Trajectory planning for bertha—a local, continuous method," in *Intelligent Vehicles Symposium*, 2014, pp. 450–457.

[48] X. Qian, I. Navarro, A. de La Fortelle, and F. Moutarde, "Motion planning for urban autonomous driving using bézier curves and mpc," in *Intelligent Transportation Systems Conference*, 2016, pp. 826–833.

[49] R. Lattarulo and J. Pérez Rastelli, "A hybrid planning approach based on mpc and parametric curves for overtaking maneuvers," *Sensors*, vol. 21, no. 2, p. 595, 2021.

[50] D. Li and L. Chen, "Mitigating motion sickness in automated vehicles with vibration cue system," *Ergonomics*, vol. 65, no. 10, pp. 1313–1325, 2022.

[51] D. Li, B. Xu, L. Chen, and J. Hu, "Automated car-following algorithm considering passenger motion sickness," in *Proc. Int. Symp. Future Act. Saf. Technol. Toward Zero Traffic Accidents*, 2021, pp. 1–6.

[52] C. Certosini, R. Capitani, and C. Annicchiarico, "Optimal speed profile on a given road for motion sickness reduction," *arXiv preprint arXiv:2010.05701*, 2020.

[53] Z. Htike, G. Papaioannou, E. Siampis, E. Velenis, and S. Longo, "Fundamentals of motion planning for mitigating motion sickness in automated vehicles," *Transactions on Vehicular Technology*, vol. 71, no. 3, pp. 2375–2384, 2022.

[54] D. Li and J. Hu, "Mitigating motion sickness in automated vehicles with frequency-shaping approach to motion planning," *Robotics and Automation Letters*, vol. 6, no. 4, pp. 7714–7720, 2021.

[55] I. S. Organization, *Mechanical vibration and shock-evaluation of human exposure to whole body vibration. part 1: General requirements. international*, 1997.

[56] J. Golding, H. Markey, and J. Stott, "The effects of motion direction, body axis, and posture on motion sickness induced by low frequency linear oscillation.," *Aviation, Space, and Environmental Medicine*, vol. 66, no. 11, pp. 1046–1051, 1995.

[57] B. E. Donohew and M. J. Griffin, "Motion sickness: Effect of the frequency of lateral oscillation," *Aviation, Space, and Environmental Medicine*, vol. 75, no. 8, pp. 649–656, 2004.

[58] A. Domahidi and J. Jerez, "Forces professional. embotech gmbh (http://embotech.com/forces-pro)," *t uly (cit. on p. 30)*, 2014.

[59] T. Irmak, K. N. de Winkel, D. M. Pool, H. H. Bülthoff, and R. Happee, "Individual motion perception parameters and motion sickness frequency sensitivity in fore-aft motion," *Experimental Brain Research*, vol. 239, no. 6, pp. 1727–1745, 2021.

[60] B. Alrifaee and J. Maczijewski, "Real-time trajectory optimization for autonomous vehicle racing using sequential linearization," in *Intelligent Vehicles Symposium*, 2018, pp. 476–483.

[61] H. Arioui, L. Nehaoua, and H. Amouri, "Classic and adaptive washout comparison for a low cost driving simulator," in *International Symposium on Control and Automation*, 2005, pp. 586–591.

[62] N. Dużmańska, P. Strojny, and A. Strojny, "Can simulator sickness be avoided? a review on temporal aspects of simulator sickness," *Frontiers in Psychology*, vol. 9, p. 2132, 2018.

[63] K. N. de Winkel, T. Irmak, V. Kotian, D. M. Pool, and R. Happee, "Relating individual motion sickness levels to subjective discomfort ratings," *Experimental Brain Research*, vol. 240, no. 4, pp. 1231–1240, 2022.

[64] T. Irmak, V. Kotian, R. Happee, K. N. de Winkel, and D. M. Pool, "Amplitude and temporal dynamics of motion sickness," *Frontiers in systems neuroscience*, vol. 16, p. 866 503, 2022.

[65] S. Nordhoff, J. de Winter, W. Payre, B. Van Arem, and R. Happee, "What impressions do users have after a ride in an automated shuttle? an interview study," *Transportation Research Part F: Traffic Psychology and Behaviour*, vol. 63, pp. 252–269, 2019.

[66] R. Krueger, T. H. Rashidi, and J. M. Rose, "Preferences for shared autonomous vehicles," *Transportation Research Part C: Emerging Technologies*, vol. 69, pp. 343–355, 2016.

[67] V. Jain, A. Lazcano, R. Happee, and B. Shyrokau, "Motion cueing algorithm for effective motion perception: A frequency-splitting mpc approach," in *Proceedings of the Driving Simulation Conference Europe, Antibes, France*, 2023.

[68] N. J. Garrett and M. C. Best, "Model predictive driving simulator motion cueing algorithm with actuator-based constraints," *Vehicle System Dynamics*, vol. 51, no. 8, pp. 1151–1172, 2013.

[69] F. Ellensohn, F. Oberleitner, M. Schwienbacher, J. Venrooij, and D. Rixen, "Actuator-based optimization motion cueing algorithm," in *2018 IEEE/ASME International Conference on Advanced Intelligent Mechatronics*, 2018, pp. 1021–1026.

[70] H. Asadi, T. Bellmann, M. C. Qazani, S. Mohamed, C. P. Lim, and S. Nahavandi, "A novel decoupled model predictive control-based motion cueing algorithm for driving simulators," *IEEE Transactions on Vehicular Technology*, vol. 72, no. 6, pp. 7024–7034, 2023.

[71] A. Mohammadi, S. Mohamed, H. Asadi, and S. Nahavandi, "Stabilizing model predictive control with optimized terminal sample weight for motion cueing algorithm," in *2019 IEEE International Conference on Industrial Technology (ICIT)*, IEEE, 2019, pp. 1363–1368.

[72] A. Mohammadi, H. Asadi, S. Mohamed, K. Nelson, and S. Nahavandi, "Mpc-based motion cueing algorithm with short prediction horizon using exponential weighting," in *2016 IEEE International Conference on Systems, Man, and Cybernetics (SMC)*, 2016, pp. 000 521–000 526.

[73] S. Munir, M. Hovd, Z. Fang, S. Olaru, and A. Kemeny, "Complexity reduction in motion cueing algorithm for the ultimate driving simulator," *IFAC-PapersOnLine*, vol. 50, no. 1, pp. 10 729–10 734, 2017.

[74] B. Karg and S. Lucia, "Efficient representation and approximation of model predictive control laws via deep learning," *IEEE transactions on cybernetics*, vol. 50, no. 9, pp. 3866–3878, 2020.

[75] L. H. Csekő, M. Kvasnica, and B. Lantos, "Explicit mpc-based rbf neural network controller design with discrete-time actual kalman filter for semiactive suspension," *IEEE Transactions on Control Systems Technology*, vol. 23, no. 5, pp. 1736–1753, 2015.

[76] M. C. Veltena, "Movement simulator," pat. US 2012/0029703 A1, Patent, Feb. 2012.

[77] J. Haasnoot, R. Happee, V. van der Wijk, and A. L. Schwab, "Validation of a novel bicycle simulator with realistic lateral and roll motion," *Vehicle system dynamics*, vol. 62, no. 7, pp. 1802–1826, 2024.

[78] M. R. C. Qazani, H. Asadi, S. Khoo, and S. Nahavandi, "A linear time-varying model predictive control-based motion cueing algorithm for hexapod simulation-based motion platform," *IEEE Transactions on Systems, Man, and Cybernetics: Systems*, vol. 51, no. 10, pp. 6096–6110, 2019.

[79] J. A. Houck, R. J. Telban, and F. M. Cardullo, "Motion cueing algorithm development: Human-centered linear and nonlinear approaches," Tech. Rep., 2005.

[80] J. R. Van der Ploeg, D. Cleij, D. M. Pool, M. Mulder, and H. H. Bülthoff, "Sensitivity analysis of an mpc-based motion cueing algorithm for a curve driving scenario," in *Proceedings of the Driving Simulation Conference 2020 Europe, Antibes, France*, 2020, pp. 37–44.

[81] G. Papaioannou, M. Cvetkovic, C. Messiou, V. Kotian, B. Shyrokau, and R. Happee, "A novel experiment to unravel fundamental questions about postural stability and motion comfort in automated vehicles," in *Comfort Congress*, 2023, p. 123.

[82] H. Bellem, M. Klüver, M. Schrauf, H.-P. Schöner, H. Hecht, and J. F. Krems, "Can we study autonomous driving comfort in moving-base driving simulators? a validation study," *Human factors*, vol. 59, no. 3, pp. 442–456, 2017.

[83] M. Kolff, C. Himmels, J. Venrooij, A. Parduzi, D. M. Pool, A. Riener, and M. Mulder, "Effect of motion mismatches on ratings of motion incongruence and simulator sickness in urban driving simulations," *Transportation Research Part F: Traffic Psychology and Behaviour*, vol. 115, p. 103 370, 2025.

[84] M. Grottoli, D. Cleij, P. Pretto, Y. Lemmens, R. Happee, and H. H. Bülthoff, "Objective evaluation of prediction strategies for optimization-based motion cueing," *Simulation*, vol. 95, no. 8, pp. 707–724, 2019.

[85] L. J. Hettinger and G. E. Riccio, "Visually induced motion sickness in virtual environments," *Presence: Teleoperators & Virtual Environments*, vol. 1, no. 3, pp. 306–310, 1992.

[86] A. H. J. Jamson, *Motion cueing in driving simulators for research applications*. University of Leeds, 2010.

[87] M. J. Griffin, *Handbook of human vibration*. Academic press, 2012.

[88] J. E. Steele, "The symptomatology of motion sickness," in *Fourth Symposium on the Role of the Vestibular Organs in Space Exploration*, Scientific and Technical Information Division, Office of Technology, 1970, pp. 89–98.

[89] V. Kotian, D. M. Pool, and R. Happee, "Personalising Motion Sickness Models: Estimation and Statistical Modeling of Individual-Specific Parameters," *Frontiers in Systems Neuroscience*, vol. 19, p. 1 531 795, ISSN: 1662-5137.

[90] C.-Y. Liao, S.-K. Tai, R.-C. Chen, and H. Hendry, "Using eeg and deep learning to predict motion sickness under wearing a virtual reality device," *Ieee Access*, vol. 8, pp. 126 784–126 796, 2020.

[91] B. Keshavarz, K. Peck, S. Rezaei, and B. Taati, "Detecting and predicting visually induced motion sickness with physiological measures in combination with machine learning techniques," *International Journal of Psychophysiology*, vol. 176, pp. 14–26, 2022.

[92] M. Recenti, C. Ricciardi, R. Aubonnet, I. Picone, D. Jacob, H. Á. Svansson, S. Agnarsdóttir, G. H. Karlsson, V. Baeringsdóttir, H. Petersen, *et al.*, "Toward predicting motion sickness using virtual reality and a moving platform assessing brain, muscles, and heart signals," *Frontiers in Bioengineering and Biotechnology*, vol. 9, p. 635 661, 2021.

[93] D. Li and J. Hu, "Mitigating motion sickness in automated vehicles with frequency-shaping approach to motion planning," *Robotics and Automation Letters*, vol. 6, no. 4, pp. 7714–7720, 2021.

[94] T. Van Leeuwen, D. Cleij, D. Pool, M. Mulder, and H. H. Bülthoff, "Time-varying perceived motion mismatch due to motion scaling in curve driving simulation," *Transportation research part F: traffic psychology and behaviour*, vol. 61, pp. 84–92, 2019.

[95] O. X. Kuiper, J. E. Bos, C. Diels, and K. Cammaerts, "Moving base driving simulators' potential for carsickness research," *Applied Ergonomics*, vol. 81, p. 102 889, 2019.

[96] V. Kotian, D. M. Pool, and R. Happee, "Modelling individual motion sickness accumulation in vehicles and driving simulators," in *Proceedings of the Driving Simulation Conference*, 2023.

[97] T. Wada, J. Kawano, Y. Okafuji, A. Takamatsu, and M. Makita, "A computational model of motion sickness considering visual and vestibular information," in *2020 IEEE International Conference on Systems, Man, and Cybernetics (SMC)*, IEEE, 2020, pp. 1758–1763.

[98] V. Kotian, T. Irmak, D. Pool, and R. Happee, "The role of vision in sensory integration models for predicting motion perception and sickness," *Experimental brain research*, vol. 242, no. 3, pp. 685–725, 2024.

[99] J. F. Golding, "Predicting individual differences in motion sickness susceptibility by questionnaire," *Personality and Individual Differences*, vol. 41, no. 2, pp. 237–248, Jul. 2006, ISSN: 0191-8869. DOI: 10.1016/J.PAID.2006.01.012. [Online]. Available: https://www.sciencedirect.com/science/article/pii/S0191886906000602.

[100] J. E. Bos, S. N. MacKinnon, and A. Patterson, "Motion sickness symptoms in a ship motion simulator: Effects of inside, outside, and no view," *Aviation, space, and environmental medicine*, vol. 76, no. 12, pp. 1111–1118, 2005.

[101] S. Casas, R. Olanda, and N. Dey, "Motion cueing algorithms: A review," *International Journal of Virtual and Augmented Reality*, vol. 1, 1 2016, ISSN: 2473-537X.

[102] M. A. Nahon and L. D. Reid, "Simulator motion-drive algorithms - a designer's perspective," *Journal of Guidance, Control, and Dynamics*, vol. 13, 2 1990.

[103] A. Beghi, M. Bruschetta, and F. Maran, "A real time implementation of mpc based motion cueing strategy for driving simulators," in *Conference on Decision and Control*, 2012, pp. 6340–6345.

[104] M. N. Zeilinger, C. N. Jones, and M. Morari, "Real-time suboptimal model predictive control using a combination of explicit mpc and online optimization," *IEEE transactions on automatic control*, vol. 56, no. 7, pp. 1524–1534, 2011.

[105] Y. Zheng, B. Shyrokau, T. Keviczky, M. Al Sakka, and M. Dhaens, "Curve tilting with nonlinear model predictive control for enhancing motion comfort," *Transactions on Control Systems Technology*, vol. 30, no. 4, pp. 1538–1549, 2022.

[106] Y. Zheng and B. Shyrokau, "A real-time nonlinear mpc for extreme lateral stabilization of passenger vehicles," in *International Conference on Mechatronics*, 2019, pp. 519–524.

[107] I. Maurović, M. Baotić, and I. Petrović, "Explicit model predictive control for trajectory tracking with mobile robots," in *International Conference on Advanced Intelligent Mechatronics*, 2011, pp. 712–717.

[108] P. Bemporad, "Explicit model predictive control," in *Encyclopedia of Systems and Control*, J. Baillieul and T. Samad, Eds. London: Springer London, 2013, pp. 1–9.

[109] A. Chadha, "Hybrid mpc-based motion cueing algorithm for driving simulators," M.S. thesis, Delft University of Technology, 2022.

[110] *Emovert controller manual*, E2M Technologies B.V, 2019.

[111] M. Bruschetta, C. Cenedese, and A. Beghi, "A real-time, mpc-based motion cueing algorithm with look-ahead and driver characterization," *Transportation research part F: traffic psychology and behaviour*, vol. 61, pp. 38–52, 2019.

A

APPENDICES CHAPTER 2

A

A.1. ACCELERATED SICKENING PATH DESIGN

The objective of the road generation is to extract the maximum sickening stimuli out of the road path.

The inputs that the optimisation chooses to maximise the MSDV are a_x and β i.e. the longitudinal acceleration and the side slip angle. The overall algorithm for the path optimisation is:

$$\max_{u \in U} \quad MSDV \tag{A.1}$$

$$s.t.: \quad Ax' = f(x,u,s) \tag{A.2}$$

$$u_{min} \leq u(k) \leq u_{max} \tag{A.3}$$

$$x_{min} \leq x(k) \leq x_{max} \tag{A.4}$$

where, Equation A.3 and Equation A.4 define the constraints to the inputs and the states of the model in the optimal control problem.

The equations of motion for the vehicle model used for the road generation in Equation A.2, are presented below:

$$\begin{aligned}
\dot{v_x} &= a_x + \dot{\psi} v_y \\
\dot{v_y} &= \dot{\psi} v_x \\
\dot{X} &= V\ cos(\psi + \beta) \\
\dot{Y} &= V\ sin(\psi + \beta) \\
\dot{s} &= V \\
\dot{\psi} &= \frac{V}{L}\ cos(\beta)\ tan(\delta) \\
a_x &= a\ cos(\psi) \\
a_y &= a\ sin(\psi) \\
V &= \sqrt{{v_X}^2 + {v_y}^2} \\
\delta &= tan^{-}1\left(\frac{\beta L}{l_r}\right)
\end{aligned} \tag{A.5}$$

where, V is the vehicle velocity; X and Y are the longitudinal and lateral positions in the global frame of reference; β is the side slip angle, and ψ is the heading angle; L is the wheelbase.

The vehicle model is allowed to take any actions within the specified limits, that make the movement feasible for a real vehicle according to the constraints in Table 2.2. A constraint is added on the local lateral displacements of the vehicle as well. This local lateral displacement limit is added considering the full workspace limit of the driving simulator (1 m). It shall be noted that the actual lateral displacement (see Figure 2.8) is larger due to vehicle yaw rotation.

The optimisation outputs a set of longitudinal acceleration and sideslip angle data to achieve maximum MSDV. Through this data and the initial conditions, all the states can be calculated. As the aim of this work is to obtain the accelerated sickening road path, the longitudinal and lateral distances (X and Y as described in equations A.5 and A.5) in global frame of reference are calculated and recorded. The sickening path is shown in Figure 2.8.

A.2. INDIVIDUAL MISC RESPONSES

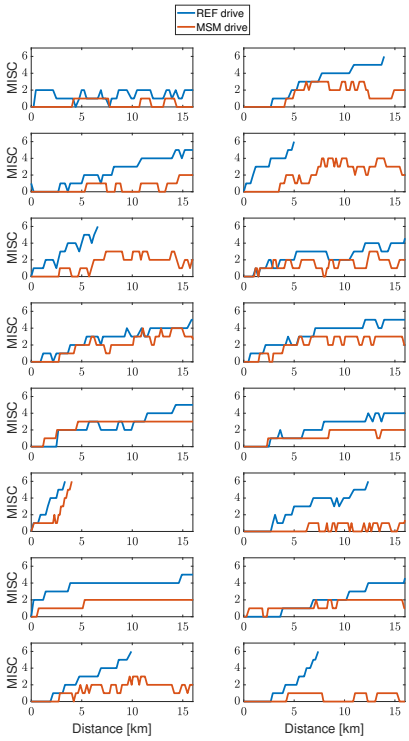

Figure A.1: Individual MISC scores for all the participants

A

A.3. NOMENCLATURE TABLE

Annotation	Description	Unit
AVs	Automated vehicles	-
a_x	Longitudinal vehicle acceleration in local frame of reference	m/s^2
$a_{x,w}(t)$	Frequency-weighted longitudinal acceleration	m/s^2
a_y	Lateral vehicle acceleration in local frame of reference	m/s^2
$a_{y,w}(t)$	Frequency-weighted lateral acceleration	m/s^2
$C_{\alpha f}$	Cornering stiffness of the front tyres	N/rad
$C_{\alpha r}$	Cornering stiffness of the rear tyres	N/rad
f_v	Function defining the nonlinear state space relation	-
g	Acceleration due to gravity	m/s^2
I_z	Moment of inertia of the vehicle about vertical axis	kgm^2
J_c	Cost function for the optimal control problem	-
J_x	Longitudinal jerk in vehicle's local frame of reference	m/s^3
k	Current simulation step	-
L_f	Distance of front axle from the vehicle COG	m
L_r	Distance of rear axle from the vehicle COG	m
m	Mass of the vehicle	kg
MISC	MIsery SCale (Subjective motion sickness rating scale)	-
MS	Motion sickness	-
MSAQ	Motion sickness assessment questionnaire	-
MSDV	Motion sickness dose value	$m/s^{1.5}$
MSM-drive	Motion sickness mitigation drive (proposed algorithm)	-
N_c	Length of the control horizon/ shifting horizon window	-
OCP	Optimal control problem	-
p	Generalised parameter	-
p'	Partial derivative of the generalised parameter w.r.t. space	-
s	Distance travelled by the vehicle	m
r	Vehicle yaw rate	rad/s
REF-drive	Reference automation drive (benchmark driving style)	-
s_0	Start-point of the road	m
s_f	End-point of the road	m
s_n	Lateral deviation of the vehicle from the lane center-line	m
T	Travel time	s
u	Control inputs (J_x and d_δ)	-
u^{guess}	Initial guess for the optimised inputs of the OCP	-
u_{opt}	Optimal control input	-
v_x	Longitudinal vehicle velocity in local frame of reference	m/s
v_y	Lateral vehicle velocity in local frame of reference	m/s
w_m	Weighting coefficient for MSDV in the cost function	-
w_t	Weighting coefficient for travel time in the cost function	-
x^{guess}	Initial guess for the states of the OCP	-
x_v	Vehicle states	-
α	Deviation of the vehicle heading angle from the road heading	rad
d_δ	Rate of change of steering wheel angle	rad/s
δ	Steering angle	rad
κ	Curvature of the road	m^{-1}
μ	Friction coefficient of the road	-
θ	Road heading angle	rad
ψ	Vehicle heading angle	rad

A.4. SOLVER SETTINGS

Parameter	Value
Algorithmic differentiation tool	CasADi 3.5.1
Prediction horizon for the sliding window	100 m
Step size	1 m
Shifting step size (Sliding window)	1 m
Integrator	ERK4
Integrator nodes	5
Solver method	PDIP NLP
Solver maximum iterations	2000
Tolerance	10^{-6}

B

APPENDICES CHAPTER 3

B.1. QUESTIONNAIRE

Two questionnaires were administered to the participants. The post scenario questionnaire involved providing absolute grades for each algorithm after its simulation. The post experiment administered upon completion of both scenarios, aimed to compare the FS and AW algorithms.

Post scenario questionnaire

- How closely did the ride's motion correspond to the video?

  [0 = Not at all, 5 = Completely coherent]

- How close did the cornering feel compared to a real car?

  [0 = Not at all, 5 = Exactly like a real car]

- How realistic did the deceleration feel compared to a real vehicle drive?

  [0 = Not at all, 5 = Exactly like a real car]

- How aggressive were the different sections of the drive?

  [0 = Not at all, 5 = Aggressive like a race car]

  - Section 1 (Multi-turns)
  - Section 2 (Slalom)
  - Section 3 (Lane change)

- Was the ride disorienting or sickening?

  [0 = Not at all, 5 = Extremely sickening]

- Were there any unnatural motions that did not match real driving?

  [0 = Not at all, 5 = A lot of them]

Post experiment questionnaire

- Which algorithm provided a more realistic driving experience?
- Which algorithm provided a more aggressive drive?
- Which algorithm provided higher instances of abrupt/unnatural motion during the simulation?

B.2. ABBREVIATIONS AND NOTATIONS

Table B.1: Notations used and their description.

Notation	Description
A_{hex}	System (state) matrix describing the hexapod motion
B_{hex}	Input matrix governing the hexapod motion
U_{hex}	Control input(s) for the system (hexapod)
X_{hex}	State vector for the platform
$\hat{X}_{hex}$	Neutral position of the platform
$\hat{Y}_{hex}$	References for the outputs of the state space
$Y(x_k, u_k)$	Output vector depending on the states and inputs
f_{spec}	Specific force (total)
G_{loc}	Tilt component or the gravitational force vector in occupant's frame of reference
W_Y	Penalisation weight for the output terms
W_X	Penalisation weight for the state terms
w_θ	Penalisation weight on the tilt angle of the platform
w_s	Penalisation weight on the displacement of the platform
$[k_1,\ k_2,\ k_3]$	Constants defining the shape of the non-linear weights (w_s; w_θ)
W_u	Penalisation weight on the input
$w_{G,loc}$	Penalisation weight for tilt-coordination reference tracking
$w_{f,trans}$	Penalisation weight for translational reference tracking
$w_{f,spec}$	Penalisation weight for the total specific force tracking
J_k	Platform jerk values (translation and rotation)
W_J	Weight penalisation on jerk
j_{trans}	Translational jerks
j_{ang}	Angular/rotational jerks
$w_{j,trans}$	Weight penalisation on translational jerks
$w_{j,ang}$	Weight penalisation on rotational jerks
ω_{thd}	Threshold for the tilt rate based on perception threshold
w_δ	Weight penalisation on the slack variable
δ	slack variable
s_{dyn}	Dynamic constraint relation for displacement
θ_{dyn}	Dynamic constraint relation for tilt angle
$[c_v, c_w, c_u, T_{dyn,s}, T_{dyn,\theta}]$	Constant gains used in the Dynamic constraint relation
Δ	Small value to keep non-linear weights from reaching infinity
ν_{FS}	Cut-off frequency for the high pass and low pass filters used in the MPC framework
ν_{yaw}	Cut-off frequency used for the yaw washout filter
s_{hex}	Platform displacement (all directions)
v_{hex}	Platform velocity (all directions)
a_{hex}	Platform acceleration (all directions)
θ_{hex}	Platform angular orientation
ω_{hex}	Platform angular velocity
α_{hex}	Platform angular acceleration
J_{hex}	Platform jerk (all directions)
j_{ang}	Angular jerks for the platform
s_{lim}	limit of displacement for the platform
θ_{lim}	limit of tilt angle for the platform
J_c	The cost function for the MPC
g	Acceleration due to gravity
R	Transformation matrix that resolves gravitational force to its components in global frame of reference
R_x	Transformation matrix to resolve the coordinates of a vector subjected to rotation along the x-axis
R_y	Transformation matrix to resolve the coordinates of a vector subjected to rotation along the y-axis
R_z	Transformation matrix to resolve the coordinates of a vector subjected to rotation along the z-axis

Table B.2: Abbreviations used and their description

Abbreviation	Description
MCA	Motion cueing algorithm
MPC	Model predictive control
FS MCA	Frequency-splitting MCA
AW MCA	Adaptive washout MCA
Dof/dof	Degrees of freedom
DAVSi	Delft Advanced Vehicle Simulator
HP	High pass
LP	Low pass
PDIP	Primal dual interior point
DWM	Direct workspace management
Acc/dec	Acceleration/ deceleration
std.	Standard deviation
IQR	Interquartile range
comp.	Component

B.3. VISUALISATION

IPG Carmaker is selected for visualisation purposes due to its exceptional capabilities in accurately depicting and simulating the experimental data, ensuring a robust and comprehensive representation of the driving scenarios under investigation. The data collected in the experiment is used to generate the visualisation for the driving simulator. Specifically, the vehicle's positional data is harnessed to construct a dynamic path. This path is subsequently traced by the vehicle, with predefined velocity references derived from the recorded experimental dataset.

B.4. BENCHMARK MPC-BASED MCA VS PROPOSED ALGORITHM FOR REAL DRIVING DATA

An analysis of the simulations comparing the results obtained using MPC-based MCA and proposed algorithm at different prediction horizon lengths is tabulated in Table B.3a. The workspace utilisation for the same conditions are tabulated in Table B.3b. It can be seen that the proposed algorithm is capable of rendering results faster than the MPC-based MCA.

B.5. SPECIFIC FORCE COMPOSITION

The specific force tracking, along with its translational and tilt components, is presented in Figure B.1 and Figure B.2. These plots illustrate how accurately the specific force is tracked and how the individual components contribute to its reconstruction.

Table B.3: Performance and workspace utilisation of MPC-based MCA and frequency-splitting algorithms at different prediction horizons for the scenario with real driving data for a 120-second simulation. The time step for this analysis is $T_s = 0.05\,\text{s}$. Real-time factors ≤ 1 (in green) indicate real-time feasibility.

(a) Specific force tracking performance and real-time feasibility

Algorithm	**Prediction horizon (Steps)**	RMSE long.	RMSE lat.	RMSE total	**Real-time factor**
MPC-based MCA	20	0.0884	0.7013	0.7068	0.3137
FS MCA	20	0.0772	0.6489	0.6535	0.2994
MPC-based MCA	40	0.0646	0.4429	0.4476	0.7133
FS MCA	40	0.0630	0.4141	0.4189	0.6010
MPC-based MCA	60	0.0662	0.2688	0.2768	1.1167
FS MCA	60	0.0675	0.2519	0.2608	0.8490
MPC-based MCA	80	0.0826	0.2390	0.2529	1.4982
FS MCA	80	0.0751	0.2359	0.2476	1.2607
MPC-based MCA	100	0.0709	0.2314	0.2420	1.7722
FS MCA	100	0.0724	0.2347	0.2457	1.5552
MPC-based MCA	120	0.0683	0.2172	0.2277	11.0467
FS MCA	120	0.0691	0.2217	0.2322	9.7388
AW MCA	-	0.0846	0.3283	0.3390	-

(b) Workspace utilisation

Algorithm	**Prediction horizon (Steps)**	RMS displacement	RMS velocity	RMS angular disp.	RMS angular vel.
MPC-based MCA	20	0.0929	0.1379	4.0859	3.1824
FS MCA	20	0.0808	0.0909	3.9762	2.2418
MPC-based MCA	40	0.0647	0.0685	3.0423	2.3083
FS MCA	40	0.0872	0.0741	3.0428	2.1532
MPC-based MCA	60	0.0487	0.0696	2.6847	2.0881
FS MCA	60	0.0577	0.0657	2.6428	1.9685
MPC-based MCA	80	0.0521	0.0690	2.6486	2.0091
FS MCA	80	0.0617	0.0651	2.6014	1.8820
MPC-based MCA	100	0.0498	0.0690	2.6606	2.0059
FS MCA	100	0.0600	0.0630	2.5900	1.8674
MPC-based MCA	120	0.0777	0.0918	2.7145	2.4701
FS MCA	120	0.0704	0.0649	2.5904	2.3803
AW MCA	-	0.0536	0.0429	2.8041	1.7905

B.6. PRE-POSITIONING

Pre-positioning is a phenomenon observed in MPC-based MCAs. An MPC can anticipate future maneuvers and prepare accordingly by moving the platform in advance. The specific force remains (close to) zero before the maneuver starts. However, no-

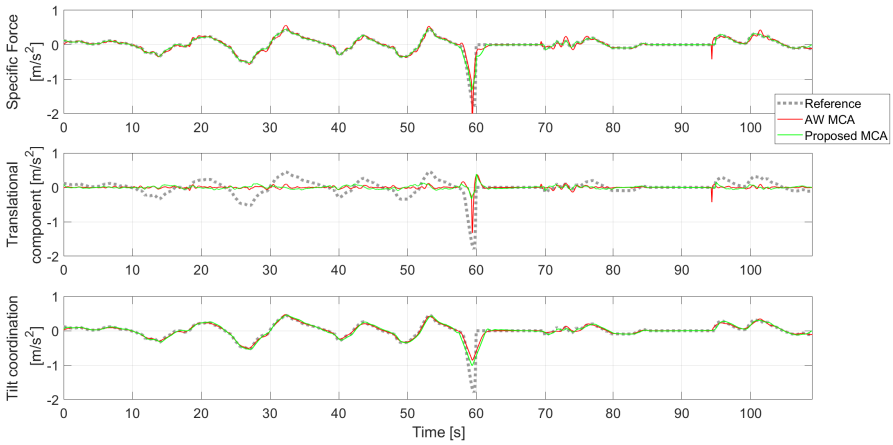

Figure B.1: Specific force tracking along with its linear and translational components corresponding to Figure 3.10.

table platform translations and rotations occur. These result in specific force components acting in opposite directions, whereby the translational component cancels out the tilt component. The movement of the platform can still be perceived in such a case. Pre-positioning primarily occurs when the tilt coordination cannot generate the desired specific force component promptly, given the tilt-rate restriction due to the perception threshold. Figure B.3 shows instances of pre-positioning. It can be seen that the first corner does not exhibit any pre-positioning because the platform had enough time to generate the desired specific force component through tilt coordination. This is evident from the omega (angular velocity) in the same figure, where omega does not saturate (reach the 3°/s limit) during the initial maneuver. Therefore, the platform could generate the specific force within the required time, avoiding pre-positioning. However, around time instances 50 and 80, the tilt-rate saturates indicating insufficient time for the platform to generate the desired specific force component through tilt-coordination. Consequently, the platform starts tilting in advance and the specific force components arising from the tilt of the platform are cancelled by the translational component.

B.7. PENALIZATION VARIATION SPECIFIC FORCE, ACCELERATION, TILT

Here we varied the elements of W_y (defined in Equation 3.6). Figure B.4. shows that these changes have limited effects.

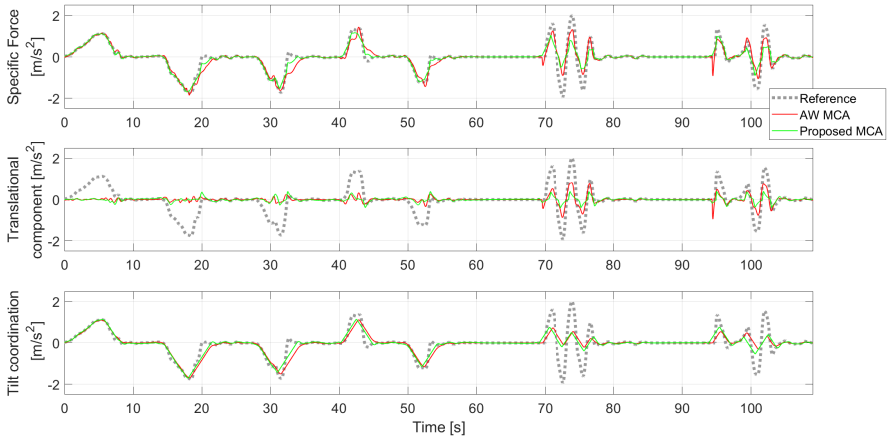

Figure B.2: Specific force tracking along with its linear and translational components corresponding to Figure 3.11.

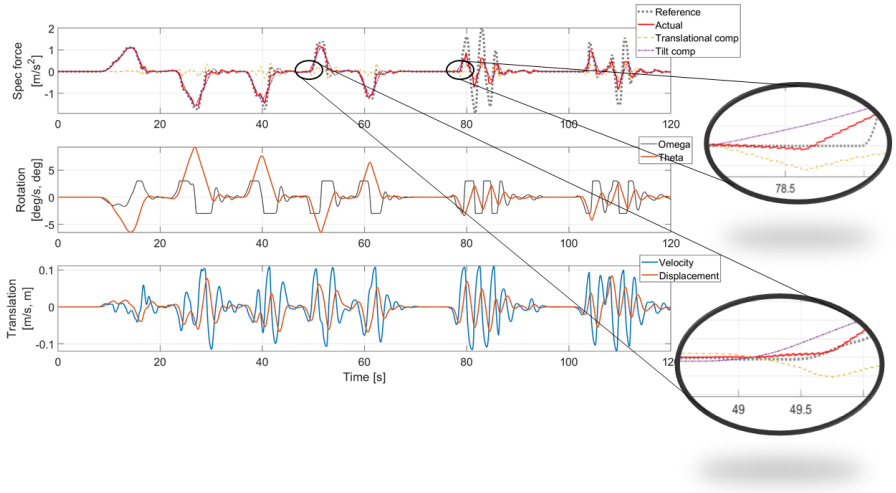

Figure B.3: Lateral specific force tracking for the settings corresponding to the experiment. The zoomed in regions highlight the pre-positioning problem that occurs in MPC based MCAs.

B

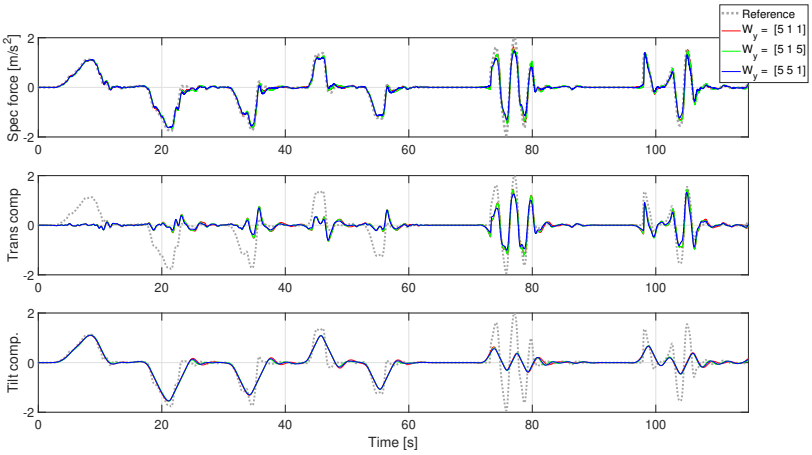

Figure B.4: Variations in W_y (penalization on the output terms [Total specific force; Translational component; Tilt component]) The red line represents the penalization used throughout the paper, the green line shows the solution with increased penalisation on the tilt component, and the blue line corresponds to a solution with higher penalisation on the translational component.

C

APPENDIX CHAPTER 4

C.1. SPECIFIC FORCE AND KINEMATIC TRACKING OF PLATFORM MOTION

The platform translational and rotational velocity and displacement along with the specific force tracking is presented in Figure C.1 for lateral and Figure C.2 for the longitudinal direction. It can be seen that both FS MCA and autoscaling MCAs create similar magnitudes of specific force as well as the tilt angles. Confirming that the algorithm matches the performance of other MPC-based MCAs while reducing preposition in tilt coordination.

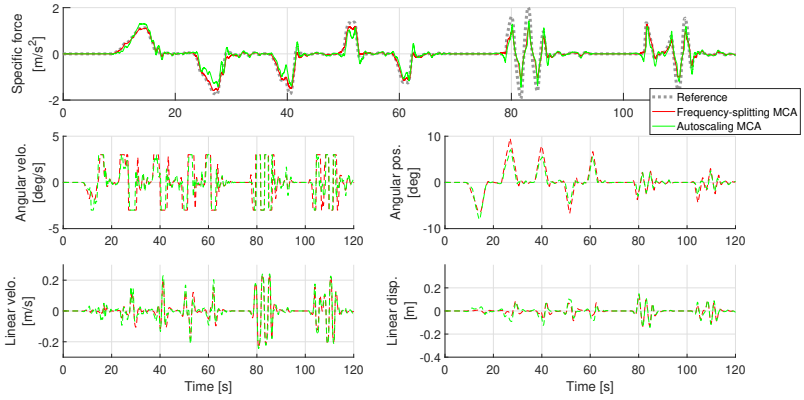

Figure C.1: The specific force tracking along with linear and angular velocity and displacement for lateral direction, corresponding to Figure 4.3

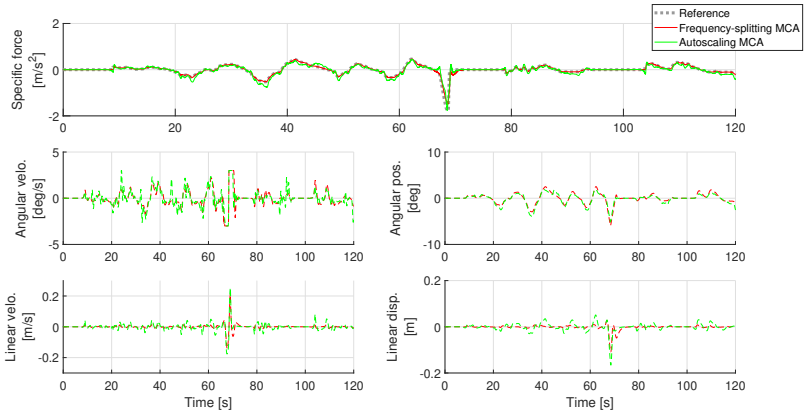

Figure C.2: Specific force tracking along with linear and angular velocity and displacement in the longitudinal direction, corresponding to Figure 4.2.

Additionally, the higher use of translational workspace can also be observed in the Figure C.1 and Figure C.2 via higher use of translational velocity and displacement.

D

APPENDICES CHAPTER 5

D.1. ALGORITHM WEIGHT SETTINGS

For the simulations presented in this chapter, the optimisation is conducted using `ForcesPro` [58], using Primal dual interior point (PDIP) algorithm. The maximum iterations are chosen to be 200, to ensure convergence and avoid sub-optimal solutions. The optimisation has been performed on Intel(R) Xeon(R) W-2223 CPU @3.60GHz with 32GB RAM.

In this work, we consider two major contribution terms that define the primary objective of the algorithm, along with several minor terms that help guide the Model Predictive Control (MPC) problem toward the desired performance. The two primary objective terms should have the highest contribution in the cost function.

Since the cost terms have different units, their relative contributions cannot be directly determined by the weights alone. To address this, we normalise the cost terms in the cost function. This is done by running a sample simulation and recording the maximum values attained by each error term. The cost terms are then scaled by dividing them by their corresponding maximum error values.

D.2. WEIGHT SELECTION

For the initial analysis, a penalisation weight of unity is set for specific force tracking. Additionally, the penalisation weights on the angular orientation and the platform displacement is a dynamical non-linear weight which changes based on the platform state (see Subsection 3.3.2 under workspace management) the penalisation weight chosen for this quantity just scales the overall non-linear shape of the weight based on the platform state.

PENALISATION WEIGHT FOR ANGULAR ORIENTATION

The weight on angular orientation was varied between 1e-4 and 1e-1. The weight of 1e-1 provides deteriorated specific force tracking performance, while the weights 1e-2, 1e-3 and 1e-4 provide almost identical responses. Hence, the weight of 1e-4 is chosen as it provides desirable performance, while keeping a lower contribution in the cost term.

PENALISATION WEIGHT FOR ANGULAR VELOCITY

The weight on angular velocity was also varied between 1e-4 and 1e-1. While all the weights provided a very similar response in the specific force generation, the weights had very differnet responses for the angular velocities. The weight of 1e-1 provides almost no excessive motion, whereas all other weights show excess oscillations in angular velocity. Thus the authors choose the weight of 1e-1 for the penalisation on angular velocity.

PENALISATION WEIGHT FOR DISPLACEMENT

The weight on translational displacement was varied between 1e-4 and 1e-1 as well. While a weight of 1e-4 tracks the specific force desirably for the majority of the simulation, at various instances, it performs a jerky motion when it reaches the limits of the workspace. With the weight 1e-3 we obtain desirable specific force tracking performance, however oscillations are observed in the sngulsr velocity eith this setting. The weight 1e-1 and 1e-2 provide a very similar response with no excess oscillation in the angular velocity. Thus due to its lower contribution towards the overall objective function, 1e-2 is chosen as the preffered weight for the simulations.

PENALISATION WEIGHT FOR TRANSLATIONAL JERK

The weight on translational jerk was varied between 1e-4 and 1e-1 as well. All the explored weights provided near identical responses via the algorithm. Thus the weight of 1e-4 is used to have the lowest possible contribution to the objective function, while providing a desirable performance.

PENALISATION WEIGHT FOR ANGULAR JERK

The weight on angular jerk was varied between 1e-5 and 1e-2 as well. Weight of 1e-2 renders a profile that does not follow the reference specific force properly. While the weight of 1e-3 traces the specific force, it exhibits oscillations in the tilt rate. The weights 1e-5 and 1e-4 provide a desirable specific force tracking, with the weight of 1e-4 also attaining slightly lower tilt rate values. Thus the weight of 1e-4 is selected for the simulations in this work.

D.3. SPECIFIC FORCE AND KINEMATIC TRACKING OF PLATFORM MOTION

The platform translational and rotational velocity and displacement along with the specific force tracking is presented in Figure D.1 for lateral and Figure D.2 for the longitudinal direction. It can be seen that AW and $MPC_{w_{con0}}$ produce similar levels of tilt angles, however $MPC_{w_{con0.9}}$ generates lower tilt angles in order to reduce motion sickness.

However the AW MCA uses a higher translational workspace in terms of displacements. However the $MPC_{w_{con0}}$ and $MPC_{w_{con0.9}}$ majorly stays near the neutral position.

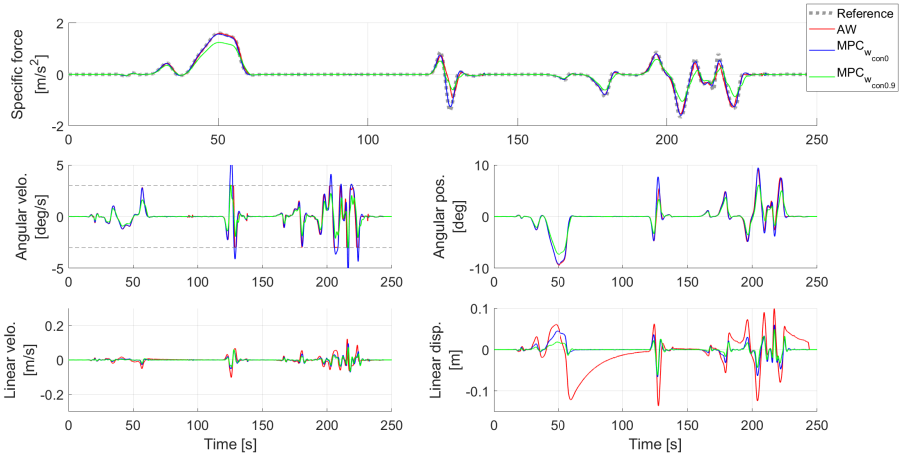

Figure D.1: Specific force tracking along with linear and angular velocity and displacement for the lateral direction, corresponding to Figure 5.3.

D

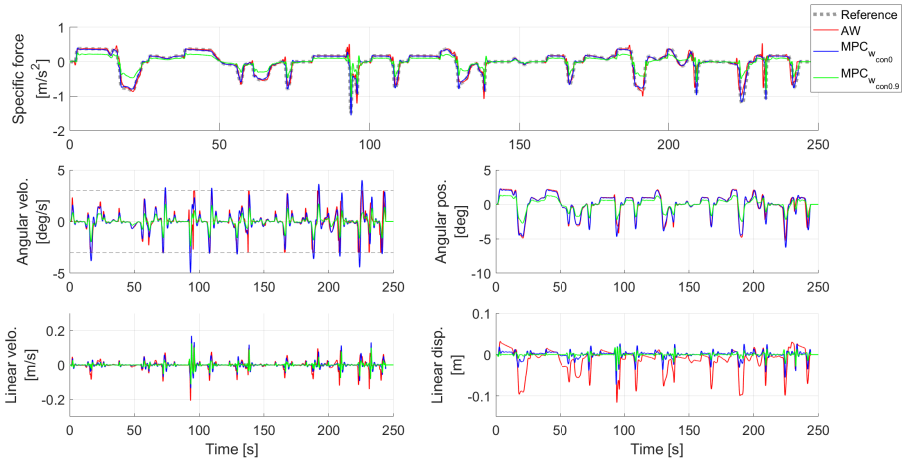

Figure D.2: Specific force tracking along with linear and angular velocity and displacement for the longitudinal direction, corresponding to Figure 5.3.

CURRICULUM VITÆ

Vishrut JAIN

14-10-1995	Born in Jabalpur, India.

EDUCATION

2013 - 2017	Bachelor of Technology VIT University, Chennai, India
2017 - 2019	MSc. in Mechanical Engineering (sp. Vehicle Engineering) TU Delft, South Holland, The Netherlands
2020 - 2025	PhD. candidate at Delft University of Technology TU Delft, South Holland, The Netherlands *Thesis:* Towards Sickness-free Automated Driving: Control Algorithms for Motion Sickness Mitigation in Automated Vehicles and Enhanced Immersion in Driving Simulators *Promotor:* Prof. Dr. Ir. R. Happee *Promotor:* Dr. B. Shyrokau *Collaborator:* Toyota Motor Europe

PROFESSIONAL EXPERIENCE

2019 - 2020	Part-time researcher at Swaayatt Robots
2018 - 2019	Teaching Assistant at TU Delft
2016-2017	Lead Design Engineer for Team Saksham International, Chennai, India
2014-2015	Chassis designer for Team Saksham International, Chennai, India
2014	Intern at BHEL, Bhopal

List of Publications

Publications included in the thesis

1. **V. Jain**, S. Kumar, G. Papaioannou, R. Happee and B. Shyrokau, "Optimal trajectory planning for mitigated motion sickness: Simulator study assessment.", in IEEE Transactions on Intelligent Transportation Systems vol. 24, no. 10, pp. 10653-10664, 2023. (Chapter 2)
2. **V. Jain**, A. M. R. Lazcano, R. Happee, B. Shyrokau "Motion Cueing Algorithm for Effective Motion Perception: A frequency-splitting MPC Approach". In: Proceedings of the Driving Simulation Conference Europe, Antibes, France. 2023. (parts of Chapter 3)
3. **V. Jain**, A. M. R. Lazcano, R. Happee, B. Shyrokau "Frequency-Splitting: Bridging Filter-Based and Optimization-Based Motion Cueing with Human-in-the-Loop Driving Simulator Validation".. (based on Chapter 3)
4. **V. Jain**, A. M. R. Lazcano, R. Happee, B. Shyrokau "Autoscaling: Minimizing Immersion Disruption in Motion Cueing Using Model Predictive Control". In Proceedings of the Driving Simulation Conference Europe, Stuttgart, Germany, 2025. (Chapter 4)
5. A Chadha, **V. Jain**, A. M. R. Lazcano, and B. Shyrokau, "Computationally-efficient motion cueing algorithm via model predictive control." in IEEE International Conference on Mechatronics, Loughborough, United Kingdom, 2023, pp. 1-6. (Chapter 6)
6. A. M. R. Lazcano, X. Akutain, **V. Jain**, R. Happee, B. Shyrokau "Method and calculator device for calculating at least one control value, and simulator" (Patent under review [Patent No. EP4492165A1]). (based on Chapter 3)
7. **V. Jain**, V. Kotian, A. Lazcano, D. M. Pool, R. Happee, B. Shyrokau "Easing the misery of a driving simulator ride: Motion Cueing for Motion Sickness Mitigation", (Manuscript in preparation) (Chapter 5)
8. A. M. R. Lazacano, X. Akutain, **V. Jain**, V. Kotian, D. M. Pool, R. Happee, B. Shyrokau "*Patent title to be decided*" (Patent under preparation). (based on Chapter 5)
9. A. M. R. Lazcano, X. Akutain, **V. Jain**, R. Happee, B. Shyrokau "AutoScaling: Motion Cueing Algorithm minimising immersion disruption and false cues" (Patent under preparation). (based on Chapter 4)

Previous Publications

1. S. Baldi, D. Liu, **V. Jain** & W. Yu, "Establishing platoons of bidirectional cooperative vehicles with engine limits and uncertain dynamics". in IEEE Transactions on Intelligent Transportation Systems vol. 22, no. 5, pp. 2679-2691, 2020.
2. D. Liu, S. Baldi, **V. Jain**, W. Yu, & P. Frasca. "Cyclic communication in adaptive strategies to platooning: The case of synchronized merging". IEEE Transactions on Intelligent Vehicles vol. 6, no. 3, pp. 490-500, 2020.
3. **V. Jain**, D. Liu, & S. Baldi. "Adaptive strategies to platoon merging with vehicle engine uncertainty". IFAC-PapersOnLine vol 53, no. 2, pp. 15065-15070, 2020.
4. T. Tao, **V. Jain**, & S. Baldi. "An adaptive approach to longitudinal platooning with heterogeneous vehicle saturations". IFAC-PapersOnLine vol. 52, no. 3, pp. 7-12, 2019.

Propositions accompanying the dissertation
TOWARDS SICKNESS-FREE AUTOMATED DRIVING
CONTROL ALGORITHMS FOR MOTION SICKNESS MITIGATION IN AUTOMATED VEHICLES AND ENHANCED IMMERSION IN DRIVING SIMULATORS
by

Vishrut JAIN

1. A motion planning algorithm that ignores motion sickness will be fit for cargo, but not for humans. *This proposition pertains to Chapter 2.*
2. A well-designed motion cue is like a good melody—it resonates not by being loud, but by being harmoniously timed. *This proposition pertains to Chapters 3, 4 and 5.*
3. High-fidelity models advance scientific understanding and enable real-world solutions, while low-fidelity approximations support real-time applications. *This proposition pertains to Chapters 2, 5*
4. Humans, even in controlled experiments, exhibit inherent variability, underscoring the need for statistically significant human-in-the-loop validation. *This proposition pertains to Chapters 2, 3, 4 and 5*
5. Curiosity is essential in research—until it becomes a detour from research objectives.
6. The more a PhD suffers, the more insightful propositions they can write.
7. Discomfort is often the price of meaningful development.
8. As eager as the world is to move towards electric vehicles it is not prepared.
9. Widespread international condemnation in times of war often provokes irrational responses.
10. It is often in our most vulnerable moments that we learn who we are, not from within, but through the care and presence of others.

These propositions are regarded as opposable and defendable, and have been approved as such by the promotors Prof. Dr. Ir. Riender Happee and Dr. Barys Shyrokau